POLITECNICO DI TORINO

LAUREA IN INGEGNERIA ENERGETICA E NUCLEARE
Innovazione nella produzione di energia

Master Thesis

Methane production through a solid oxide electrolyser with primary renewable source and carbon dioxide capture

Supervisors:
Prof. Maria Serra Prat
Prof. Attila Peter Husar
Prof. Massimo Santarelli

Candidate:
Edoardo Chiadò

Academic year 2018-2019

In collaboration with:

UNIVERSITAT POLITÈCNICA
DE CATALUNYA
BARCELONATECH

Institut de Robòtica
i Informàtica Industrial

During the Erasmus Exchange Programme:

Erasmus+

Acknowledgements

In this page I would like to thank all the people who supported me during this important chapter of my life.

En primer lugar quiero agradecer a mis Profesores Maria Serra Prat y Attila Peter Husar que me apoyaron y me ayudaron durante el desarrollo de este proyecto de tesis en el departamento 'Institut de Robòtica i Informàtica Industrial' de la Universitat Politècnica de Catalunya. Fue un placer trabajar con ustedes dos durante estos meses. Un cordiale ringraziamento va al Prof. Massimo Santarelli, mio relatore presso il Politecnico di Torino.

Ci tengo a ringraziare fortemente i miei genitori che mi sono sempre stati accanto e aiutato a superare i momenti di difficoltà incontrati durante questi cinque intensi anni. Un abbraccio va a mia sorella Eleonora che con la sua simpatia ha contribuito a rendere più leggero questo percorso. Un sentito grazie lo voglio anche rivolgere alle mie due nonne Maria e Pina per l'affetto e la vicinanza che mi hanno sempre dimostrato; spero da lassù nonna Pina tu sia fiera di me.

I want to thank all the incredible people I met during my Erasmus experience in Barcelona. In particuar, I will bring with me forever all the amazing moments I spent with my flatmates Alberto, Jesus, Monika, Philipp and Viktória. Special thanks to Lukas, not just a flatmate but a close friend and my personal English teacher. Thanks to the brexiting girls Federica and Giovanna for all the dinners we shared together. Doy tambien las gracias a mi pacer preferida Mireia por su apoyo durante los entrenamiento de running.

Non può certamente mancare un sentito ringraziamento per Fil, Cla, Vector e Guido che hanno costituito la mia famiglia all'interno del Poli durante questi anni. Con voi andare all'università è stata una passeggiata, quasi un divertimento. Un grazie speciale voglio rivolgerlo ai miei amici da una vita Pupo e Giova che mi hanno sempre dimostrato il loro appoggio anche nei momenti di lontananza. Voglio ringraziare Chiara per essermi stata vicina soprattutto in questi ultimi mesi dove il traguardo sembrava non volesse mai arrivare. Infine non posso non ringraziare Ciuchiz e Vitino che mi hanno accompagnato con la loro spiccata simpatia tosco-romana. Vi voglio bene.

Abstract

Renewable electric energy can be transformed into storable methane via electrolysis and subsequent methanation. Power to Gas systems appear as a promising technology to exploit the surplus energy from renewable power plants; different gases can be produced (e.g. methane or hydrogen).
In this Master Thesis work, two different Power to Gas systems are modelled using Matlab Simulink: a Solid Oxide Electrolyser with a CO_2-methanator and a Solid Oxide Co-Electrolyser with a CO-methanator. This latter component can operate with an inlet H_2/CO-ratio equale to 3 or larger. A ratio of 5 is also considered. The CO_2, coming from biogas produced in the Waste Water Treatment Plant of *EDAR Riu Sec* situated in Sabadell (Barcelona), is captured and processed in order to obtain methane. Additionally, according to the Master Thesis' objectives, a photovoltaic power plant and a CO_2 storage are sized. An averaged power profile produced by a PV plant located in Barcelona is obtained with the *PV*SOL* programme. Therefore, the installation of a P2G system allows to achieve two positive effects: firstly, the CO_2 is not released to the atmosphere. Secondly, the CO_2 is reused to produce methane without getting it, in a more polluting way, from natural gas or coal.
Nowadays not all the technologies analysed in this work are mature. Due to the complexity and partial lack of information simplified models and assumptions in operating conditions have been employed.
The main goal is to evaluate what is the most efficient Power to Gas choice in terms of installed nominal power to exploit the entire amount of the carbon dioxide over one year of operation. Furthemore the photovoltaic power plant is sized assuming operativity only during the summer period; the differences with respect to yearly operation are illustrated in terms of required power and storage capacity.
According to the results achieved in this work, the optimal Power to Gas system is the co-electrolyser coupled with a CO-methanator with a H_2/CO-ratio equal to 3. Considering the worst case of operation, thus during winter, a PV plant of 1.2 MW has to be installed to process the entire amount of CO_2 available; regarding only summer operation, a smaller plant of 0.8 MW plant is needed. The capacity of the storage, assuming only summer operation, is also reduced of almost 30% with respect to winterly operation, where 995 m^3 of storage are needed. The molar fractions of the outlet gas mixture, after methanation process, are around 30% CH_4, 60% H_2O and 10% CO_2.
To obtain more precise results, improvements should be apported to the developed models, enhancing the learning of the operating conditions.

Contents

List of Figures

Chapter 1

Introduction

1.1 Motivation and context

Carbon dioxide is the primary greehouse gas emitted through human activities [66]. CO_2 emissions represent one of the major cause to global warming and account for almost 80% of all EU greenhouse gas emissions [67]. This gas is naturally present in the atmosphere as part of the Earth's carbon cycle. However, human activities are provoking changes in this natural cycle by adding more CO_2 to the atmosphere or influencing the ability of natural sinks to remove CO_2 from the atmosphere. Combustion of fossil fuels for energy and transportation are mainly responsible for human CO_2 emissions [66]. Thus, in the last decades, the concentration level of CO_2 in the atmosphere is growing as highlighted in fig.1.1. The main index of global warming is the increase of the surface temperature, respect to the pre-industrial period. Looking at fig.1.2, it is clearly visible that eighteen of the 19 warmest years have all occured since 2001, with the exception of 1998 [62].

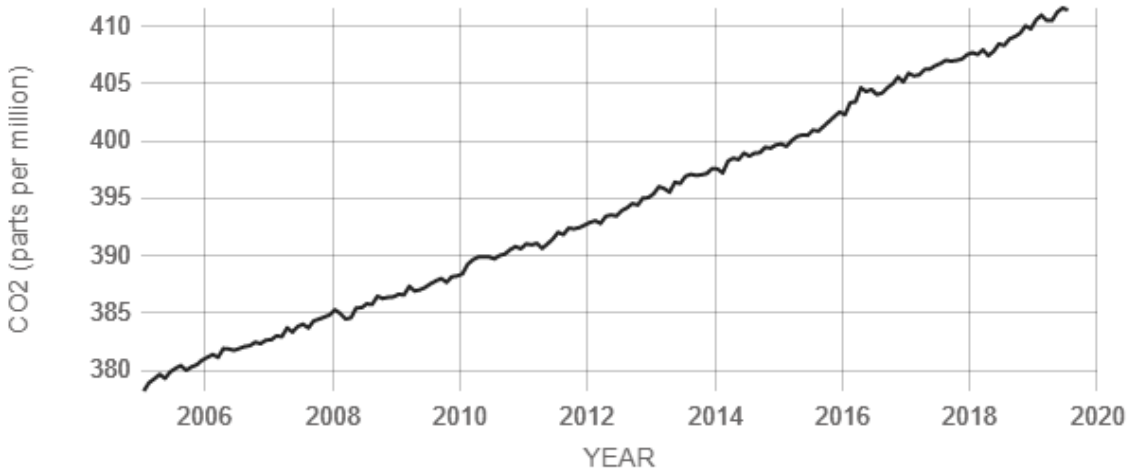

FIG: 1.1. Atmospheric CO_2 levels measured at Mauna Loa Observatory, Hawaii in recent years [62]

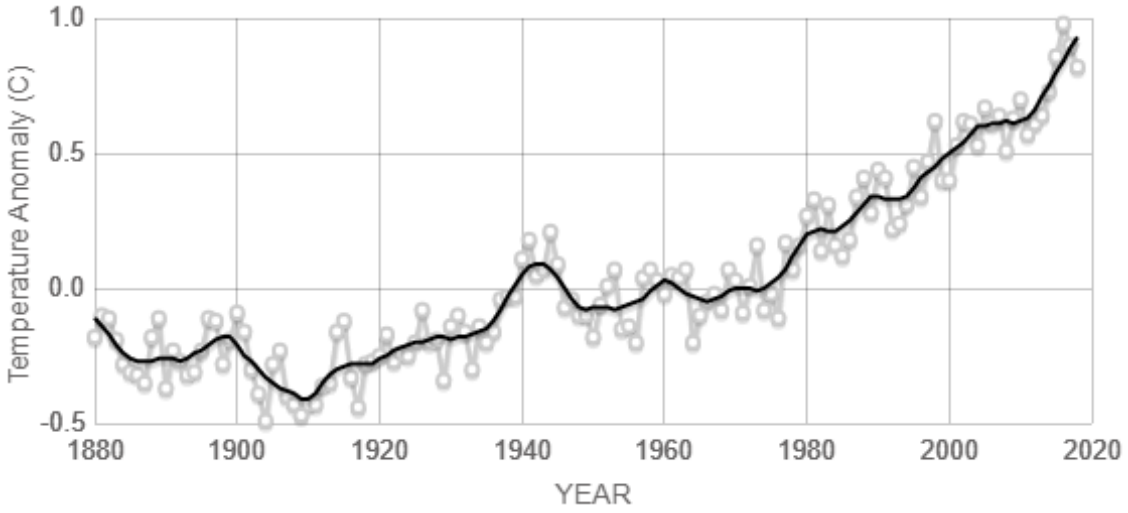

FIG: 1.2. Change in global surface temperature relative to 1951-1980 average temperature [62]

To mitigate the greenhouse gas emissions, the *Paris Agreement*, an agreement within the United Nations Framework Convention on Climate Change (UNFCCC), has been signed in 2016. The main long-term aim is: "Holding the increase in global average temperature to well below 2 °C above pre-industrial levels and to pursue efforts to limit the temperature increase to 1.5 °C above pre-industrial levels, recognizing that this would significantly reduce the risks and impacts of climate change" [68]. Under the *Paris Agreement*, the EU has approved to cut its greenhouse gas emissions by at least 40% below 1990 levels by 2030. Furthermore, in November 2018 the European Commission presented a long-term strategy for the EU to achieve a climate-neutral economy by 2050 [69].
Simultaneously, renewable energy sources (RES) have played an important role in recent decades. As a matter of fact, the awareness of climate change and the need to develop alternative energetic sources are influencing their exponential growth [1]. The EU, with its Renewable Energy Roadmap, has decided to reach a target of 20% renewable energies in the overall energy mix by 2020 [2]. In 2017 30% of the electricity in Europe was produced by renewable energy sources [60]. Neverthless, RES are charaterized by intermittence and unpredictable profile of electrical productivity; moreover, they have to be balanced for electrical grid stability. Therefore, to avoid overloads or blackouts, the electrical energy has to be stored.
Researchers are focusing their attention in electric energy storage coupled with carbon capture and storage (CCS) systems. PtG technology seems to be a promising way to manage these issues. This process is made up of two consecutive steps: H_2 production by water electrolysis and H_2 conversion with a CO or CO_2 source to CH_4 via methanation [1] [2].
The Universitat Politecnica de Catalunya (specifically the Institut de Robotica i Informatica Industrial), where this Master Thesis work has been developed, with the collaboration of Maria Serra and Attila Husar, is partner of *CoSin* project. *CoSin* is a project by the *RIS3CAT Energy Community*, financed by the Regional Goverment of Catalonia; its main objective is to obtain synthetic fuels using biogenical sourced carbon and water. This PtG project is based on converting and storing surplus of electricity from renewable resources

in methane; inside this plant, built in Sabadell, only water and carbon dioxide from biogas are used as reactants. Another advantage is that this renewable gas can be transported using the existing natural gas pipelines. The operation of the pilot plant began in May 2018 and is planned to last for 18 months [71].

1.2 Objectives

The present Master Thesis work has been carried out during an exchange programme from March to September 2019 at Universitat Politecnica de Catalunya (IRI). The idea for this project is based on from the cooperation of the University with the Institut de Recerca en Energia de Catalunya (IREC) and the partners of the *CoSin* project. The topic is the capture of carbon dioxide, produced during the operation in *EDAR Riu Sec* a Waste Water Treatment Plant located in Sabadell (Barcelona), and its conversion in methane feeding the spanish natural gas network. Two positive effects are reached: the reduction of CO_2 emissions and of imports of fossil-based natural gas.
Particularly, two different systems are analysed and compared: a Solid Oxide Electrolyser with a CO_2-methanator and a Solid Oxide co-Electrolyser with a CO-methanator. The overall operating schemes are visible in fig. 1.3 and 1.4.
The work is divided in several parts; after a theoretical study of the four main devices (SOE,COSOE and two methanators), their dynamic models have been developed using Matlab-Simulink. After that, for each system, a renewable plant (photovoltaic power plant) has been designed and, thus, the four devices have been sized to use the electric power available. Furthermore, CO_2 storage has also been implemented. This component can store carbon dioxide when there is a lack of power or release it when needed.
The main objective of this work is to evaluate which one of the two systems requires the least installed nominal power of the PV plant to exploit all the CO_2 available during one year. Thus, all the components have been sized to reach this obejective. This way, the most efficient system can be found. Secondly, the sole operation during summer months is considered and the same study is repeated. Concerning the system represented in fig.1.4, the CO-methanator can work with a different feeding ratio between hydrogen and carbon monoxide produced by the COSOE; hence, another objective is to discover which ratio allows to produce more methane.

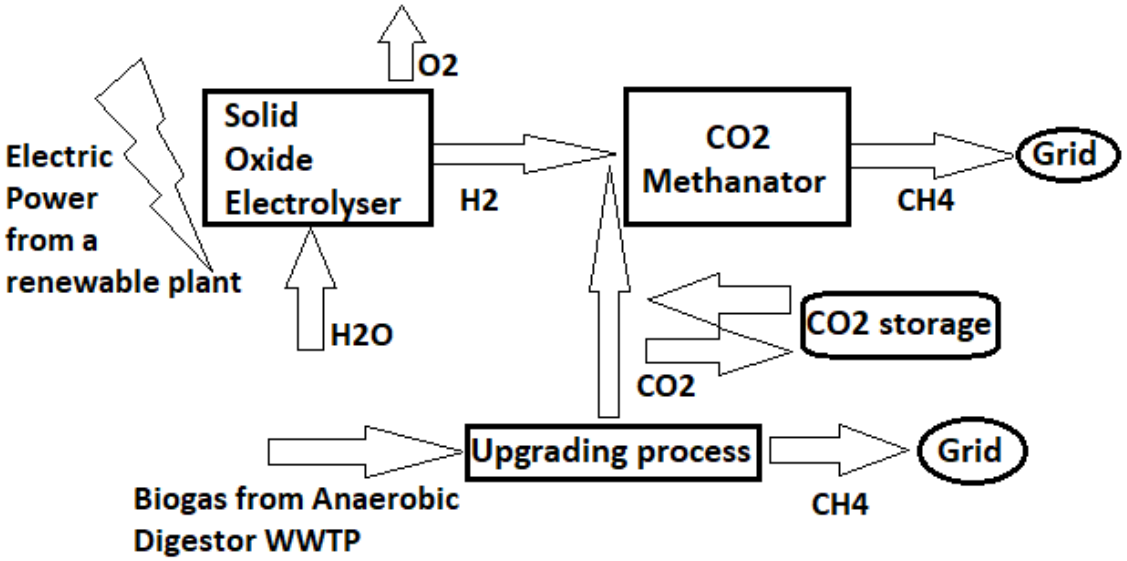

FIG: 1.3. 'SOE + CO_2-methanator' system scheme

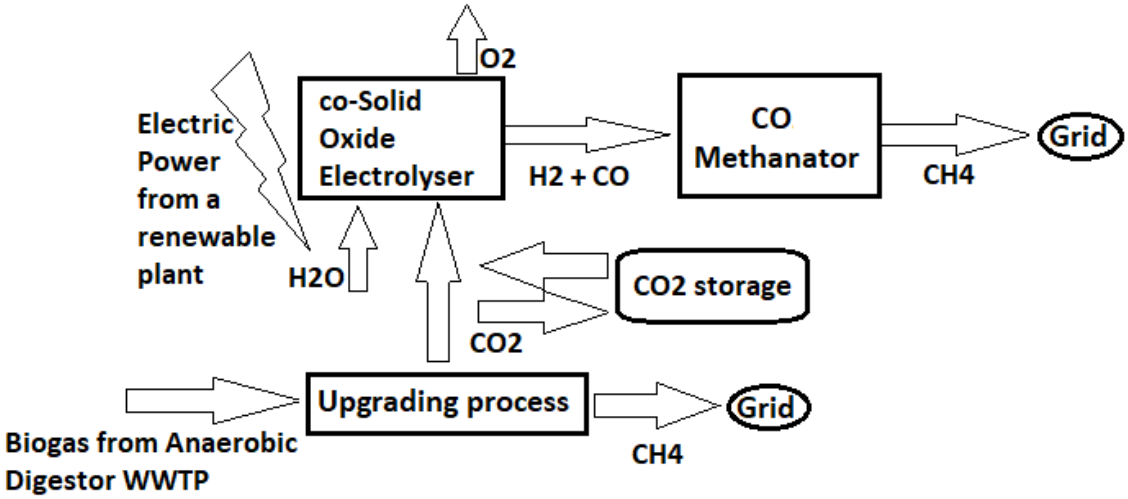

FIG: 1.4. 'COSOE + CO-methanator' system scheme

Chapter 2

State of the art

2.1 Wastewater treatment plant

The wastewater treatment is a process that converts wastewater which comes from households and industries, in another effluent. This latter can be released to the water cycle, minimizing the environmental impact, or directly reused. This process takes place inside a Waste Water Treatment Plant (WWTP) and it plays an important role in the field of sanitation. Sanitation, indeed, includes the handling of human waste and solid waste as well as stormwater management. From a WWTP multiple products can be obtained as coarse solids and sewage sludge that can be treated and used to produce biogas. There are two main types of sludge named as 'primary' and 'secondary' sludge that present different characteristics and allow to produce different biogas quantities [63]. Fig.2.1 shows an overall operating scheme of a WTTP; the different steps are described, mainly focused on the Anaerobic Digestor that produces biogas that can be employed for different energetic scopes.

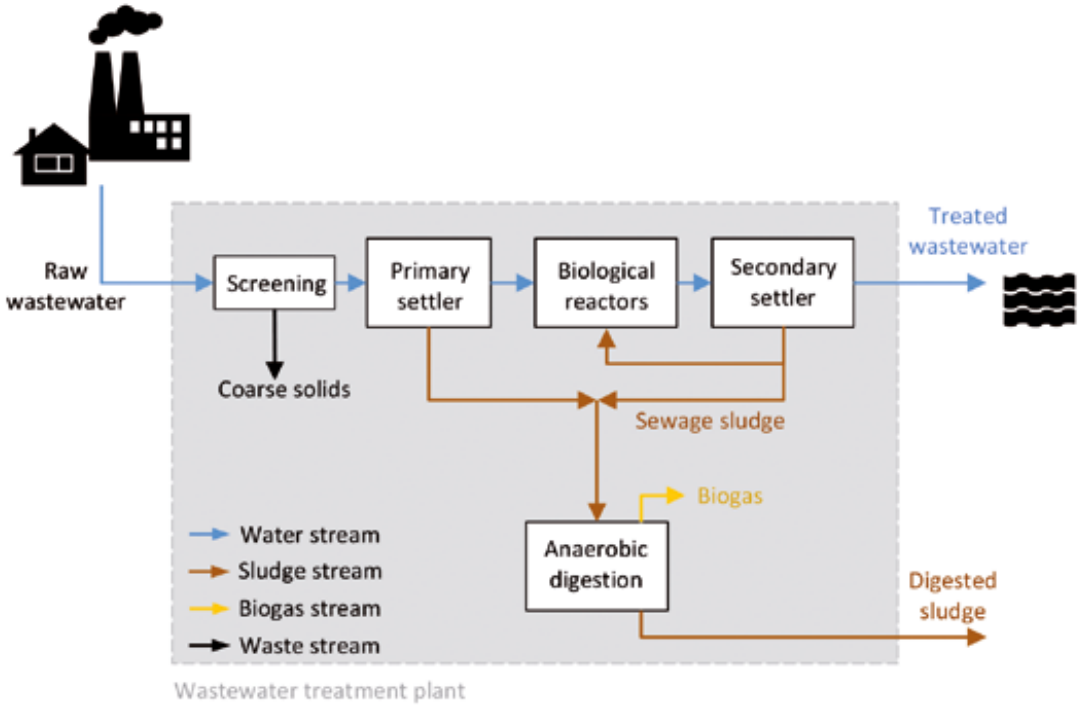

FIG: 2.1. WWTP scheme [3]

2.1.1 Operation process of a WWTP

1. The Primary settler is fed in by a raw wastewater flux and by means of a gravitational sedimentation, usually by a clarifier, the primary sludge is produced; it is characterized by an high content of organic matter and it is easily degradable. During the process, its energy has not yet been consumed and it is an higher biogas production potential. According to [VSA], 2010 and Zhang, 2010, in optimal digestion conditions a methane yield of 315-400 Nm^3 per ton of organic dry matter (ODM) can be expected [3].

2. Inside the biological reactors, microorganisms are used to consume the organic matter of the wastewater; they, indeed, feed on the biodegradable material of the wastewater and then flow in the Secondary settler.

3. By means of a secondary clarifier, inside the Secondary settler, the biomass is deposited and removed as secondary sludge; in this latter case, this sludge is characterized by a lower energetic content and degradable fraction. Therefore, in optimal conditions, the methane yield is 190-240 Nm^3 per ton of ODM. It can be noticed that a part of this sludge may be again treated inside the biological reactors; another output is the completely treated water released to the environment [3].

4. At this point of the process, the sewage sludge can flow inside the anaerobic digestors; often it is sieved and thickened to a dry solids content of up to 7% to avoid high energy consumptions due to the amount of water content. By-products are biogas and the digested sludge that are analysed further more in details. Inside the digestors, microorganisms transform the organic dry matter into biogas (according

to Bachmann, 2009, Tietze, 2006, VSA, 2010, 45-55% is converted equivalent to one third of solid matter); to understand better the process some parameters must be taken into account: the hydraulic retention time (HRT) and the temperature [3] [64]. The first one is defined according to the following formula:

$$HRT[days] = \frac{Netdigestervolume[m^3]}{Feedstockinput[\frac{m^3}{day}]} \tag{2.1}$$

The HRT represents the theoretical period that the sludge should stay inside the AD. If this index is too small, e.g. due to residual sediments inside the digestor, this can cause an incomplete or no degradation; thus, low biogas yields are achieved. The second key parameter is the temperature: to optimize the ratio between heating energy needed and the energy gain; considering moreover that the sewage sludge presents an high water content the system shall operate ad mesophilic temperatures in the range between 35-39 °C (Lindtner, 2008, VSA, 2010). As rule of thumb, a typical range is between 16-25 days (based on Kind et al.,2012, VSA, 2010) .
According to types of sludge, its degradation rate and operating conditions of the anaerobic digestor, based on Bachmann, 2009, VSA, 2010, a gross gas production around 450-500 l/kg ODM can be expected [3] [64]. As illustrated above in fig.2.1, the two products are the digested sludge and the biogas.

- **Digested sludge**
  Depending on the further utilization, the sludge is pressed, centrifuged or even heat dried to remove as much water as possible. It can then be utilised in agriculture due to its high fertilizing value or send to an incineration plant even if its lower heating value is limited; its final disposal depends mainly on legal constraints and costs. The liquid fraction, originating from the dewatering process of the digested sludge, could be reinserted at the entrance of the WTTP and mixed with the one coming from the households and industries.
- **Biogas**
  This represents the second output of the anaerobic digestor and it is the most relevant product from an energetic point of view; the biogas technology, indeed, represents one of the most attractive solutions to convert organic residues into a renewable energy carrier; it also plays an important role to achieve the target set by the *European Commission* in 2009 to cover the 20% of final energy consumptions shall be provided by renewable sources. The sustainable biogas production is increasing in this years; it is, thus, needed to analyse more in details its composition and possible employments. The raw biogas produced inside the AD is a mixture of different gases: mainly it contains methane (63-67% based on Bachmann, 2009, Kind et al., 2012, Kolisch, 2010), carbon dioxide (35-40%) and trace gases. This outcome is not still ready to be used and a gas treatment, including drying and trace substances removal, has to be carried out to obtain a good quality combustible.
  Another important index that has to be evaluated inside a WWTP is the utilization of the biogas produced that indicates how much of the produced biogas is converted into power, heat or biofuel; based on VSA, 2010 the best range is

between 95-99% [3].
Now three viable employments of the biogas are explained:

- **Heat production**: this is the least efficient and suitable disposal;
- **Combined heat and power production**: this is recommended for all biogas plants and it is the most exploited;
- **Upgrading to bio-methane**: this third solution is still in development in the smaller biogas plants but it is already used in the larger plants with biogas production rates greater than 100 Nm^3/h. The biomethane obtained can be either sold as biofuel or injected directly into the grid. This last employment is the most important with respect to this work's objectives. During the upgrading process, the biogas is treated and separated into biomethane and carbon dioxide. Regarding this latter gas, this work focuses its attention; usually, after the upgrading process, the carbon dioxide is released into the atmosphere and not reused anymore. Considering that the CO_2 is an important pollutant for the environment, the idea at this point would be to collect it and try to produce new methane using a Power to Gas system. The required electrical power may come from a renewable system, e.g. photovoltaic or wind plant [3]. The upgrading process' operational conditions are out of the scopes of this MT and, therefore, in fig. 2.2, a schematic and brief explanation is provided without entering into further details.

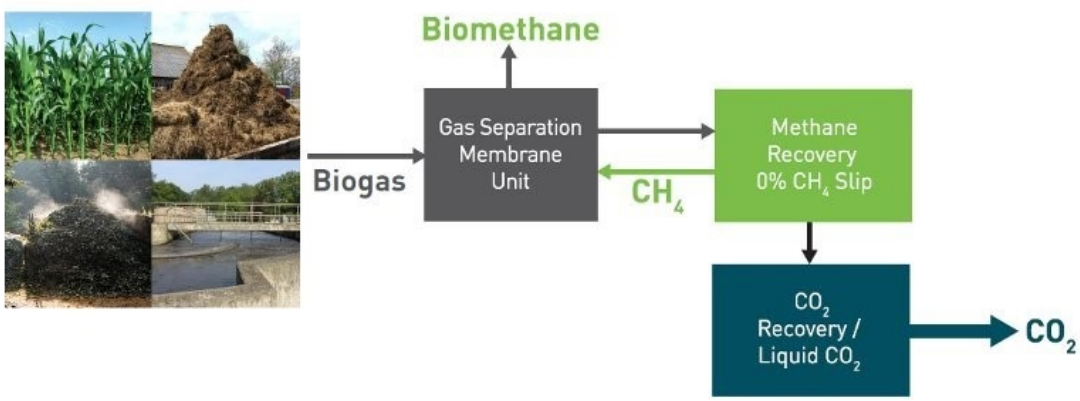

FIG: 2.2. Upgrading process scheme [65]

2.2 Solid oxide electrolyser

One of the main component treated in this work is the electrolyser that uses electrical power to convert water into hydrogen; the electrolyser operates in 'reverse mode' with respect to the fuel cells, electrochemical devices able to produce electricity using hydrogen and oxygen. The electrolysers represent the most promising carbon free technology for the hydrogen production according to high conversion efficiencies and lower energy input required with respect to similar systems (thermochemical and photocatalytic devices) [4]. Several types of reversible fuel cells are nowadays known. However, the proton membrane exchange electrolyser (easily named PEM) and the solid oxide electrolyser (SOE) are the most relevant. According to the purposes of this work, even if the PEM-electrolyser represents the most mature technology, only the latter has been employed due to different reasons that are now explained. The SOE operates in a temperature range, that varies from 600 °C to 1000 °C with respect to PEM technology, that works usually below 100 °C. Increasing the temperature, the electrical demand or Gibbs free energy progressively decreases; as a result, the efficiency of the system is higher. In SOE the theoretical efficiency can reach 100% compared with the usual 65-80% in a PEM [5] [7]. As shown in fig.2.3, increasing the temperature the heat demand grows nevertheless the total energy demand slightly varies. Moreover, the high temperature reactions are favourable from the point of view of kinetics and electrolyte conductivity. If an high temperature heat source is available, the process is very convenient.

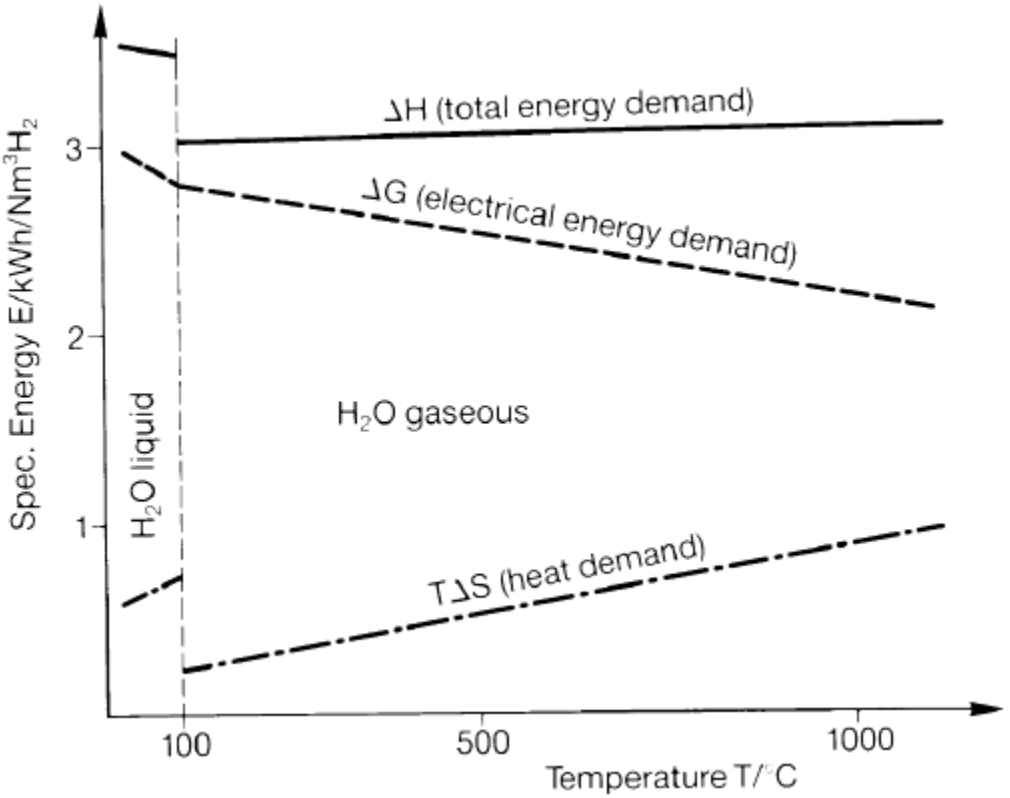

FIG: 2.3. Electricity, heat and total energy demand [7]

In a solid oxide electrolyser cell the steam water is fed into the porous cathode and,

when a certain voltage is applied, the steam moves towards the electrolyte-cathode interface where, the water reduction takes place and H_2 and O_2 ions are produced and separated: the hydrogen crosses the cathode again in the opposite direction and it is collected on the cathode surface. Meanwhile, the oxygen ions conduct through the electrolyte and reach the electrolyte-anode interface where the oxidation occurs and pure oxygen is obtained and collected. It has to be noticed that the electrolyte has to be dense enough in order to avoid the diffusion of the gases and the consequent recombination of hydrogen and oxygen ions [5] [7]. According to [8], the reaction sites are named "triple phase boundaries" (TPB), because the reaction requires three phases: a gas phase supplies and removes the gas species, an electric conduction phase brings the electrons to the reaction site and an oxygen ionic conductor transfers away the oxygen ions from the reaction site. If one of these three phases is missing, the electrochemical reactions cannot take place.
Therefore, as also shown in fig.2.4 and 2.5, a solid oxide electrolyser is made up of three main elements:

- **ANODE** named also as "Oxygen Electrode"; here the following oxidation reaction occurs:
$$O^{2-} \rightarrow \frac{1}{2}O_2 + 2e^- \tag{2.2}$$
The anode is built up with a porous material (usually the most commonly used is the Lanthanum Strontium Manganate LSM) that guarantees high performances, creating, under electrolysis conditions, vacancies that allow the oxygen diffusion;

- **CATHODE** also named as "Fuel Electrode"; here the following reduction reaction happens:
$$H_2O(g) + 2e^- \rightarrow H_2(g) + O^{2-} \tag{2.3}$$
The cathode is built up again with a porous material: the most commonly used is a Nickel cathode doped with Yttria-Stabilized Zirconia. Other solutions are under development because the high steam partial pressure and the low hydrogen partial pressure can lead to an irreversible degradation due to the Nickel's oxidation at the $Ni - YSZ$ interface;

- **ELECTROLYTE**: this third element is usually made up of Zirconia Dioxide doped with $Y_2\ O_3$ and together this constitutes the YSZ. These two elements guarantee high strength, high melting points, resistance to corrosion and during fast cooling down the phase transition from monoclinic to tetragonal is reduced, thus avoiding the presence of cracks and the decrement of conductive properties; They are important for the electrolyte's operating function [70].

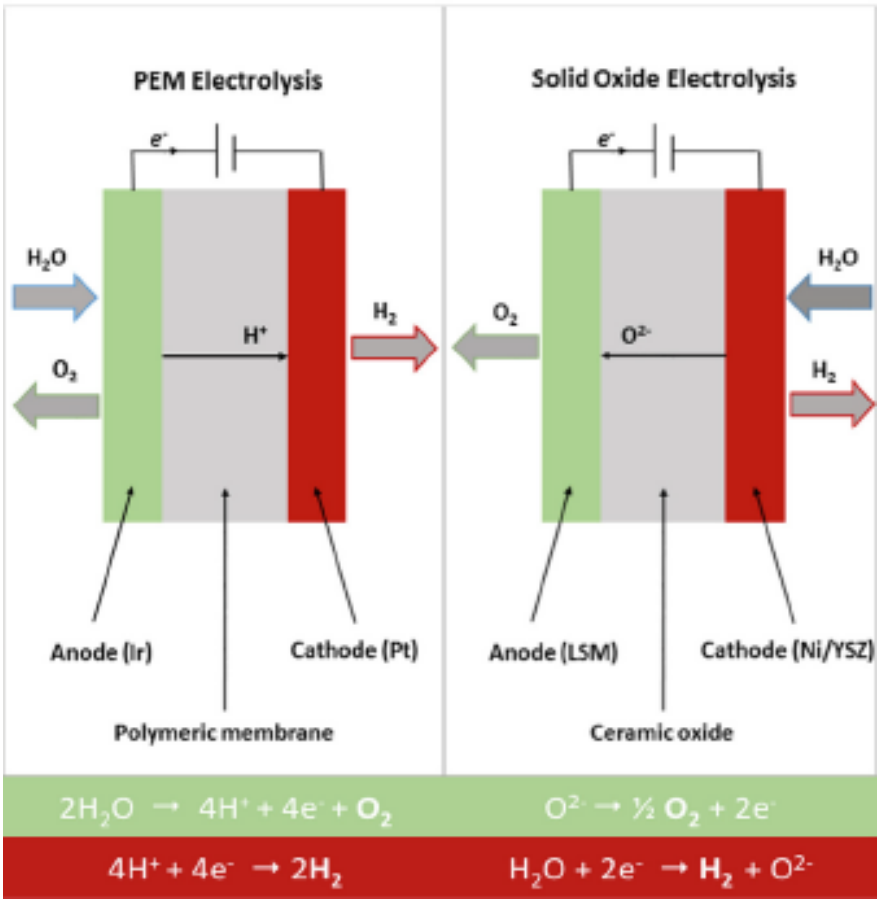

FIG: 2.4. Comparison between PEM and SOE technology [6]

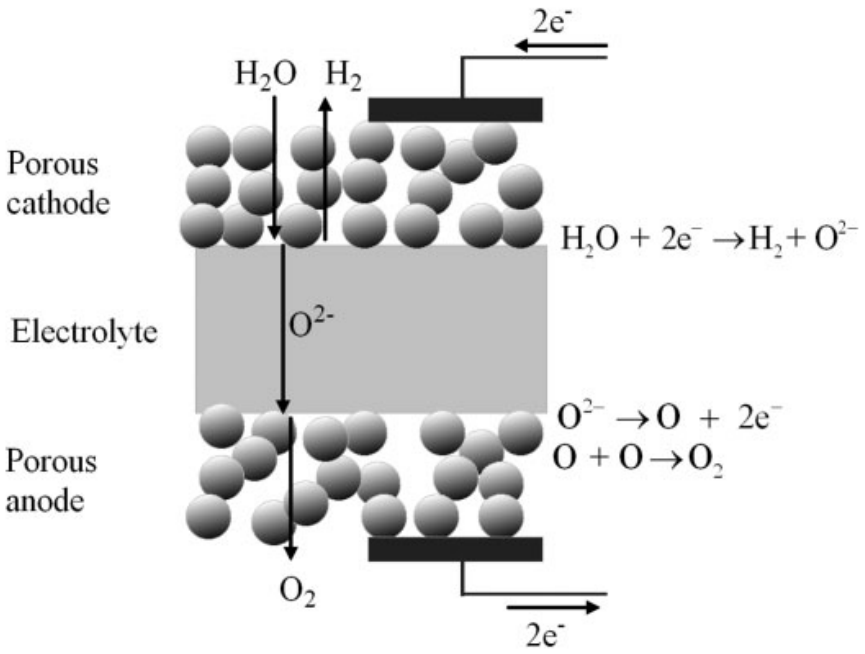

FIG: 2.5. Structure of a soe cell [13]

In a solid oxide electrolyser modelling, different quantities have to be taken into account to correctly describe this component. First of all, there is a linear correlation between the hydrogen produced or converted water and the amount of current that flows inside the device; Faraday's law for electrolysis determines this relationship. The current density is, in this case, the sole parameter used to evaluate the electrochemical performance and product composition [9]. Furthermore, the number of electrons involved in the water electrolysis reaction are taken into account and Faraday's law is following:

$$H_{2_{produced}} \text{ or } H_2O_{converted} = \frac{j \cdot A \cdot N}{n_e \cdot F} \tag{2.4}$$

Where:

- $j[\frac{A}{cm^2}]$ is the current density expressed usually in $\frac{A}{m^2}$ or $\frac{A}{cm^2}$;
- $A[cm^2]$ is the operating area of each cell of the electrochemical stack;
- N is the number of cells connected in series with the aim to increase the voltage;
- n_e represents the electrons involved in the chemical reaction (in this case 2);
- F is the Faraday constant: 96485,3365 $\frac{C}{mol}$.

Secondly, another key factor is the voltage that must be applied to the cells during the hydrogen production mode and it can be defined according to the following formula:

$$V_{SOE} = E_{rev} + \eta^{SOE}_{conc,anode} + \eta^{SOE}_{conc,cathode} + \eta_{act,anode} + \eta_{act,cathode} + \eta_{ohmic} \tag{2.5}$$

According to [11],[12],[13] and [14], the first term on the right side of the equation is the reversible or minimum voltage and it is defined as the minimum electrical energy required by the cell in order to have water electrolysis, in other terms, the split of water into hydrogen and oxygen; this quantity is represented by the free Gibbs energy variation as follows in the equation:

$$E_{rev} = \frac{\Delta G}{n_e \cdot F} \tag{2.6}$$

Where:

- ΔG $[\frac{kJ}{mol}]$ is the Gibbs free energy variation and it is defined as the difference between products and reactants with the proper molar ratio;
- n_e is the number of electrons associated with the electrochemical reaction;
- F $[\frac{C}{mol}]$ is the Faraday constant.

Under standard conditions at 298 K, the ΔG^0 for $H_2O(l)$ is equal to 237,2 kJ/mol and thus the standard reversible voltage is:

$$E^0_{rev} = 1.23V \tag{2.7}$$

Moreover, an enthalpy variation ΔH is associated to the water electrolysis; this quantity takes into account the overall energy balance of the cell and it is correlated with the Gibbs free energy and the entropy generation following the equation:

$$\Delta G = \Delta H - T \cdot \Delta S \tag{2.8}$$

By means of enthalpy variation, it is possible to define the thermoneutral voltage of the cell in this way:

$$E_{tn} = \frac{\Delta H}{n_e \cdot F} \tag{2.9}$$

This value represents the operating voltage of a cell with 100% thermal efficiency e.g. no waste heat produced/consumed by the reaction; under standard conditions at 298 K, the ΔH^0 for $H_2O(l)$ is equal to 285,84 kJ/mol and thus thermoneutral voltage is:

$$E^0_{tn} = 1.481V \tag{2.10}$$

When a cell operates with an higher voltage an excess of heat is generated (exothermic mode): this means there is an excess of electric power provided with respect to enthalpy variation; on the opposite, when the voltage is lower than the thermoneutral one an endothermic operation is experienced and a certain amount of heat has to be supplied to the system. When the device operates at the thermoneutral voltage the internal ohmic losses compensate exactly the heat required and no external heat is needed. In fig.2.6 extrapolated from the model built in this work, the endothermic/exothermic modes are visible in comparison with the cell voltage and they follow exactly the predictions.

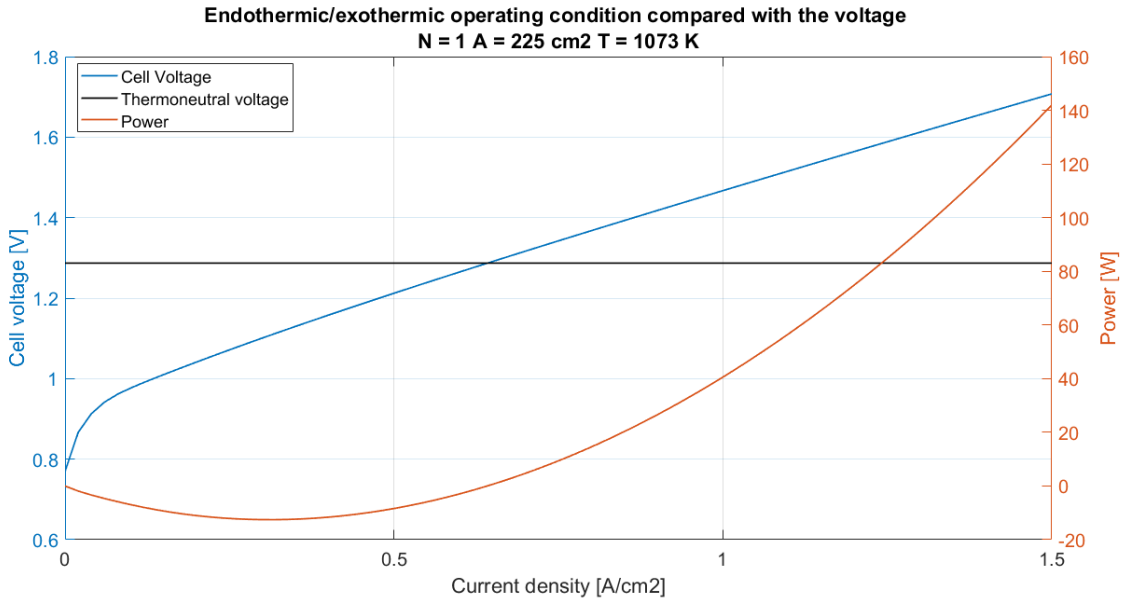

FIG: 2.6. Thermoneutral voltage and solid oxide electrolyser operation

Coming back to eq.(2.6), the reversible potential, named also Nernst potential, is calculated through the following equation:

$$E_{rev} = E^0_{rev} + \frac{R \cdot T}{2 \cdot F} \cdot ln(\frac{p_{H_2} \cdot p^{0.5}_{O_2}}{p_{H_2O}}) \tag{2.11}$$

Where:

- $E^0[V]$is the standard potential depending on the operating temperature of the cell;
- $R[\frac{J}{mol \cdot K}]$ is the universal gas constant;

- $T[K]$ is the absolute temperature;
- $F[\frac{C}{mol}]$ is the Faraday constant;
- p_{H_2},p_{O_2},p_{H_2O} are the partial pressures of hydrogen, oxygen and water respectively.

All the other terms that contribute to define the operating voltage of a solid oxide electrolyser cell are overpotentials i.e. losses; now, a more detailed explanation is provided.

1. **Concentration overpotentials**
   The concentration overpotentials are related to the resistances occurred during the transport of reactants close to the reaction site and the transport of products leaving it as well [7]; the difference between gas and electrons speeds generates concentration gradients close to each electrode; the higher the current density is the greater are the losses. Two different concentration overpotentials are considered for anode and cathode:

$$\eta_{conc,cathode} = \frac{R \cdot T}{n \cdot F} \cdot ln(\frac{1 + \frac{J \cdot R \cdot T \cdot \sigma_c}{2 \cdot F \cdot D^{eff}_{H_2O} \cdot p_{H_2}}}{1 - \frac{J \cdot R \cdot T \cdot \sigma_c}{2 \cdot F \cdot D^{eff}_{H_2O} \cdot p_{H_2O}}}) \tag{2.12}$$

$$\eta_{conc,anode} = \frac{R \cdot T}{n \cdot F} \cdot ln(1 + \frac{J \cdot R \cdot T \cdot \sigma_a}{4 \cdot F \cdot D^{eff}_{O_2} \cdot p_{O_2}})^{0.5} \tag{2.13}$$

   Where:

   - $J[\frac{A}{m^2}]$ is the current density;
   - D^{eff}_i $[\frac{m^2}{s}]$ is the effective Knudsen coefficient for the species i;
   - σ_a and σ_c are the thickness of anode and cathode respectively;
   - p_{H_2},p_{O_2},p_{H_2O} are the partial pressures of hydrogen, oxygen and water respectively;
   - $R[\frac{J}{mol \cdot K}], T[K], F[\frac{C}{mol}]$ are universal gas constant, absolute temperature and Faraday constant respectively.

2. **Activation overpotentials**
   The activation overpotentials are related to the electrode kinetics at the reaction site; this is due to the activation needed for charge transfer. The activation overpotential is valid both for anode and cathode and can be estimated with the following formula:

$$\eta_{act,i} = \frac{R \cdot T}{2 \cdot F} \cdot \ \sinh^{-1}(\frac{J}{2 \cdot J_{0,i}}) \tag{2.14}$$

   Where:

   - $J[\frac{A}{m^2}]$ is the current density;
   - $J_{o,i}$ $[\frac{A}{m^2}]$ is the exchanged current density: this parameter is linked to the kinetics of the electrode reaction and represents the readiness of the electrode to proceed with the electrochemical reaction [14][15]; it comes from the Arrhenius law that shows the dependence on temperature as follows:

$$J_{0,i} = k_i \cdot \exp(-\frac{E_{act,i}}{R \cdot T}) \tag{2.15}$$

Where:

- k_i is the pre-exponential factor for anode/cathode;
- $E_{act,i}$ $[\frac{J}{mol}]$ is the activation energy for anode/cathode;
- $R[\frac{J}{mol \cdot K}], T[K], F[\frac{C}{mol}]$ are the universal gas constant, the absolute temperature and the Faraday constant respectively.

3. **Ohmic losses**
The Ohmic overpotential is linked to the resistance to ions conduction through the electrolyte and electrodes; this overpotential grows linearly with the current density and can be estimated by means of Ohm's law. Usually the electrical interconnector and the electrodes have a much greater electrical conductivity with respect to electrodes; thus, their effect can be neglected and just the electrolyte part is considered [16]. Its effect is evaluated with the following formula:

$$\eta_{ohmic} = J \cdot L \cdot \Phi \tag{2.16}$$

Where:

- $J[\frac{A}{m^2}]$ is the current density;
- $L[m]$ is the electrolyte length;
- Φ $[Ohm \cdot m]$ is the electrical resistivity.

2.3 Solid oxide co-electrolyser

Another component, analysed in this work, is the solid oxide co-electrolyser. It offers a promising way to split steam and carbon dioxide into a mixture of hydrogen and carbon monoxide using electrical energy [17]. It has been demonstrated that co-electrolysis of CO_2 and H_2O is feasible for simultaneous production of H_2 and CO [15]. This system is similar to the simpler soe; a detailed explained was given in the previous section. The water electrolysis takes always place but two more reactions are involved in this component: CO_2 electrolysis and water gas shift reaction (WGSR). Furthermore, according to [15], the reversible WGSR should always contribute to CO production, even if its relative weight is not still clear [18]. These solid oxide cells can also operate in a reverse way (fuel cell mode) converting the chemical energy back into electricity [17]. Moreover, high-temperature electrolysis is more efficient than low temperature electrolysis [19]: running the co-electrolyser at 1373 K allows to save 30% and 20% of the electricity needed to consume respectively CO_2 and water with respect an operation at 373 K [20] [21]. Fig.2.7 shows the temperature effect on the thermodynamics of the co-electrolysis reaction with an output ratio H_2/CO equal to 1. This new technology seems to be very interesting due to its significant advantages. First of all, according to [22], due to the fast overall electrochemical kinetics, the co-soec is more cost effective and energy efficient. Secondly, according to [23], a large amount of CO_2 conversion to CO proceeds in a reverse water gas shift reaction; this contributes to reduce the total electrical consumption. Third, the carbon deposition experienced in the dry CO_2 electrolysis is suppressed thanks to the steam water; thus the severe cooking and loss of cell function are avoided [24] [25]. To sum up, the high-temperature co-electrolysis is a highly efficient technology for syngas production with lower cost and enhanced durability [17].

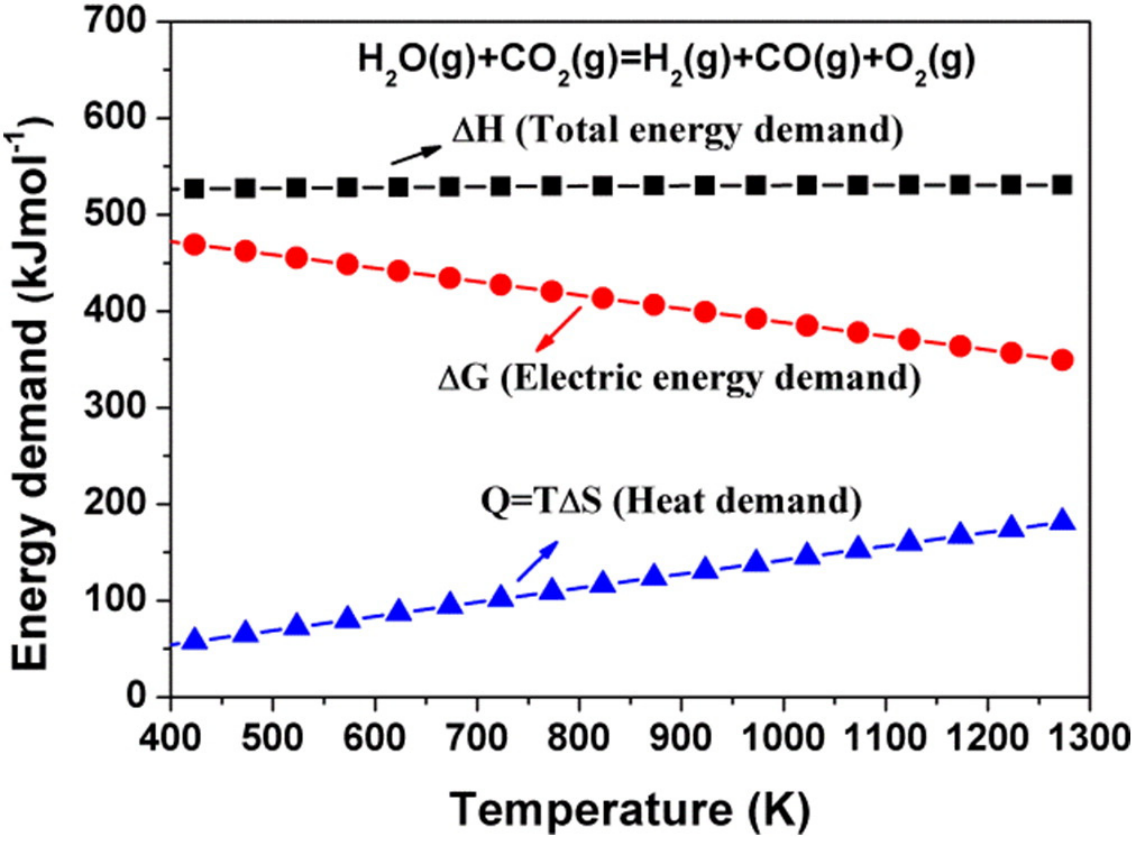

FIG: 2.7. Electricity, heat and total energy demand co-soe [17]

Fig.2.8 shows the working principle of a solid oxide co-electrolyser for syngas production. Similar to a simpler soe cell, the cell is made up of three distinct and porous layers: two electrodes and one electrolyte in between: they are [15] [17] [19]

- **CATHODE**: this layer is usually made of Nickel or a mixture of Nickel and Yttria-Stabilized-Zirconia (YSZ); the gas mixture of carbon dioxide, steam water, carbon monoxide and hydrogen flows in the cathodic channel. Inside this porous electrode, both H_2O and CO_2 molecules diffuse until they reach the triple-phase-boundary (TPB) at the cathode-electrolyte interface where the following reduction reactions happen:

$$H_2O(g) + 2e^- \rightarrow H_2(g) + O^{2-} \tag{2.17}$$

$$CO_2(g) + 2e^- \rightarrow CO(g) + O^{2-} \tag{2.18}$$

  In addition, a third important reaction occurs with a fast kinetic rate on the cathode side; this is the reversible WGSR explained in eq.(2.19). This chemical reaction is slightly endothermic ($\Delta H_{298K} = 41 \frac{kJ}{mol}$).

$$H_2O(g) + CO(g) \rightarrow H_2(g) + CO_2(g) \tag{2.19}$$

  Furthermore, two more reactions can happen; one is the coke formation expressed in eq.(2.20) and one is the methane formation, expressed in eq.(2.21), if Ni is used. To avoid carbon deposition it is recommended to work at low voltages and to prevent methane formation it is preferable to operate at temperatures higher than 973

K.

$$CO(g) \rightarrow C + \frac{1}{2}O_2 \tag{2.20}$$

$$CO(g) + 3H_2(g) \rightarrow CH_4(g) + H_2O(g) \tag{2.21}$$

- **ELECTROLYTE**: this dense layer is in between cathode and anode and it allows oxygen ions to cross and reach the TPB at the electrolyte-anode interface where the oxidation reaction takes place according to:

$$2O^{2-} \rightarrow O_2(g) + 4e^- \tag{2.22}$$

  This oxygen ion transport occurs under the driving force of applied voltage greater than the Nerst potential to overcome the oxygen partial pressure gradient.

- **ANODE**: it is constituted by a mixture of Lanthanide, Strontium and Manganese oxide (LSM) associated with YSZ material type; the oxygen molecules produced at the TPB cross the porous anode until the anode surface where they are collected; in the anode channel air flows and oxygen molecules flow.

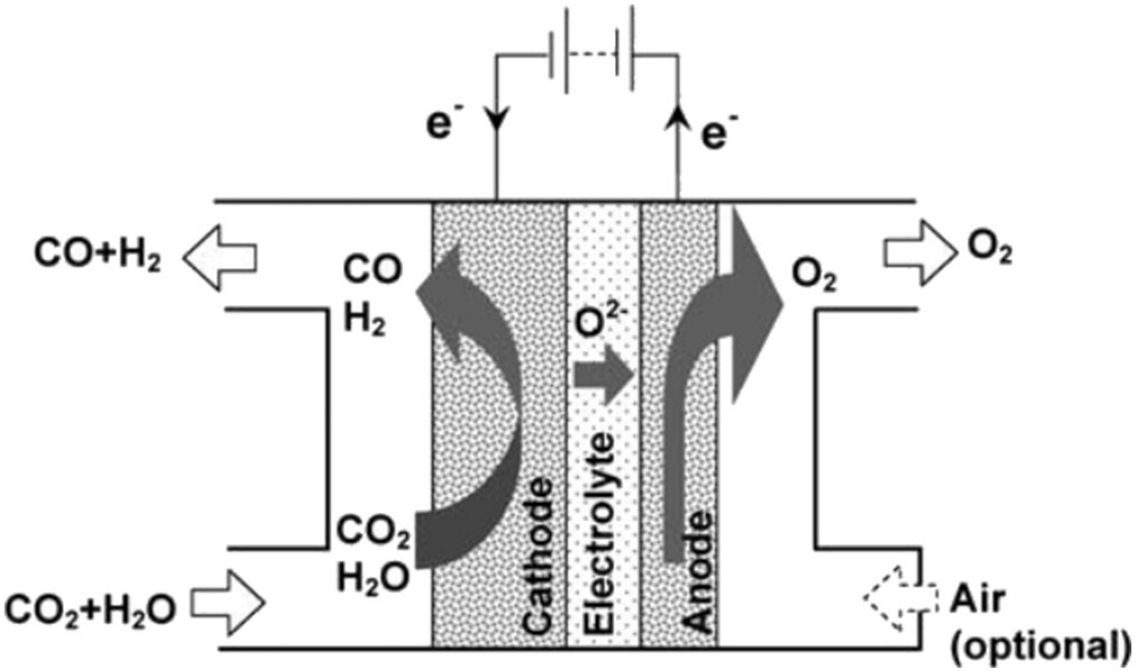

FIG: 2.8. Structure of a solid oxide co-electrolyser cell [17]

Fig.2.9, shows the triple phase boundaries (TPB). On the left side of the electrolyte (fuel electrode-cathode), H_2O and CO_2 diffuse to the TPBs and produce H_2 and CO; at the TPBs, electrons are supplied via the electric circuit and the oxygen ions cross the YSZ electrolyte. On the right side, the oxygen ions are transported to the surface of the anode and they produce molecular oxygen. The electrons are, then, transported away in the air electrode.

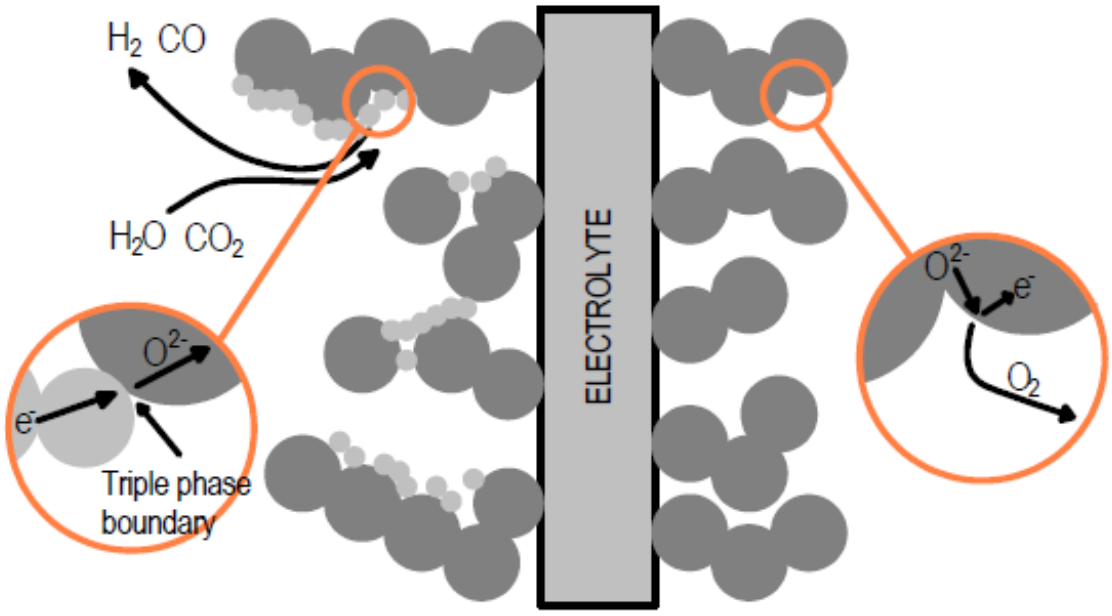

FIG: 2.9. Triple phase boundary [8]

According to [15], the required potential applied to the co-electrolyser cell can be evaluated by means of eq.(2.23) that follows the same principles already explained in the previous section about the SOE. In this case, the concentration overpotentials are not taken into account in eq.(2.23) because they are implicitly included in the reversible (Nernst) potential (E).

$$V = E_{rev} + \eta_{act,a} + \eta_{act,c} + \eta_{ohmic} \tag{2.23}$$

Now all the terms of (2.23) are presented explaining all the formulas implemented in the co-electrolyser model, that has been realized in this master thesis; further information can be found in the previous SOE section. The first term analysed is the equilibrium potential ($E[V]$), also named Nernst potential; for H_2O-CO_2 electrolysis reactions is expressed as follows:

$$E_{revH_2} = E^0_{revH_2} + \frac{R \cdot T}{2 \cdot F} \cdot ln(\frac{p_{H_2} \cdot p^{0.5}_{O_2}}{p_{H_2O}}) \tag{2.24}$$

$$E_{revCO} = E^0_{revCO} + \frac{R \cdot T}{2 \cdot F} \cdot ln(\frac{p_{CO} \cdot p^{0.5}_{O_2}}{p_{CO_2}}) \tag{2.25}$$

Where:

- $E^0[V]$ is the standard potential depending on the operating temperature of the cell; its value can be calculated from the thermodynamics using the Gibbs free energy; according to [15], for H_2 standard voltage at 600 K and 1200 K it is 1.109017 V and 0.940172 V, respectively. Similarly, the values for CO are 1.195502 V and 0.923869 V, respectively. If a linear variation of E^0 is assumed in the range 600-1200 K the Nernst potentials, that include the concentration overpotentials can be written as:

$$E_{revH_2} = 1.253 - 0.00024516 \cdot T + \frac{R \cdot T}{2 \cdot F} ln(\frac{p_{H_2} \cdot p^{0.5}_{O_2}}{p_{H_2O}}) \tag{2.26}$$

$$E_{revCO} = 1.46713 - 0.0004527 \cdot T + \frac{R \cdot T}{2 \cdot F} ln(\frac{p_{CO} \cdot p_{O_2}^{0.5}}{p_{CO_2}}) \tag{2.27}$$

- $R[\frac{J}{mol \cdot K}]$ is the universal gas constant;
- $T[K]$ is the absolute temperature;
- $F[\frac{C}{mol}]$ is the Faraday constant;
- p_{H_2},p_{O_2},p_{H_2O},p_{CO},p_{CO_2} are the partial pressures of hydrogen, oxygen, water, carbon monoxide and carbon dioxide, respectively;

$\eta_{act,a}$,$\eta_{act,c}$ are the activation overpotentials of anode and cathode, respectively; in the literature, the Butler-Volmer equation is the most widely adopted formula to describe the activation overpotentials; of course, activation losses are referred to hydrogen and carbon monoxide; however, in this work, a linear equation that correlates these losses and the current density is adopted [15]:

$$\eta_{act,H_2,i} = \frac{R \cdot T \cdot J_{H_2}}{\eta_{H_2} \cdot F \cdot J^o_{H_2,i}} \tag{2.28}$$

$$\eta_{act,CO,i} = \frac{R \cdot T \cdot J_{CO}}{\eta_{CO} \cdot F \cdot J^o_{CO,i}} \tag{2.29}$$

Where:

- $J[\frac{A}{m^2}]$ is the current density;
- $J^0_{H_2}$,J^0_{CO} $[\frac{A}{m^2}]$ is the exchanged current density for H_2O and CO_2 electrolysis, respectively. This parameter is evaluated with the Arrhenius law, that shows the dependence with the temperature. At 1073 K, Chan and Xia [26] recommend the values of $J^0_{H_2,c}$ and J^0_a to be 5300 $\frac{A}{m^2}$ and 2000 $\frac{A}{m^2}$, respectively. Moreover, experiments have shown how the rate of electrochemical oxidation of hydrogen is about 2.5 times that of carbon monoxide; thus, the exchange current density of the cathode for CO_2 electrolysis is evaluated as:

$$J^0_{CO,c} = 0.4 \cdot J^0_{H_2,c} \tag{2.30}$$

Where:

- k_i is the pre-exponential factor for anode/cathode;
- $E_{act,i}$ $[\frac{J}{mol}]$ is the activation energy for anode/cathode;
- $R[\frac{J}{mol \cdot K}], T[K], F[\frac{C}{mol}]$ are the universal gas constant, the absolute temperature and the Faraday constant, respectively.

η_{ohmic} is the well-known Ohmic overpotential and according to Ohm's law can be calculated as [27]

$$\eta_{ohmic} = 2.99 \cdot 10^{-5} \cdot J \cdot exp(\frac{10300}{T}) \tag{2.31}$$

Where:

- $J[\frac{A}{m^2}]$ and $L[m]$ are the current density and the thickness of the electrolyte, respectively.

2.4 CO_2 Methanator

The main goal of the methanator is to produce methane from hydrogen and CO_x; CO and CO_2 methanation processes have been discovered by Sabatier and Senderens at the beginning of the 20^{th} century. Nowadays, these chemical reaction are widely applied in ammonia synthesis plants to remove traces of carbon oxides from hydrogen-rich feed streams and to reduce its poisoning effect on catalyst [28][29][30][31]. Moreover, in the 60's decade, it has been proposed to produce synthetic natural gas (SNG) due to the high demand of natural gas. However, in these last years, the CO_2/CO methanation is constantly gaining more interest in the context of Power-to-Gas (PtG) technology: the electricity is converted into hydrogen (via H_2O electrolysis) and then into methane. Therefore, it is possible to store excess electrical energy from renewable sources; furthermore, methane can more easily be stored and transported than hydrogen [32]. The CO_2 methanation eq.(2.32) is an exothermic catalytic reaction that operates in the temperature range 200-550 °C depending on the used catalyst:

$$CO_2(g) + 4H_2(g) \leftrightarrow CH_4(g) + 2H_2O(g) \text{ with: } \Delta_r H = -165\frac{kJ}{mol} \tag{2.32}$$

According to [33], no general consensus exists on the reaction's operating mechanism due to the uncertainty in establishing the intermediate compound involved in the rate determining step [34][35]. One idea involves the direct hydrogenation of CO_2 to CH_4 following eq.(2.32); the second one assumes a two-step reaction mechanism: first of all, as shown in eq.(2.33), carbon dioxide and hydrogen are converted into carbon monoxide and water (WGSR):

$$CO_2(g) + H_2(g) \leftrightarrow CO(g) + H_2O(g) \text{ with: } \Delta_r H = 41\frac{kJ}{mol} \tag{2.33}$$

Afterwards, methane is formed according to CO-methanation reaction:

$$CO(g) + 3H_2(g) \leftrightarrow CH_4(g) + H_2O(g) \text{ with: } \Delta_r H = -206\frac{kJ}{mol} \tag{2.34}$$

Moreover, among the products, high saturated hydrocarbons can be found (e.g. ethane eq.(2.35)) or carbon precipitation can occur eq.(2.36):

$$CO_2(g) + 3.5H_2(g) \leftrightarrow 0.5C_2H_6(g) + 2H_2O(g) \text{ with: } \Delta_r H = -132\frac{kJ}{mol} \tag{2.35}$$

$$CO_2(g) + 2H_2(g) \leftrightarrow C + 2H_2O(g) \text{ with: } \Delta_r H = -90\frac{kJ}{mol} \tag{2.36}$$

However, in this work, a simplified model of the system is built (the last two reactions are not taken into account) and no further considerations have been carried out on this topic. Carbon dioxide methanation is thermodynamically favoured at low temperatures and high pressure [32]. Fig. 2.10 shows the Gibbs free energy with temperature for the reactions above explained; when $\Delta G = 0$ the reaction is in equilibrium. If $\Delta G < 0$, the reaction is favoured and the equilibrium is shifted towards the products [36]. Thus, it is clear that the CO_2 methanation reaction is favoured up to 600 °C but the lower the temperature

the better. Otherwise, the carbon monoxide formation from WGSR is favoured at temperatures higher than 800 °C; therefore, it is reasonable to keep temperature and the CO concentration as low as possible. Fig.2.11 shows, on the opposite, the CO_2 conversion is depending on temperature and pressure; it is demonstrated that increasing pressure and decreasing temperature allows an higher CO_2 conversion rate to methane.

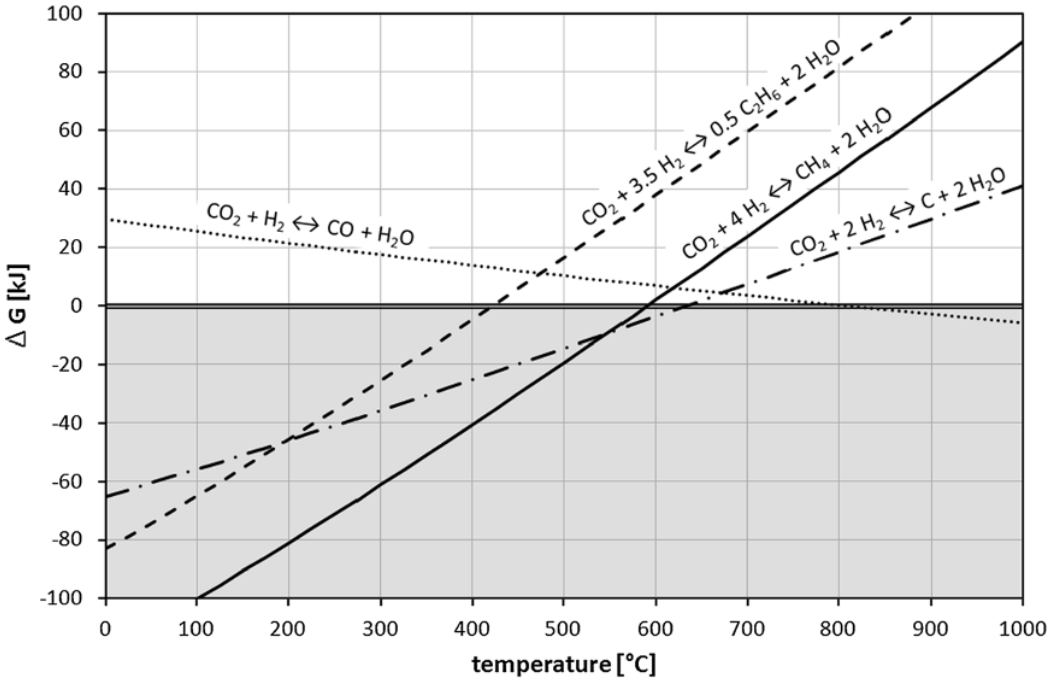

FIG: 2.10. Gibbs free energy and temperature [36]

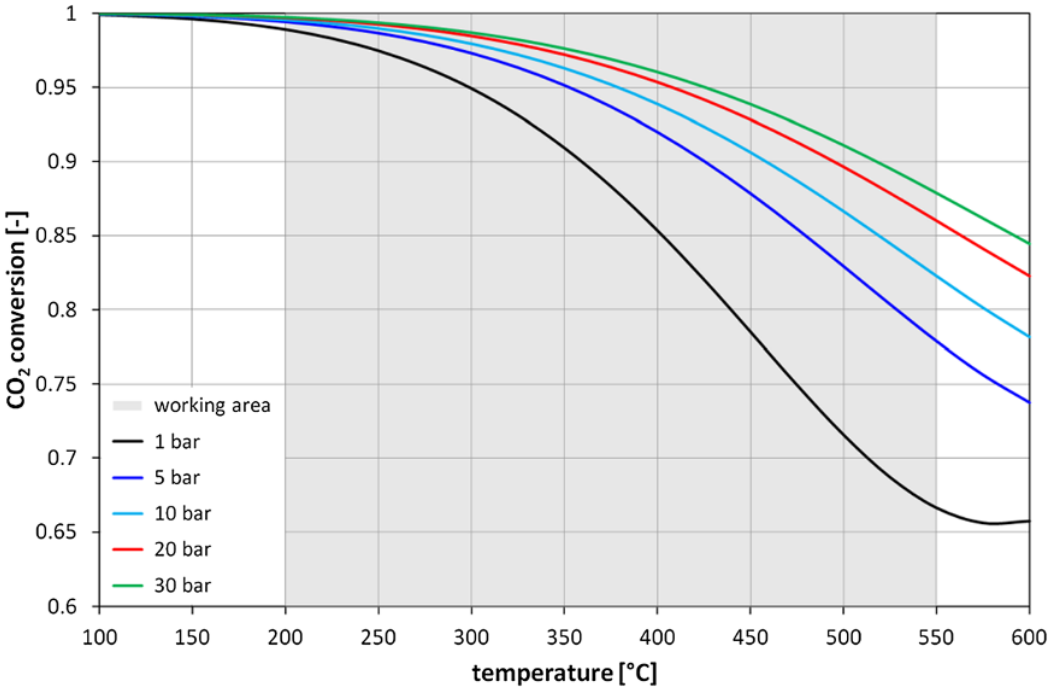

FIG: 2.11. CO_2 conversion depending on temperature and pressure [36]

Concerning the structure of a methanator, the adopted catalyst plays a key factor; the state of the art catalyst is based on Ni due to its high activity and low price; however, it has to withstand fast temperature changes between 50 °C and 100 °C occurring in few seconds [36]. This material is used for high temperature methanator (i.e. >250 °C) because when it works under 200°C there is the possibility to form highly toxic nickel carbonyl ($Ni(CO)_4$) from carbon monoxide. Under this operating condition (i.e. <200 °C) , a more expensive Ru-based catalyst is preferable [37][38]. Sintering and carbon deposition might cause the catalyst deactivation when the operating temperature exceeds 550 °C [39]. To sum up, the optimal temperature operating range is between 200 °C and 550 °C; generally, catalysts effective for CO methanation are also effective for CO_2 methanation [38]. Catalysts lifetime usually varies between 5 and 10 years, nevertheless, some manufactures ensure a period up to 24 years [28][37].

One of the major issues is the highly exothermic nature of the methanation reaction; thus, it is crucial to have a good thermal control over the system. It is estimated that per each percent of CO_2 conversion an adiabatic rise in temperature of 60 °C is expected [36][37]; consequently, the heat generated has to be continuously removed. The state of the art reveals that two reactor types are used for this process: two-phase fixed bed reactors and fluidized bed reactors. The first one is a cylindrical tube filled with catalyst pellets with reactants flowing through the bed and being converted into products; the catalyst can have different configurations (e.g. one large bed, several horizontal beds or several parallel packed tubes) depending on the temperature control chosen within the system; the pellets, whose range is between 0.25-1 cm can be spherical, cylindrical or with a random shape. The second device consists in small suspended particles of catalyst; the motion of the fluid is upward. The flowrate is usually high enough to mix the particles without exceeding the edges of the reactor. Usually the particles are much smaller (10-300 microns) than the ones used in the fixed bed technology and therefore have lower cost. With this latter technology it is possible to achieve a uniform temperature inside the reactor [72]. Other technologies, for instance slurry reactors, exist but are not described in this work. On the one hand, fixed bed reactors are simple, flexible and easy to scale up; on the other hand, high cost, multiple reactors in parallel are needed for larger plants and large catalyst particles are the main disadvantages [73]. Regarding fluidized bed reactors, pro arguments are: higher efficiency in heat exchange and better temperature control compared to fixed bed technology; on the opposite, arguments against are complexity in operability, difficult separation of catalyst particles and erosion problems due to the high velocities [74][40][41].

According to [36], an effective way to reduce the temperature is the reduction of the reactive feed by means of a controlled dilution of the inlet gas stream; this can be performed cooling down and recirculating parts of the outlet gas stream. Another strategy is to operate under isothermal conditions avoiding to reach high temperatures that cause sintering of the catalyst; in this case, a cooled reactor is required and the heat is transferred from the reaction zone to a cooling medium. Even so, due to the strong exothermic nature and the structure of a fixed bed reactor it is difficult to work isothermal with just one single device; as a matter of fact, at least two adiabatic reactors in series are required. Temperature control can be performed through recirculation of the outlet gas streams and

intermediate gas cooling stages [39][42][43]. Due to the properties of the fluidized bed reactor, in these reactors almost isothermal conditions can be achieved. Fig.2.12 summarizes different reactor concepts for the methanation process showing some operational data.

Process number	Process/company	Reactor type	Process stages	Operation range		Feed
				p (bar)	*T* (°C)	
(a)	TREMP/Haldor Topsøe	Fixed bed	3	30	300…700	Coal, petrol coke, biomass
(b)	Hicom/British Gas Corp.	Fixed bed	4	25…70	230…640	Coal
(c)	RMP/Ralph M. Parson Co.	Fixed bed	4…6	1…70	315…780	Coal, heavy fuel
(d)	SuperMeth, ConoMeth/Conoco	Fixed bed	4/4	Approximately 80	n. s.	Coal
(e)	CRG/British Gas Corp.	Fixed bed	2	Approximately 25	300	Naphtha (refinery residue)
(f)	Hygas/Institute of Gas Technology	Fixed bed	2	70	280…480	Coal
(g)	Lurgi, Sasol/Lurgi GmbH	Fixed bed	2	18	Approximately 450	Coal
(h)	ICI, Koppers/Imperial Chemical Industries	Fixed bed	3		400…700	Coal
(i)	Linde/Linde AG	Fixed bed	2	n. s.	n. s.	Coal
(j)	Bi-Gas/Bituminous Coal Res. Inc	Fluidized bed	1	86	n. s.	Coal
(k)	Bureau of Mines/US department of the Interior	Fluidized bed		20	200…400	
(l)	Comflux/Thysengas GmbH	Fluidized bed	1	20…60	400…500	Coal (biomass)

FIG: 2.12. Different existing CO2 methanation plants [36]

2.5 CO Methanation

Similarly, in this work, also another chemical process is analysed: this is the CO-methanation. The heterogeneously catalysed methanation is important in two main applications: removal of traces of CO in hydrogen-rich gases for the ammonia synthesis and the conversion of syngas to methane [44]. When there is a mixture of gases, where the main components are hydrogen and carbon monoxide, this can feed a CO-methanator; for instance, this mixture can be realized inside a co-electrolyser where H_2O and CO_2 react producing H_2 and CO. The system made up of a co-electrolyser and a CO-methanator is a clear example of PtG technology; inside a CO-methanator CO and H_2 react producing methane. The main reactions that occur are the following ones [45]:

$$CO(g) + 3H_2(g) \leftrightarrow CH_4(g) + H_2O(g) \text{ with: } \Delta_r H = -206\frac{kJ}{mol} \tag{2.37}$$

$$CO_2(g) + H_2(g) \leftrightarrow CO(g) + H_2O(g) \text{ with: } \Delta_r H = 41\frac{kJ}{mol} \tag{2.38}$$

$$2CO(g) \leftrightarrow C + CO_2(g) \text{ with: } \Delta_r H = -172.5\frac{kJ}{mol} \tag{2.39}$$

Eq.(2.37) is the well-known CO-methanation reaction, where the carbon oxide is hydrogenated to methane and water. Eq.(2.38) is the Water Gas Shift reaction and eq.(2.39) is the Boudouard reaction. The latter causes carbon deposition and operating conditions have to be properly chosen to avoid this unwanted reaction. According to [44], inside the methanator, other reactions can take place aswell but are not further discussed. This chemical process is performed on a catalyst: different materials have been studied (i.e. Ruthenium, Rhodium, Platinum, Iron, Nickel and Cobalt) [47]. Even so, as for the CO_2-methanator, the Ni catalyst is the most appropriate due to its selectivity, activity and price. The temperature range, similar to a CO_2-methanator, is between 200 °C and 500 °C. Moreover, the process is favoured with low temperatures and high pressures, as shown in fig.2.13, where the case with H_2/CO ratio equal to 3 is analysed. Again, the strong exothermicity of the methanation process, that results in a high temperature increase, can cause sintering and lead to carbon particle formation; therefore, temperature control strategies have to be carefully implemented to keep the temperature as low as possible removing the excess heat. The device typologies are exactly the same as in the case of the CO_2 methanation process; thus, they are not presented again in this section and detailed explanations can be found in the section "CO_2 methanation".

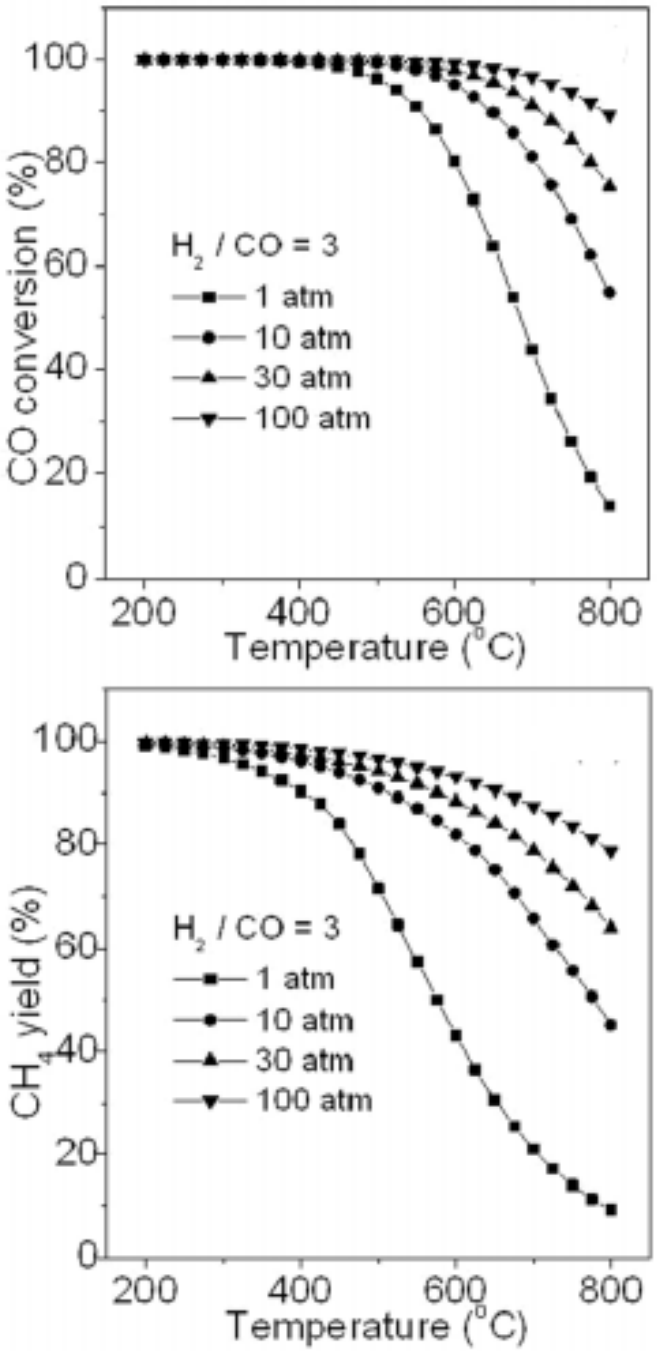

FIG: 2.13. CO conversion and CH_4 yield depending on temperature and pressure [46]

Among the reactants feeding the system, it is important to have a stoichiometric H_2/CO ratio of 3 or more; when this happens an high conversion of CO in CH_4 and H_2O is achieved through CO methanation reaction. However, the gases from coal and biomass gasifiers have lower ratios (between 0.3 and 2) that are too low for an high CO conversion. Furthermore, this also affects the catalyst lifetime. When these ratios are obtained, the WGSR can adjust the balance by converting CO with H_2O to CO_2 and H_2 [45]. Additionally, also the Boudouard reaction can lead to greater ratios even if a cat-

alyst deactivation can be observed. However, higher H_2/CO ratios seem to be the most interesting solution. As a matter of fact, as shown in fig.2.14, higher CO conversion and CH_4 yield are achieved with higher ratios (in this case 5); furthermore, when the system operates at ambient pressure and the ratio H_2/CO is 5 no carbon deposition is observed; the same phenomenon occurs when the operating pressure is 30 atm but the inlet ratio is 3 [46].

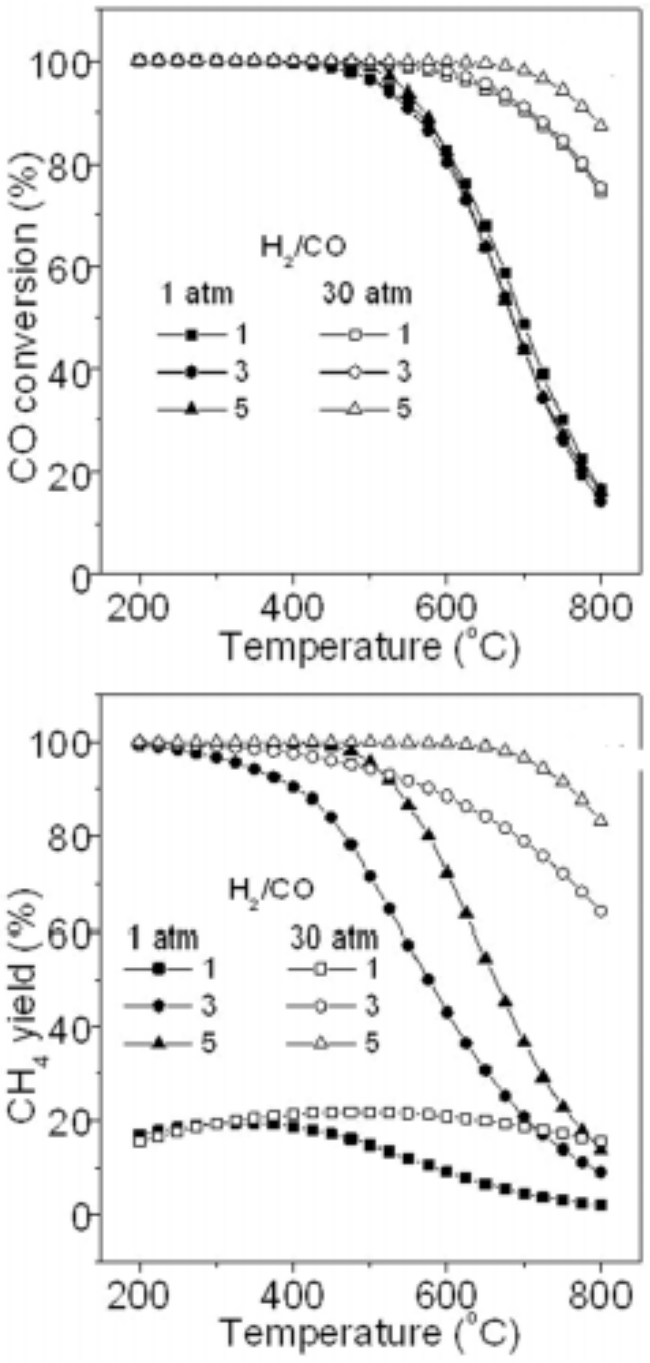

FIG: 2.14. CO conversion and CH_4 yield depending on temperature, pressure and input ratio [46]

Chapter 3

Modelling

3.1 Solid oxide electrolyser system

3.1.1 Model

The first device that has been modelled and analysed is the solid oxide electrolyser. The SOE dynamic model has been realized in Matlab – Simulink by a researcher student at Institut de Recerca en Energia de Catalunya (IREC) and below the main blocks and the "modus operandi" are explained in details.

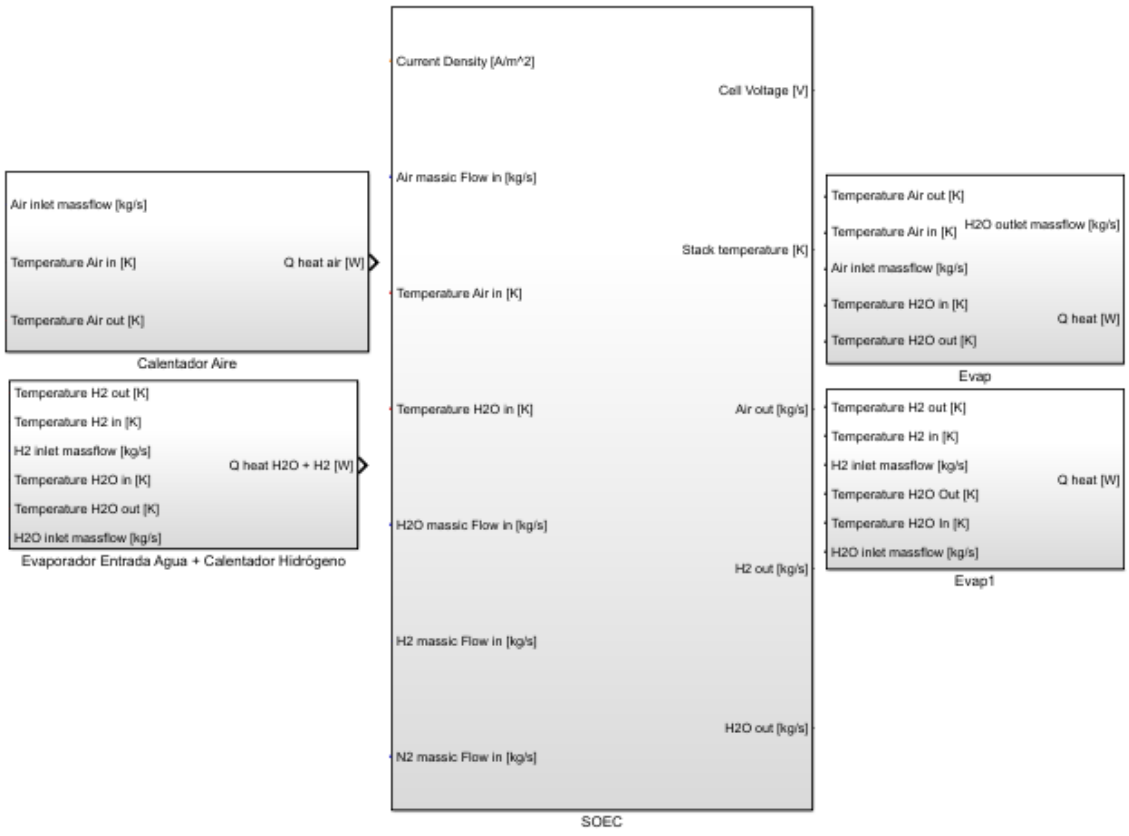

FIG: 3.1. Simulink main blocks SOE model

Looking at fig.3.1, five main blocks can be appreciated:

1. The two main subsystems on the left side of the SOEC block are needed to compute the amount of heat required to bring the reactants (air, hydrogen and water steam) of the cell from ambient temperature to the fixed inlet temperature of the system;

2. The others two on the right are used to evaluate the heat that has to be removed to cool down the SOEC outputs (hydrogen, air and steam water) to ambient temperature; concerning the gas species, the amount of heat is computed with the following formula:
$$Heat[W] = massflow \cdot c_p \cdot \Delta T \tag{3.1}$$
Regarding steam water, where additionally there is the state transformation from liquid to steam, the formula (3.1) is modified as follows:
$$Heat[W] = massflow \cdot c_p \cdot \Delta T + latentheat \tag{3.2}$$
As a reminder, these heat computations are not used in this work and these subsystems are not analysed more detailed.

3. The central block represents the solid oxide electrolyser analysed in this work: first of all, it is important to understand which are the inputs and outputs of the system: the main characteristic of this system is the current density that represents an input and inside the model the operating voltage of each cell and of the whole stack is computed. Of course, the SOE requires steam water and oxigen respectively feeding the cathode and anode. Furthermore, a small amount of hydrogen and nitrogen are considered to work properly and to avoid problems due to corrosion in a real device. All the inputs are evaluated in $\frac{kg}{s}$ and a proper stoichiometry among the reactants is defined. It is clear that, according to the current density, different amounts of reactants are required: if they were kept constant while increasing the current density a lack of reactants could be experienced. On the contrary, decreasing it, a lot of steam could flow inside the device without any electrochemical reaction. The first case must be avoided otherwise the SOE cannot operate and as well the second situation because there would be too much steam at the outlet with respect to the hydrogen produced.
This model has been modified in order to follow the current density variation along the time; basically the air flow is kept constant while a relationship between the current density and the other input flows is built; the current density value is multiplied with a constant that is expressed by the following expression:
$$\frac{A \cdot N}{n_e \cdot F \cdot UF} \tag{3.3}$$
Where:

   - $A[m^2]$ represents the area of each SOE cell;
   - N represents the number of cells connected in series;
   - n_e represents the number of electrons involved in the electrochemical reaction and in the case of water electrolysis is equal to 2;

- $F[\frac{C}{mol}]$ represents the Faraday constant;
- UF means utilization factor; eq.(3.3), without UF, indicates exactly the amount of mols per second of hydrogen is produced, and consequently water consumed, in the water electrolysis reaction; the utilization factor shows, in the water electrolysis, how much water is consumed: e.g. $UF = 1$ means 100% conversion of water in hydrogen. Usually, due to internal losses, this factor is lower than 1.

The quantity, computed in (3.3), expressed in $[\frac{mol}{s}]$, represents the total amount of inlet flows of the SOE apart from air (air is always fixed and it does not depend on the current density). After the choice of a proper utilization factor, the total flow is then split into water, hydrogen and nitrogen as follows:

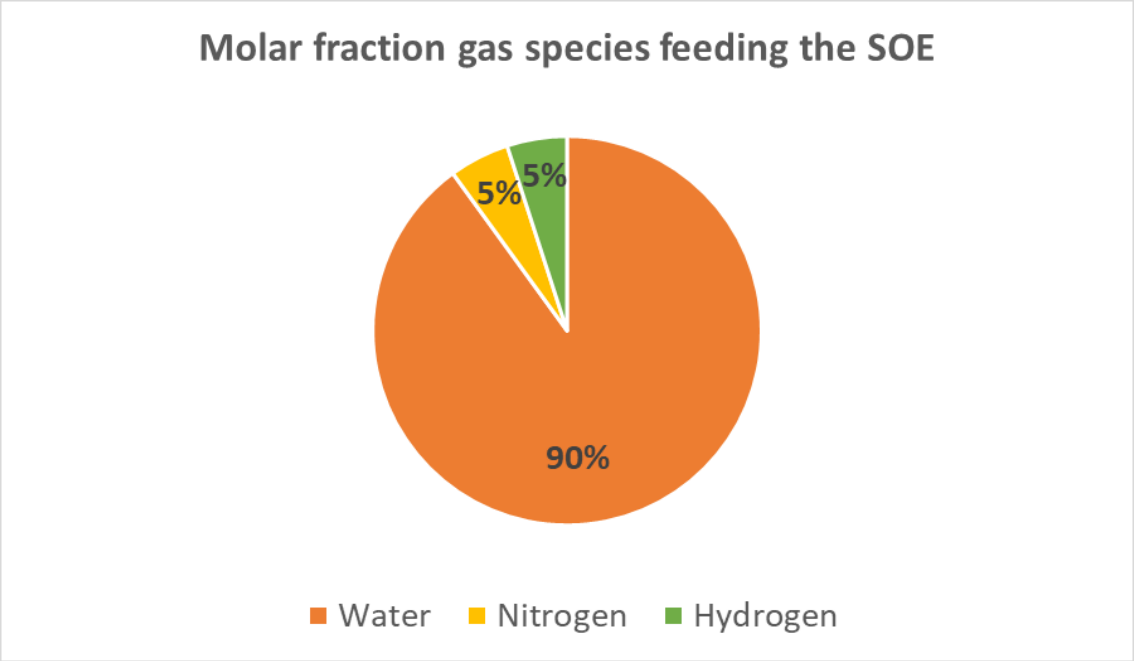

FIG: 3.2. Molar fractions inlet gas species

Afterwards, the SOEC model is divided in three subsystems:

1. **Anode and Cathode**
   The first one represents the anode and cathode of each SOE cell; in particular the two sides of the cell are divided up into three parts as explained in the figure:

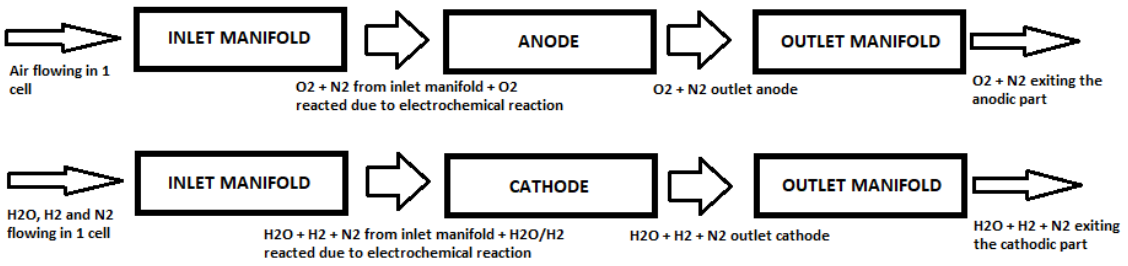

FIG: 3.3. Anodic and cathodic side of a SOE cell

The anode and the cathode respectively present one inlet manifold and one outlet manifold; as shown in fig.3.3, inside the inlet and outlet manifolds the electrochemical reaction is not taken into account because this happens just in the anode and cathode: indeed, the anode/cathode are fed in with the gas species plus what is produced/reacted due to water electrolysis. In each of these parts of the device the partial pressures of the different gases and also the total pressures are computed; before explaining the methodology to compute these pressures, it is important to notice that the pressure faced at the outlet of each segment is the internal pressure of the subsequent block.
Each block, implemented in this model, is seen as a unique volume with inputs and outputs; a discretization along the space is not present and the flow of the gases through the electrolyte between cathode and anode is not taken into account.
In the following it is explained how the partial pressure of each gas is computed: for each gas a mass balance is performed. It is defined as the difference between input and output of each element; furthermore, concerning anode/cathode, it is also taken into account how much hydrogen and oxygen are produced and how much water reacted due to electrochemical reaction with a positive and negative sign respectively. The outflows are evaluated with the following empirical formula:

$$outflow_i = K \cdot x_i \cdot \Delta p \tag{3.4}$$

Where:

- x_i is the mass fraction of each gas species computed as follows:

$$x_i = \frac{\text{mass component i}}{\text{total mass}} \tag{3.5}$$

- Δp is the pressure difference between the pressure inside the block and the pressure faced at the outlet that is the pressure inside the next block; in the case of outlet manifolds the pressure at the exit can be fixed as a constant and in this work it is considered as the ambient pressure (101325 Pa). The expression below synthetizes the computation of this pressure difference:

$$\Delta p = P_{block} - P_{next-block} \tag{3.6}$$

- K is a constant that defines the quantity of gases leaving the block and thus influences the pressures inside the blocks; the values of this constant are chosen

empirically to allow a pressure drop among the different parts. This computes the weight of the pressure drop. The greater the value of this constant is, the larger is the amount of gases which leave each block and the internal total pressure decreases.

As expected the mass balance gives zero as result when the steady state condition is reached and this means that how much enters the block is perfectly balanced with how much comes out. Fig.3.4 shows the water mass flow balance in the cathodic part of the SOE cell with certain operation conditions: during the first 1000 seconds of simulation there is the transient where there is no perfect balance between inflow and outflow and afterwards the steady state condition is reached.

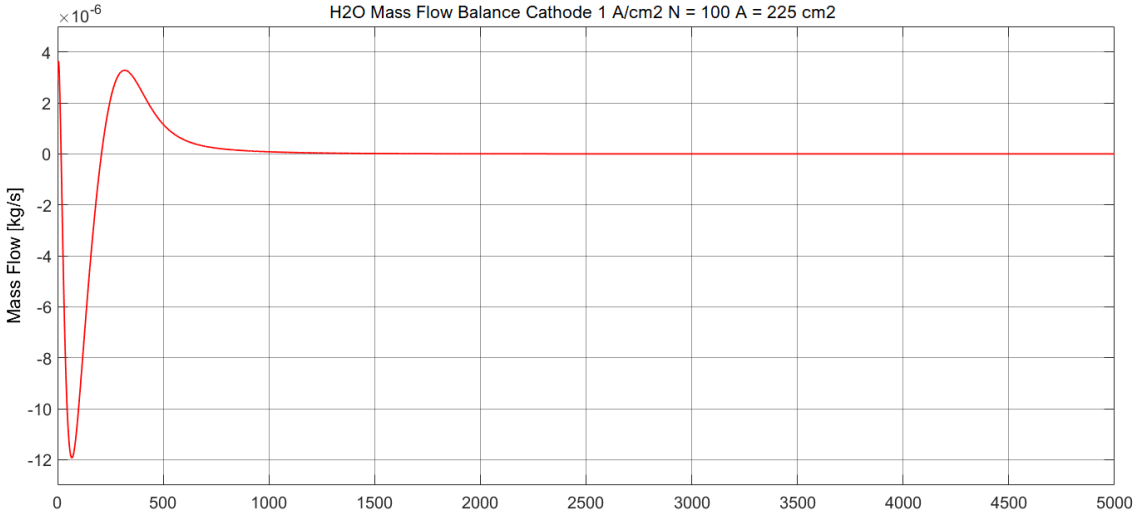

FIG: 3.4. Water mass flow balance inside the cathode

Once the bass balance is performed with the Simulink tool 'integrator' the amount of mass of each substance is computed and then converted into moles multiplying the mass with the inverse of the molar mass [76] of the relative gas. At this point each partial pressure is evaluated with the ideal gas law [75]:

$$P \cdot V = n \cdot R \cdot T \tag{3.7}$$

Where:

- $P[Pa]$ is the pressure of the gas;
- $V[m^3]$ is the volume occupied;
- $n[mol]$ is the number of gas moles involved;
- $R[\frac{J}{mol \cdot K}]$ is the ideal gas constant;
- $T[K]$ is the absolute temperature.

The trend of the partial pressure of hydrogen in the cathode under certain operating conditions is reported in fig.3.5 during the first one hundred seconds the system

needs time to stabilize and therefore the pressure is not constant but after the transient the steady state is reached and the pressure remains constant.

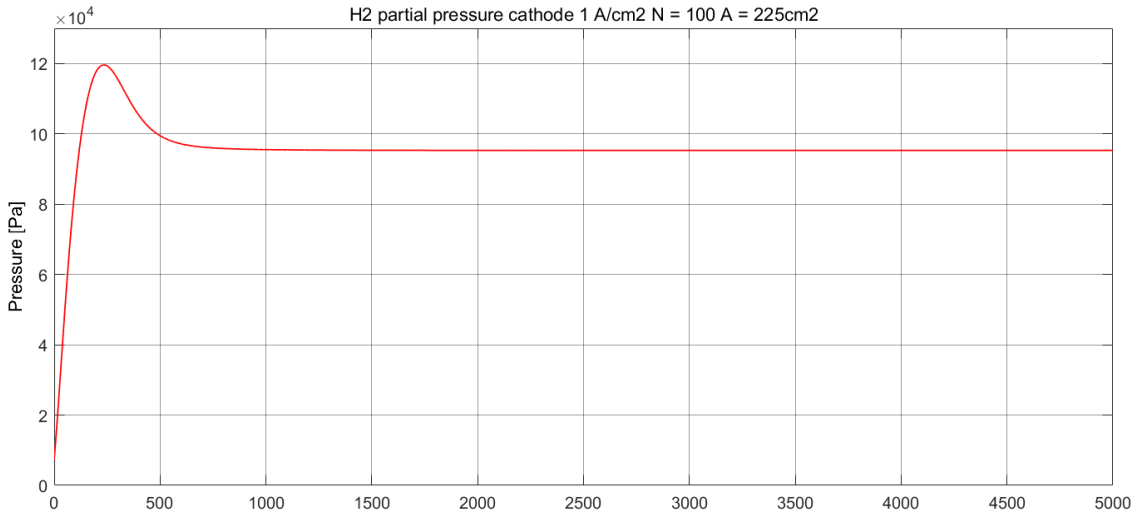

FIG: 3.5. Partial pressure hydrogen inside cathode

Summing all the partial pressures of all gases it is possible to calculate the total pressure inside every block. In fig.3.6, it is possible to notice the total pressure inside the cathode with certain operating conditions:

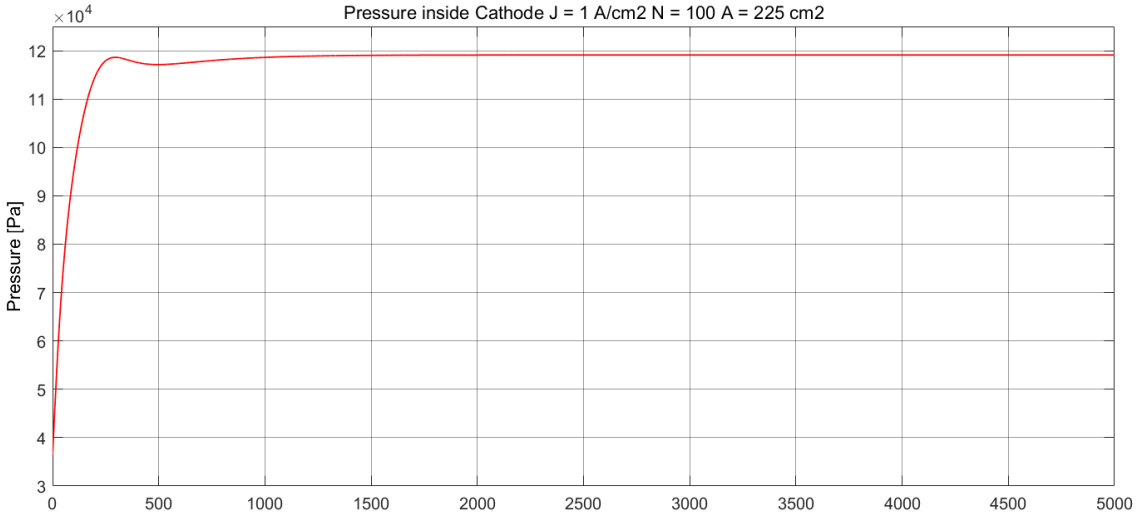

FIG: 3.6. Total pressure inside cathode

2. **Electrochemical stack**
   The second main block of the model computes the operating voltage of every cell of the stack following eq.(2.5) particularly explained in the theoretical section about the solid oxide electrolyser. Additionally this model presents an Open Circuit Voltage loss with respect to the previous overpotentials of eq.(2.5) to improve the matching of the data coming from an experimental device built at IREC.

In this part it is also possible to evaluate the amount of hydrogen and oxygen produced and at the same time water consumption following Faraday's law: as a reminder, by using 1 mol H_2O 1 mol H_2 and 0.5 mols O_2 are produced. Clearly, comparing the reacted water and the molar inflow the percentage of water decomposition can be evaluated: as explained in the section regarding SOE inputs for any current density a direct correlation that estimates the amount of water feeding the SOE is defined and when the steady state is reached, this value remains always the same for any current density value.

3. **Heat section**
   In this block all the heat correlations with the device are evaluated: for instance, the reaction heat (enthalpy variation) and the electrical power supplied to the system are computed and it is possible to observe if the reaction inside the SOE is endothermic or exothermic. Moreover, inside the model, a thermal balance is computed. All the heat losses (convection, oven and radiative) are taken into account and the internal temperature of the device is calculated. To simplify, the inside of the SOE is considered isothermal and no dynamic heat evaluation ; for this reason the different heat losses are not explained more detailed and just some comments concerning the electric power and the reaction heat are carried out in the next sections.

3.1.2 Gibbs free energy and entalphy

Fig.3.7 shows the different trends of the enthalpy and Gibbs free energy variations and entropy generation calculated by means of the SOE model and compared with the literature fig.2.3. The behaviours found with the model match the ones of the literature and what can be noticed is that, increasing the operating temperature of the cell, the electrical demand (represented by the Gibbs free energy) decreases and thus the E_{rev} is lower; on the contrary, the heat demand (represented by the entropy generation) increases. Moreover, the enthalpy variation which takes the energetical balance of the device into account is almost constant.

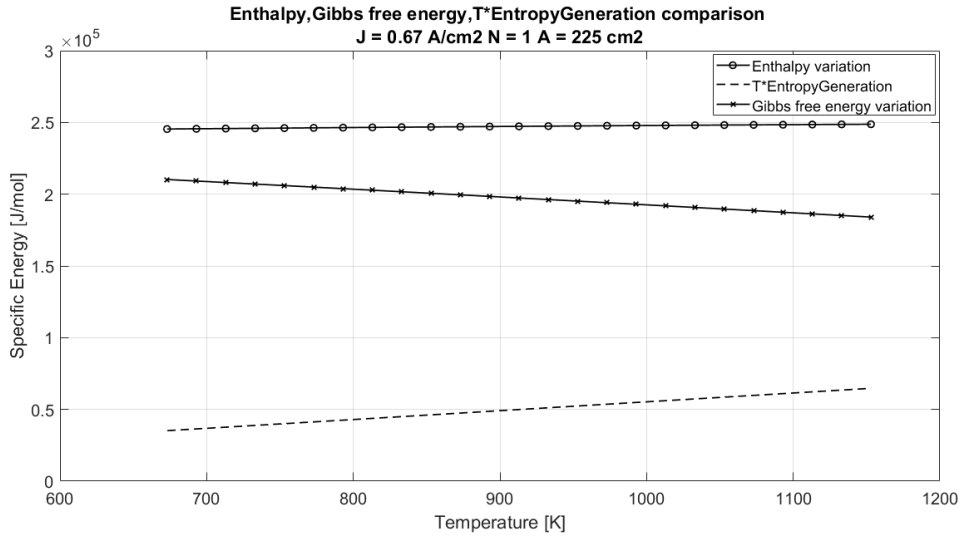

FIG: 3.7. Electrical energy and heat demand

3.1.3 Polarization curve

The polarization curve is one of the most important parameters of the solid oxide electrolyser and correlates the current density with the voltage of each cell. In particular, the model, used in this work, shows the operating voltage of each cell, computed by means of (2.5), when the device is fed with a certain current density value. It is clear that the SOE is made up of a number of cells connected in series to increase the overall voltage and the current flowing inside is constant. In fig.3.8 different polarization curves depending on temperature (isothermal operation) are plotted: as expected, increasing the operating temperature the cell voltage decrease and as shown in fig.3.7, the electrical power demand is lower. The behaviour for any operating temperature, apart from the lowest current density values, is linear; this can differ a bit with respect to what is available in the literature but it is due to how the input flows are correlated with the current density value as explained in the section above. Additionally, it is useful to explain that, during the design, it is important to define the maximum tolerated current density value. This maximum current density which can be supplied plays an important role to fix the highest electrical power demand; whenever the available power (e.g. from a renewable plant) is lower the SOE will work with lower current and voltage. Therefore, this limit is needed to size the device in order to evaluate how many cells have to be connected in series to exploit all the power available (further considerations on the sizing can be found in section 'SOE-COSOE design').

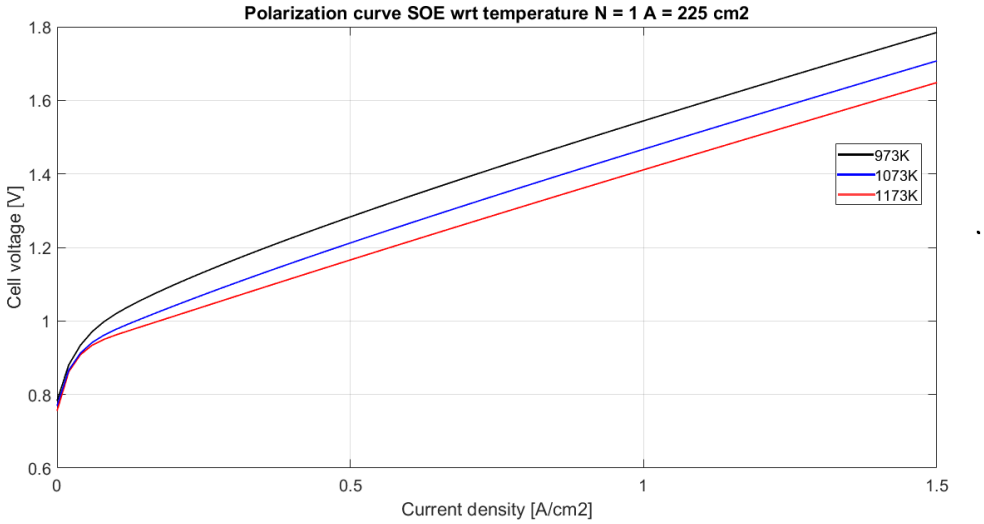

FIG: 3.8. Polarization curve depending on temperature

To clarify, fig.3.9 plots the polarization curve of one cell of the SOE operating at 1073 K that represents the isothermal condition chosen to do the simulations.

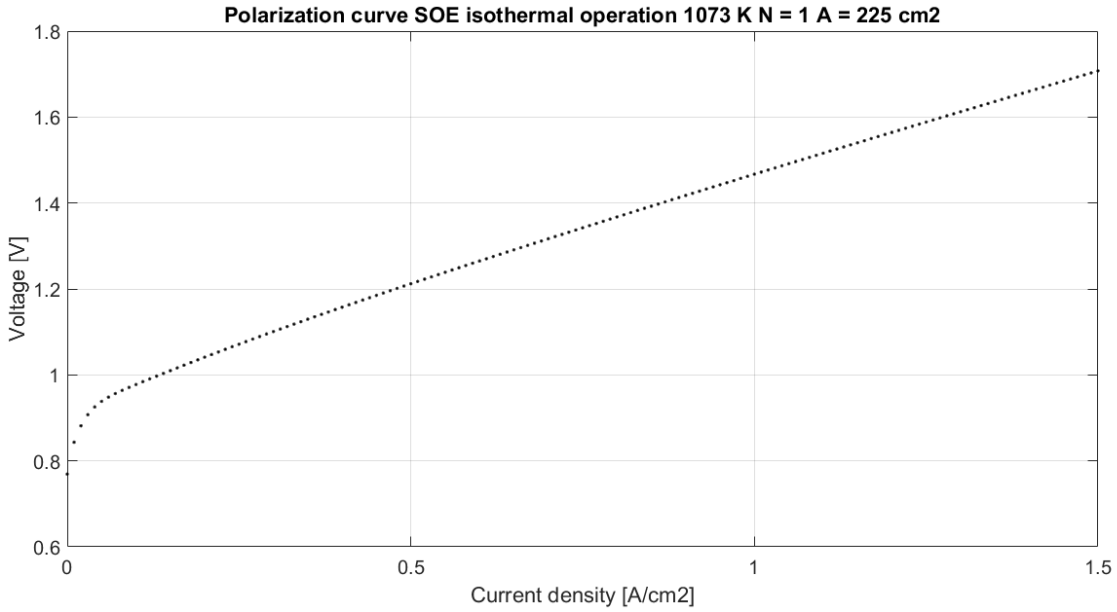

FIG: 3.9. Polarization curve one cell SOE

Fig.3.10 shows the contribution of the overpotentials to define the operating voltage of the cell: as expected, by increasing the current density the overpotentials grow. In this model the Ohmic losses are predominant and follow a linear law; concerning the activation and concentration losses, they play a marginal role especially the latter ones and they increase with current density more slowly compared to the Ohmic losses.

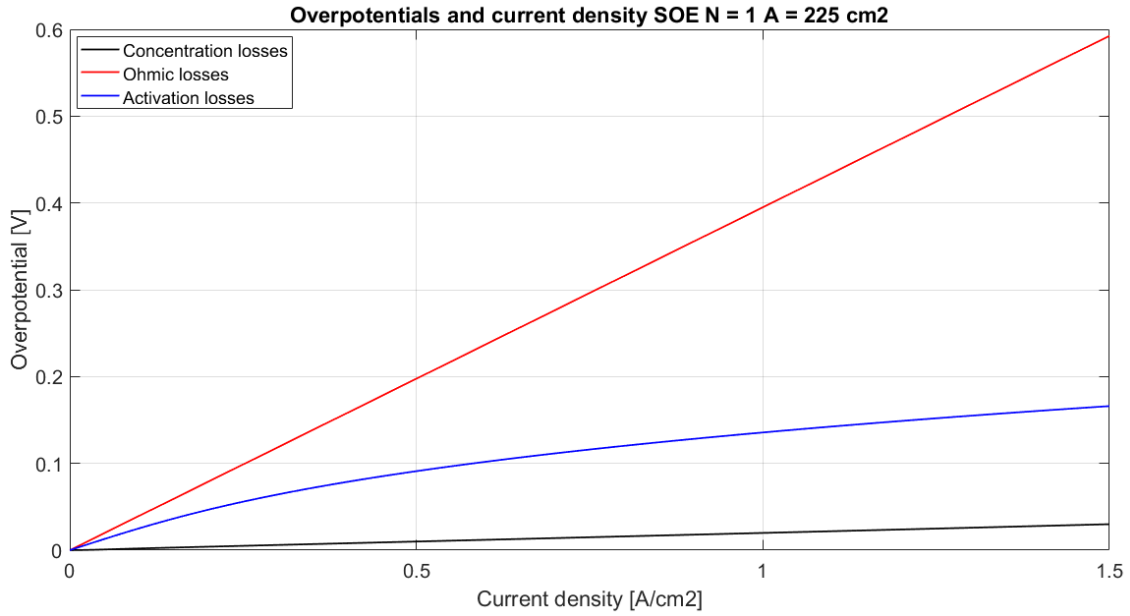

FIG: 3.10. Overpotentials depending on current density

3.1.4 Power density curve

In fig.3.11 and 3.12, the power density curves and the power curves of one cell (active area 225 cm^2) of the SOE depending on the temperature are plotted respectively; the power density curve is found by multiplying the current densities with the correlating cell voltages. The power curve is obtained considering the active cell area and the number of cells connected in series: in this case just one cell is analysed. As already commented, by increasing the temperature the electrical power demand decreases: particularly, with low current values the differences among the different power curves are not appreciable but they become more and more visible when the device is fed with higher current.

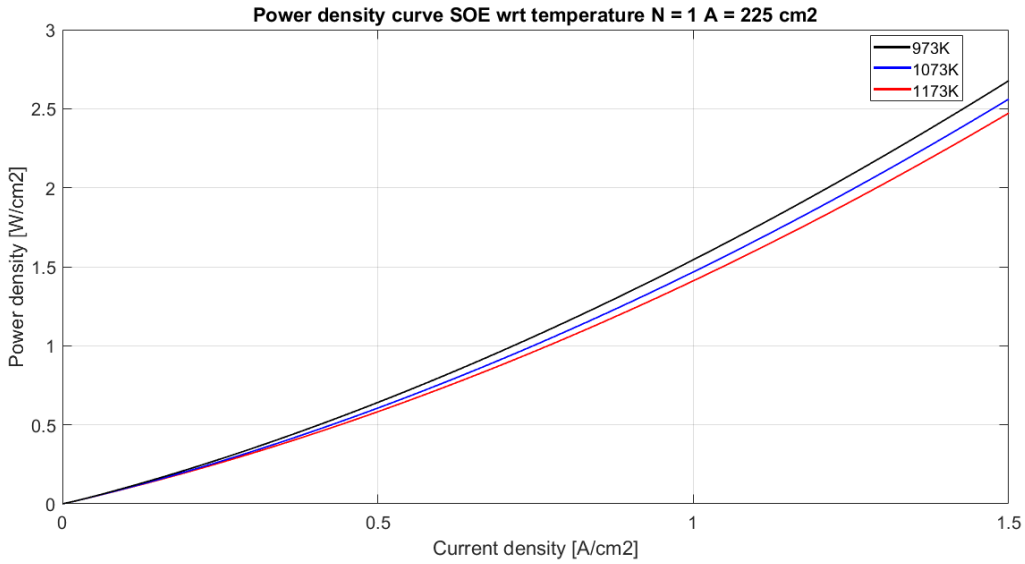

FIG: 3.11. Power density curve different isothermal temperatures

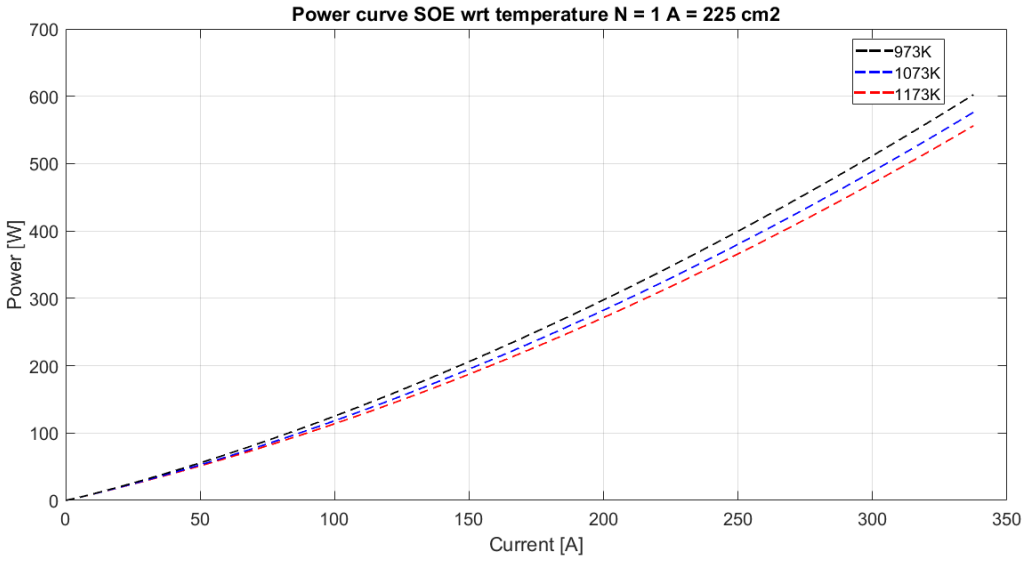

FIG: 3.12. Power curves different isothermal temperatures

3.2 Solid oxide co-electrolyser system

3.2.1 Model Anode and Cathode

The Solid Oxide Co-Electrolyser has been modelled modifying the model used to simulate the SOE; thus, the overall structure of the model is the same and in this section just the changes are highlighted and explained more detailed. As a reminder, it has to be noticed that the system works under isothermal condition and to simplify no considerations about the heat exchanges have been conducted; therefore, all the blocks concerning heat flows have not been modified and the CO_2 electrolysis is not analysed under this aspect. Inside this device the carbon dioxide and steam are respectively converted into carbon monoxide and hydrogen through electrolysis (2.17)(2.18). Additionally, the WGSR or its reverse occurs and its relative weight depends on the operating conditions: they include the inlet gas composition, temperature and applied voltage or current [48][49][50]. Therefore, the main outputs are H_2 and CO; a certain amount of steam and carbon dioxide may also be present. It is important to notice that sometimes it is required a fixed outlet ratio between H_2 and CO (e.g. 1,3,5 or more). To achieve this ratio, it is necessary to feed the system with a certain molar composition among the reactants. Now this aspect is explained more detailed. The cathode channel of the device is fed with a mixture of steam water, carbon dioxide and hydrogen; to correctly evaluate the mass balances inside the device two more inputs are considered, even if they are set to zero. They are: nitrogen and carbon monoxide. The anode channel is fed with a fixed quantity of air. Regarding the gas mixture feeding the cathodic side of the COSOE, the reactants depend on the current density value; the reasons are already explained in the SOE model. Thus, similarly, the current density value is multiplied with a constant that is expressed by the following expression:

$$\frac{A \cdot N}{n_e \cdot F \cdot UF} \tag{3.8}$$

Where:

- $A[m^2]$ indicates the area of each COSOE cell;
- N represents the number of cells connected in series;
- n_e represents the number of electrons involved in the electrochemical reaction and in the case of water/carbon dioxide electrolysis is equal to 2;
- $F[\frac{C}{mol}]$ is the Faraday constant;
- UF is the well-known utilization factor.

The total inlet molar flow is defined as follows:

$$\frac{J \cdot A \cdot N}{n_e \cdot F \cdot UF} \tag{3.9}$$

In the case of the co-electrolyser this quantity is then split into H_2O, CO_2 and a small amount of H_2 with different percentages. It has to be noticed that, in this work, the device is then connected with a CO-methanator that requires a certain ratio between hydrogen

and carbon monoxide. Particularly, the H_2/CO ratios analysed are 3 and 5: 3 is the ratio between H_2 and CO in the CO-methanation reaction; however, the literature indicates that, by increasing this ratio, a better conversion of CO into methane is reached. To obtain the desired output ratio, it is necessary to feed the device with a certain molar composition. Therefore, this inlet composition between H_2O and CO_2 (assuming 1% molar fraction of the mixture (3.9) to be H_2) has been searched through a trial and error procedure, according to the operating isothermal temperature; it has been then validated in the current density range, where the COSOE can operate. The model built is dynamic and, thus, a certain amount of time is required until the desired ratio is reached; fig.3.13 shows the time needed to get, under certain operating conditions, the ratio H_2/CO equal to 5. Fig.3.14-3.15 show the different inlet molar composition to achieve H_2/CO = 3 or 5 at the outlet.

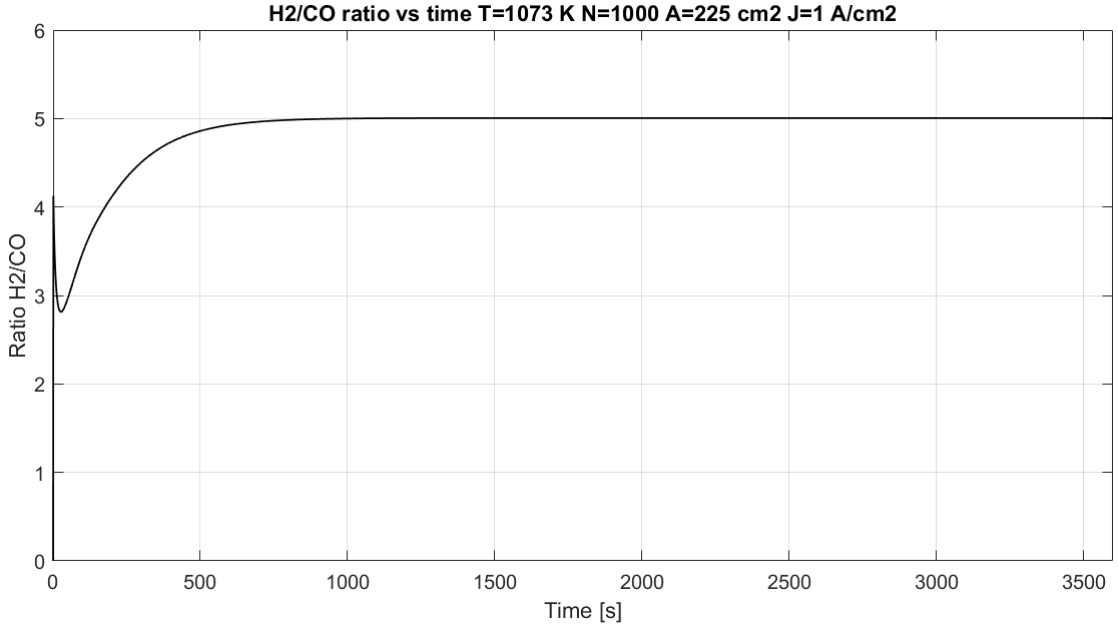

FIG: 3.13. Transient to get an output ratio H_2/CO COSOE

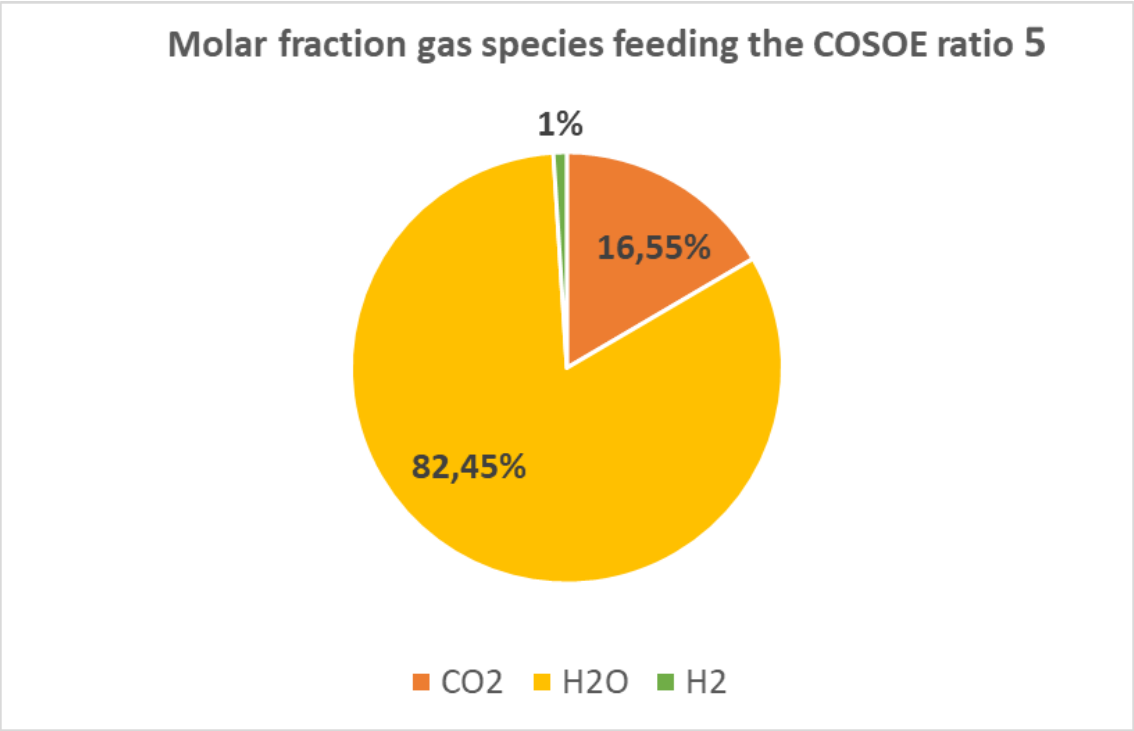

FIG: 3.14. Molar fractions ratio 5

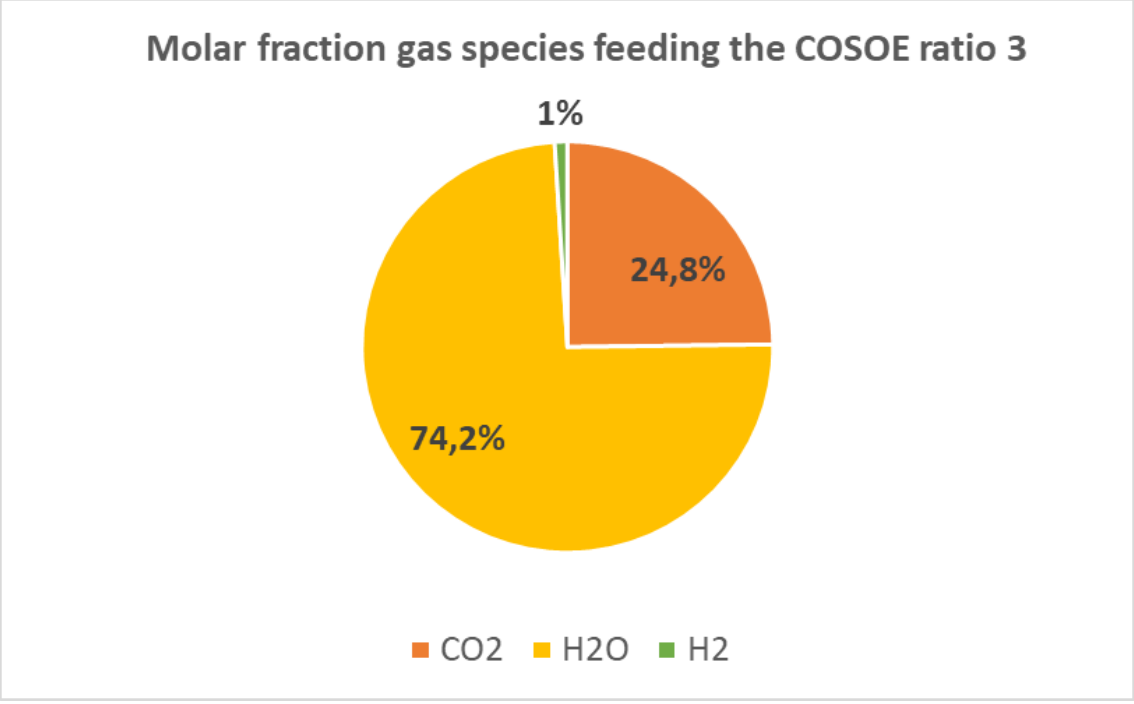

FIG: 3.15. Molar fractions ratio 3

The modelling of the structure of a solid oxide co-electrolyser cell reflects the same procedure adopted for the SOE system; it is summarized in fig. 3.16.

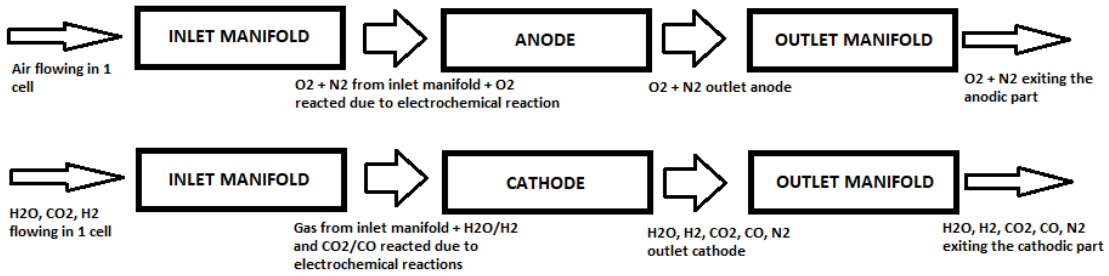

FIG: 3.16. Structure of the co-soe: anode and cathode

The anodic side is exactly the same; the cathodic side, instead, changes. Inside the two manifolds and the cathode two more mass balances are added regarding CO and CO_2: they are necessary in order to correctly evaluate the partial pressures and the total pressure inside every block. The methodology adopted to compute the pressures is the same used in the SOE system. Moreover, as shown in fig.3.16, just in the anode and cathode the electrochemical reactions occur and the amount of reactants/products is considered. Additionally, inside the co-electrolyser, in particular at the TPB cathode-electrolyte interface other chemical reactions, highlighted in (2.19)(2.20)(2.21), could take place; in this work, the operating conditions have been chosen to avoid methane and coke formation. Therefore, in the porous cathode, the transport of gas species is influenced by the reversible Water Gas Shift Reaction and by the rate of electrolysis reaction [15]. Inside the cathode, the rate of the WGSR or its reverse is computed using the formula [15]:

$$R_{WGSR} = k_{sf} \cdot (p_{H_2O} \cdot p_{CO} - \frac{p_{H_2} \cdot p_{CO_2}}{K_{ps}})[\frac{mol}{m^3 \cdot s}] \tag{3.10}$$

$$k_{sf} = 0.0171 \cdot exp(-\frac{103191}{R \cdot T(K)})[\frac{mol}{m^3 \cdot Pa^2 \cdot s}] \tag{3.11}$$

$$K_{ps} = exp(-0.2935 \cdot Z^3 + 0.6351 \cdot Z^2 + 4.1788 \cdot Z + 0.3169) \tag{3.12}$$

$$Z = \frac{1000}{T} - 1 \tag{3.13}$$

When R_{WGSR} is positive, it means that the WGSR is occurring: steam and carbon monoxide are consumed and hydrogen and carbon dioxide are produced. When it is negative, the reverse reaction occurs. As shown in (3.10), this rate depends on the partial pressures of the gas species inside the cathode and on the operating conditions of the cell. Clearly, once the rate is found, the amount of mass flows of reactants/products are evaluated and considered to compute the mass balances. In fig.3.17, the relationship between the WGSR rate and the current is shown under certain operating conditions of the model. The comparison between different output ratios is shown. The absolute value of the rate goes up linearly with the increase of the current density: increasing, indeed, the gas species inside the device, consequently, the reaction is always more favourable to occur. It has been observed that when the COSOE works with an output ratio of 1 the reverse of the WGSR occurs (contributing in this case to CO production). When the ratio is higher, CO and H_2O are consumed to produce H_2 and CO_2. According to [51][52], the common understanding is that in the co-electrolyser the WGSR always contributes to CO production; however, it is difficult to confirm this expectation and quantify the exact contribution. This work seems

to be in agreement to a similar study conducted in [15] where they found that, under certain operating conditions, the WGSR consumes CO. Additionally, if the ratio H_2/CO becomes higher than 1 CO is always consumed: greater the ratio, larger the amount of CO consumed. In fig.3.17, the contribution of the WGSR to the hydrogen production inside the co-electrolyser is highlighted; with the ratio of 3, the rate is positive and H_2 is produced through water electrolysis and WGSR: considering the current density value of 1 $\frac{A}{cm^2}$, the WGSR reaction represents the 27% of the total H_2 outlet molar flow.

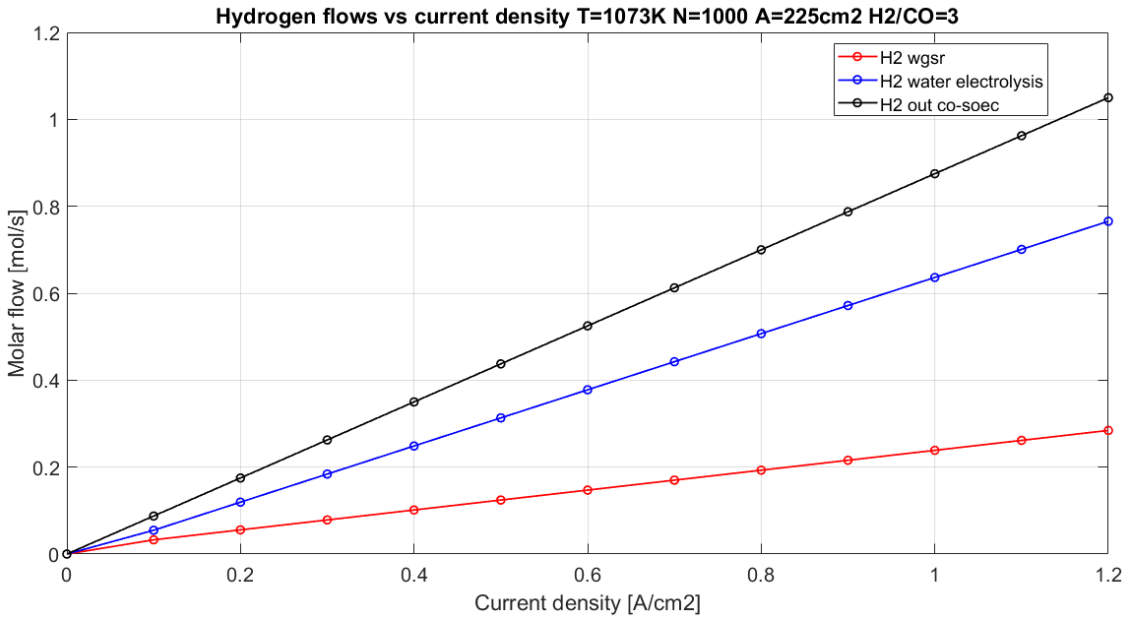

FIG: 3.17. WGSR rate and current density

3.2.2 Electrochemical reactions

In the co-electrolyser, as already explained, two electrochemical reactions occur: H_2O and CO_2 electrolysis. To realize this electrochemical process a certain voltage has to be applied to the cell; furthermore, each electrolysis reaction has its own voltage. Therefore, inside the model, two different voltages are computed: one for the H_2O electrolysis and the other for the CO_2 electrolysis. To do this, the two Nernst voltages and the relative overpotentials (activation and Ohmic) are implemented inside the model using the formulas provided in the COSOE State of the art. Moreover, as in the SOE device, an OCV loss is added for each voltage. The co-electrolyser can be studied as two electrical branches connected in parallel. Clearly, the device works with a unique voltage that depends on different parameters, including the current density. This latter parameter is, indeed, responsible for the electrochemical reaction; in the case of co-electrolysis, a certain quantity of current produce H_2O electrolysis and the remaining CO_2 electrolysis as shown in fig.3.18. Therefore, it is important to correctly evaluate how the current is split in the two branches.

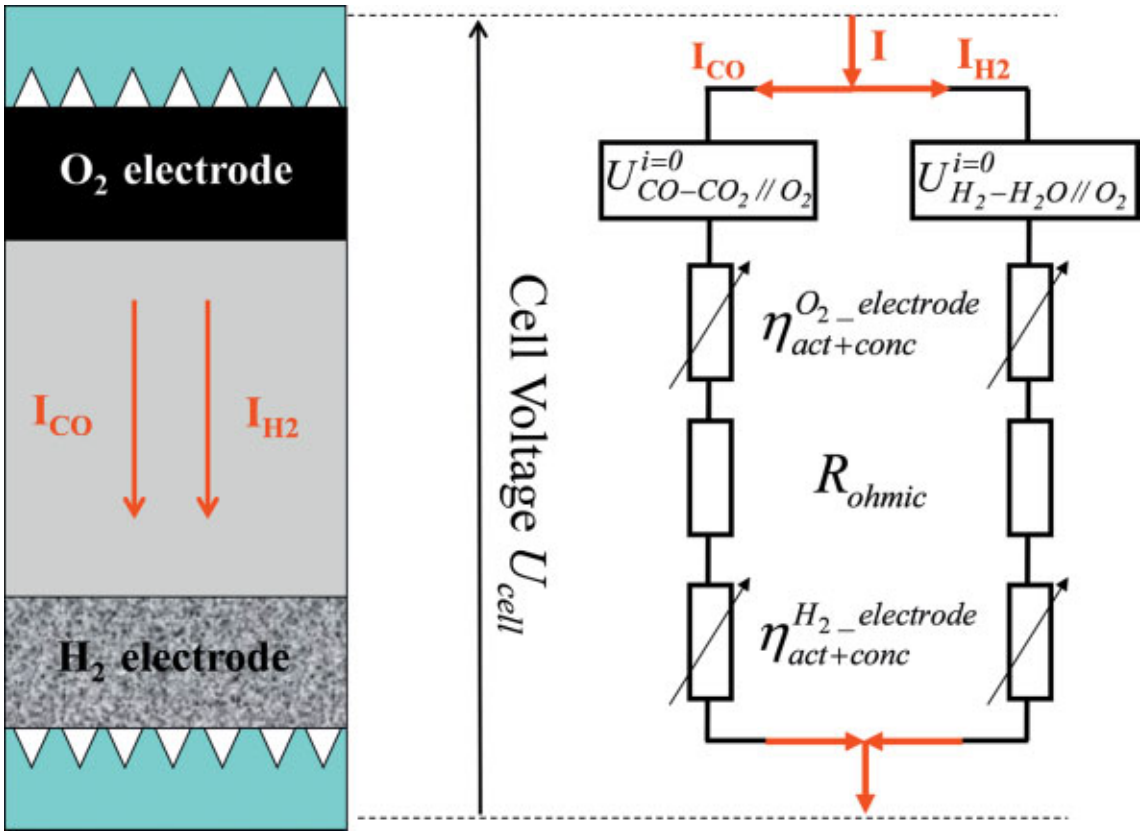

FIG: 3.18. Different paths of current in the COSOE

In the literature, different strategies have been analysed to make the two voltages equal: one of them is to divide the cathode/electrolyte surface in two different sites where the two reactions occur [53][54]. In this work, the following methodology has been adopted. The idea implemented is the splitting of the input current in two parts such that the two computed voltages become equal. Basically, during the simulation, the two voltages are always evaluated; afterwards, they are passed to a Proportional-Integral controller, carefully tuned, whose output is exactly the value of the current split. At this point, according to this parameter, the current is then divided; thus, the relative values are used to evaluate the amount of H_2 and CO produced and to compute again the overpotential losses. This strategy works well with any current density value used as input of the system except for very low current density (lower than 0.015 $\frac{A}{cm^2}$) and in open circuit voltage condition (no current). Therefore, when this situation occurs, the controller will give zero as result and all the current is used to produce CO; hydrogen is always produced with the WGSR; furthermore, the matching of ratio H_2/CO with the desired one is not achieved. Comparing the results with one author of the paper [55], it is not yet clear what precisely happen inside the device with these low current values. Even so, it has been noticed that the model shows voltage values very similar; due to this contingency, an approximation, in this work, is performed and an average value between the two voltages is considered.
In fig.3.19, the trends of the two voltages are plotted: initially, as expected, the values are different and after few seconds they become equal thanks to the current split, whose behaviour is appreciable in fig.3.20; when the split becomes constant it means that the voltages are equal. In fig.3.21, it is then shown the amounts of current involved in the two

electrochemical reactions. Fig.3.22 illustrates the open circuit voltage condition; as explained above, the two voltages are very similar and their trends are flat; in this situation, the operating voltage of the COSOE is averaged.

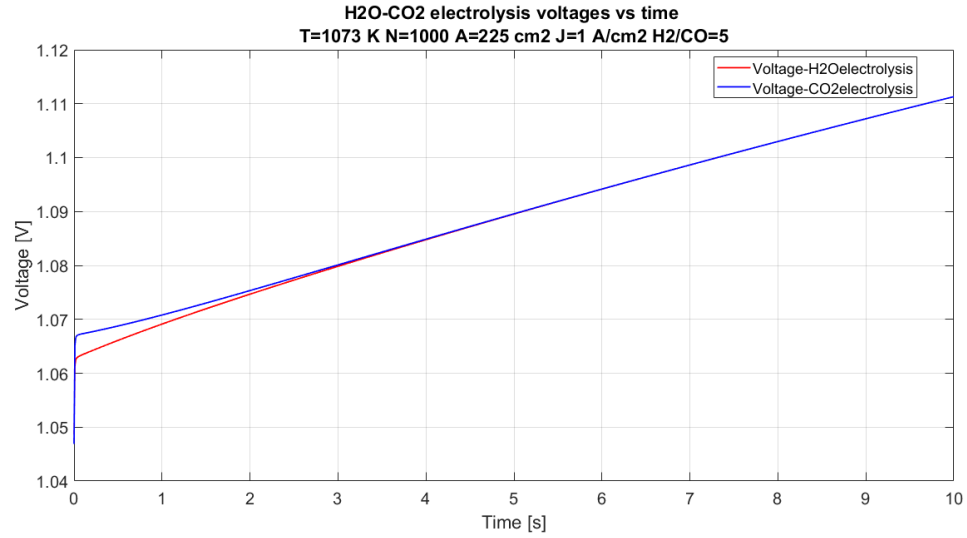

FIG: 3.19. H_2O and CO_2 electrolysis voltages

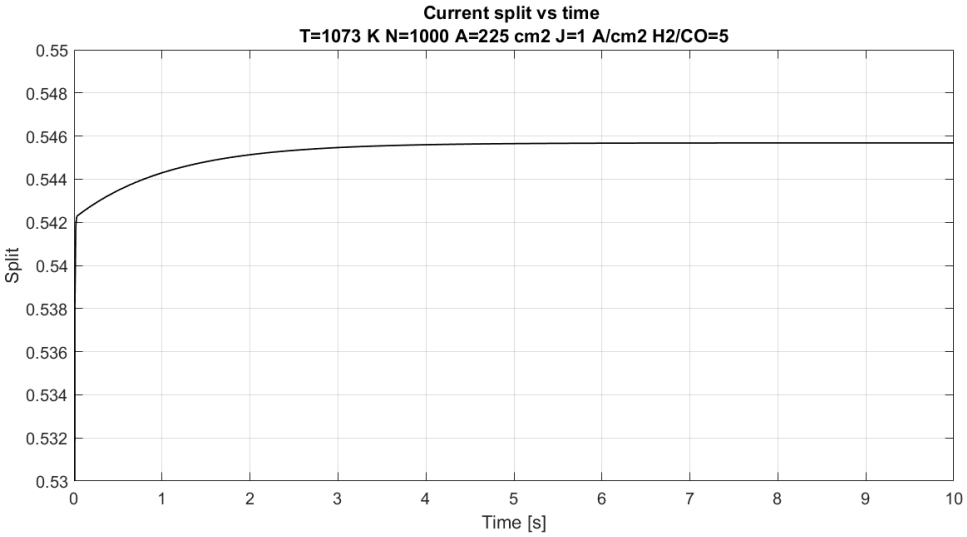

FIG: 3.20. Split of the current in the co-soe

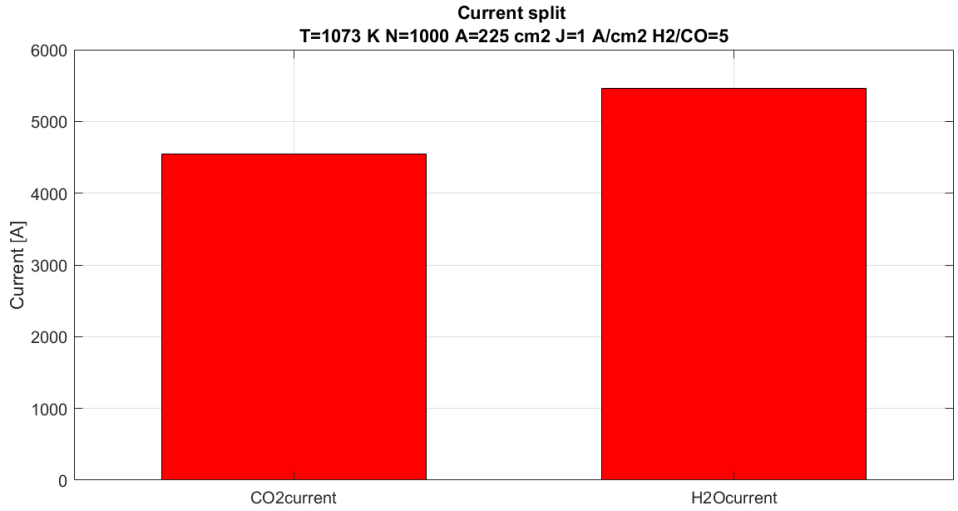

FIG: 3.21. H_2O and CO_2 currents

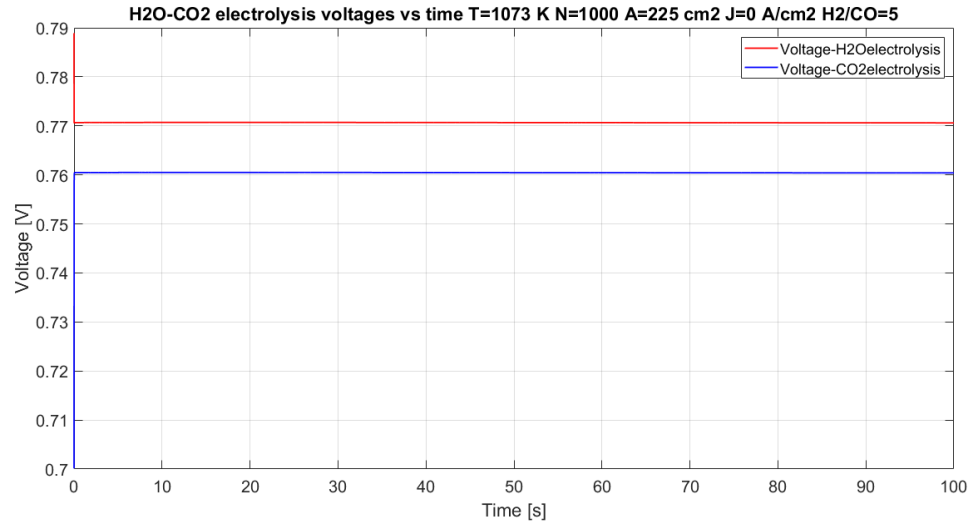

FIG: 3.22. H_2O and CO_2 open circuit voltages

3.2.3 Polarization curve

In fig.3.23, the polarization curves of the solid oxide co-electrolyser cell are plotted comparing the two different output ratios between hydrogen and carbon monoxide; the graph turns out that the output ratio does not influence the polarization curve of the device: the two curves are, indeed, identical. As explained above and due to the simplification adopted with small inputs currents the voltage behaviour does not follow the usual one: the trends are just qualitative and not match exactly the real operating conditions. The reasonings about temperature influence on the polarization curve carried out in the solid oxide electrolyser are still valid; therefore, they have not been repeated for the COSOE cell.

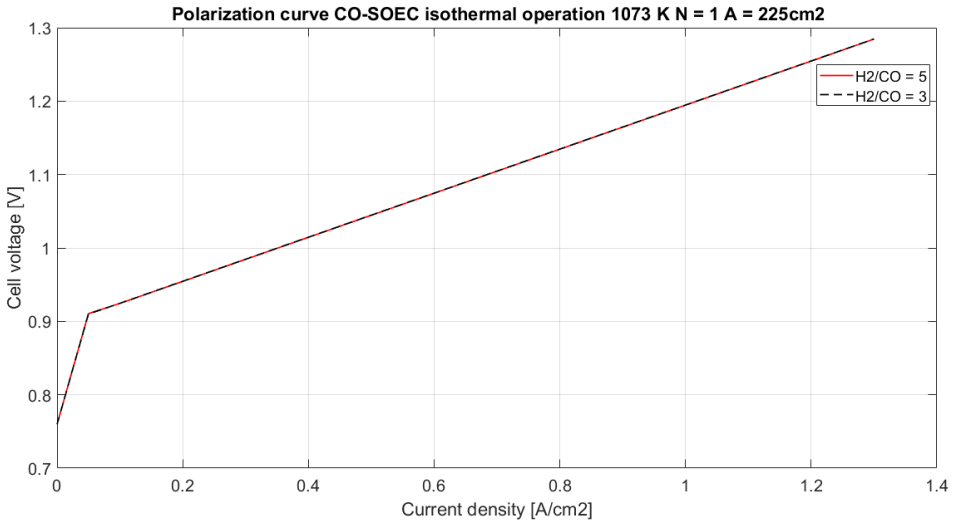

FIG: 3.23. Polarization curve co-soec

3.2.4 Power density curve

In fig.3.24, the power density curves of the co-electrolyser, when it operates with outlet $H2/CO$-ratio of 3 and 5 are plotted. They are overlapped and this means that, for any operating ratio, the co-electrolyser absorbs the same amount of power.

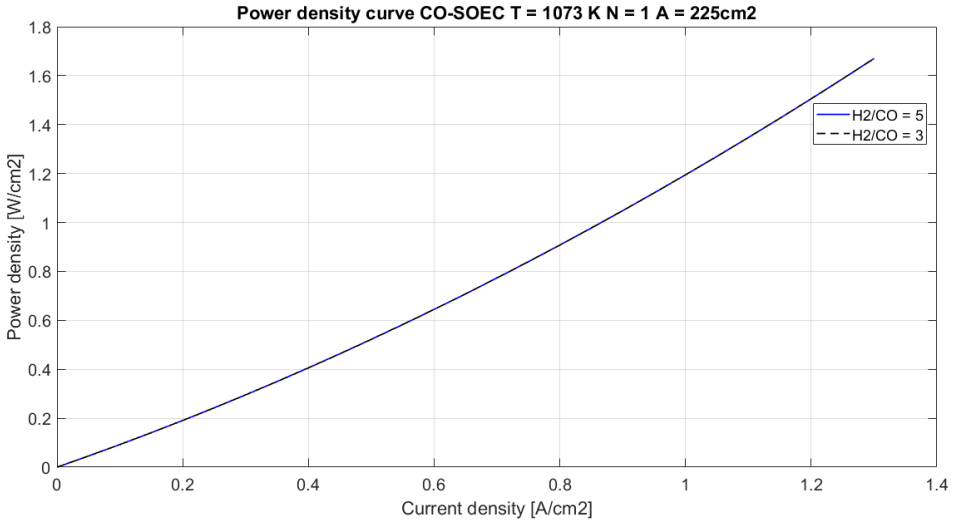

FIG: 3.24. Power density curve curve co-soec

3.3 CO-Methanator

3.3.1 Model

The third component that has been modelled in this work is the CO-methanator, i.e. the device needed to produce methane having as main inputs hydrogen and carbon monoxide. As already explained in the previous chapter in CO-methanator section, inside the methanator several chemical reactions may happen and in this work, according to [44], just two reactions are taken into account. They are:

$$COmethanation : CO(g) + 3H_2(g) \leftrightarrow CH_4(g) + H_2O(g) \tag{3.14}$$

$$WGSR : CO(g) + H_2O(g) \leftrightarrow CO_2(g) + H_2(g) \tag{3.15}$$

Thus, the Boudouard reaction is neglected and, consequently, coke formation. In order to realize a proper model of the device the methodology explained more detailed in [44] has been followed and a dynamic model of a catalytic fixed bed reactor, operating in isothermal conditions, has been realized in MATLAB-Simulink. According to [44], an isothermal reactor presents different advantages over an adiabatic one; for instance, product recycling may be reduced, cooling costs are lower and extremely high reactor exit temperatures are avoided; this latter advantage allows to preserve catalyst lifetime and internal refractory insulation, used in adiabatic reactors, is not needed.
First of all, it has to be noticed that there are five inputs: steam, carbon dioxide, carbon monoxide, hydrogen and methane; obviously, the methane molar flow is always zero but it has to be considered to evaluate the mass balances inside the methanator. Secondly, to have a more precise model the fixed bed reactor has been divided into equal sections as shown in fig.3.25. Clearly, the greater the number of smaller volumes, the higher the detail of the model is. Due to the computational time reasons during simulations, the models present a number of volumes equal to five, thus $n = 5$.

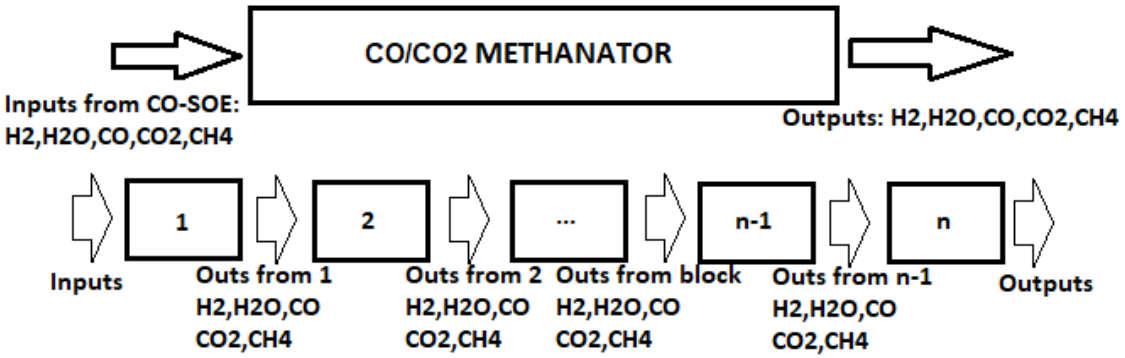

FIG: 3.25. Volumes of the CO-methanator

The model below explained presents a limitation for a correct study; it cannot distinguish, indeed, among a long and narrow or a short and large device because just the information about the total volume is considered; in this way, a more realistic analysis in terms of space is not performed. Therefore, the division in smaller volumes is the experimental approach used to simulate and analyse the realistic situation in terms of reactants/products

evolutions even if the real length cannot be expressed. Information regarding mass of the catalyst and volume will be illustrated afterwards.
The dynamics inside each volume follow the same idea implemented for anode and cathode in the SOE and CO-SOE. The partial pressures of the different species are computed after the mass balances of steam water, hydrogen, carbon monoxide, carbon dioxide and methane. The partial pressures are needed to evaluate the rates of the chemical reactions (3.14) (3.15); both are reversible and, according to the different quantities inside the volumes, the direct reaction or its reverse can occur. The methanation reactor model is based on kinetics developed by Kopyscinski over a commercial catalyst Ni/Al_2O_3 (50wt% Ni/Al_2O_3, BET surface area = 183 m^2/g) in a fixed bed reactor. The rate equations of (3.14) and (3.15) follow the Langmuir-Hinshelwood approach by the assumption of the rate-determining step (RDS) for the reaction mechanisms proposed by Kopyscinski [56]:

$$R = \frac{(kineticterm) \cdot (drivingforce)}{(adsorptionterm)} \tag{3.16}$$

The driving force for the reactions (3.14) and (3.15) are the partial pressures expressed in bar; the adsorption term takes into account the retarding effects of the adsorbed reactants and products. This step is considered as being the slowest reaction step and responsible for the overall rate; all the others are in equilibrium or irreversible. The assumed RDS for this work, according to [44], is the following one:

$$COH^* + H^* \rightarrow -CH^* + OH^* \tag{3.17}$$

Other further information can be found in reference [56]. Regarding the CO-methanation and WGS reactions the rates are the following:

$$R_{COmethanation} = \frac{k_1 \cdot K_c \cdot p_{CO}^{0.5} \cdot p_{H_2}^{0.5}}{(1 + K_c \cdot p_{CO}^{0.5} + K_{OH} \cdot p_{H_2O} \cdot p_{H_2}^{-0.5})^2} [\frac{mol}{kg_{cat} \cdot s}] \tag{3.18}$$

$$R_{WGS} = \frac{k_2 \cdot (K_a \cdot p_{CO} \cdot p_{H_2O} \cdot p_{H_2}^{-0.5} - \frac{p_{CO} \cdot p_{H_2}^{0.5}}{K_{eq}})}{(1 + K_c \cdot p_{CO}^{0.5} + K_{OH} \cdot p_{H_2O} \cdot p_{H_2}^{-0.5})^2} [\frac{mol}{kg_{cat} \cdot s}] \tag{3.19}$$

Where:

- k_1, k_2 are the rate constants, depending on temperature, that follow the Arrhenius equation:

$$k_j = k_j^0 \cdot exp(-\frac{E_{ai}}{R \cdot T}) \tag{3.20}$$

and are defined in this way:

$$k_1 = 3.34 \cdot 10^6 \cdot exp(-\frac{74000}{R \cdot T}) [\frac{mol}{kg_{cat} \cdot s}] \tag{3.21}$$

$$k_2 = 9.62 \cdot 10^{14} \cdot exp(-\frac{161740}{R \cdot T}) [\frac{mol}{bar^{1.5} \cdot kg_{cat} \cdot s}] \tag{3.22}$$

The pre-exponential factors of the kinetic rate and activation energies are taken from Kopyscinski [56];

- K_{OH}, K_c, K_a are the adsorption constants, depending on temperature, that follow the Vant Hoff equation:

$$K_j = K_j^0 \cdot exp(-\frac{\Delta H_{Rj}(T)}{R \cdot T}) \tag{3.23}$$

and are defined in this way:

$$K_{OH} = 3.97 \cdot 10^{-7} \cdot exp(\frac{72650}{R \cdot T})[bar^{-0.5}] \tag{3.24}$$

$$K_C = 8.10 \cdot 10^{-6} \cdot exp(\frac{61200}{R \cdot T})[bar^{-1}] \tag{3.25}$$

$$K_a = 9.3 \cdot 10^{-2} \cdot exp(\frac{6500}{R \cdot T}) \tag{3.26}$$

The adsorption coefficients and adsorption heats are taken from Kopyscinski [56];

- K_{eq} is the thermodynamic equilibrium constant of Water Gas Shift Reaction taken from [57]:

$$K_{eq} = exp(\frac{4400}{T} - 4.063) \tag{3.27}$$

The kinetic model illustrated above is valid in the temperature range between 473 and 673 K.

3.3.2 Methanation process

The methanator can be fed in with a different ratio between hydrogen and carbon monoxide; usually the ratio used is equal to 3, according to reaction (3.14), but this ratio can also be higher (e.g. 5,7). In fig.3.26 3.27, the differences in the outputs of the methanator, working with different inlet ratios, can be seen; in this work the ratio 3 and 5 have been considered.
It has to be noticed that the device receives as inputs the outputs of a COSOE that is set to reach the desired ratio; in the following chapter, a more detailed explanation about the working conditions of the whole system is provided. Concerning this comparison, equal sizes of $COSOE$ and CO-methanator have been considered and the same amount of CO_2 has been processed; particularly, the stack of the co-electrolyser is made up of 1000 cells connected in series (1073 K and atmospheric pressure) and the CO_2 used, expressed in mol/s, is the nominal one produced by the upgrading process of the WWTP. Further information can be noticed in the title of fig.3.26 and 3.27. The evolutions of the gas species in the two cases is quite similar: a reduction and sometimes a complete consumption of H_2, CO and CO_2 can be seen; similarly, production of H_2O and CH_4 is evident. Moreover, it is clear that in this model the CO-methanation rate is the predominant one, it is stronger in the first two volumes and afterwards the evolutions of the gas species are practically

constant. In the case of ratio 5 a bit more of methane is produced (around 0.2 mol/s) but also higher amount of steam is present and not all the hydrogen is consumed: on one hand, this is positive in terms of methane obtained but, on the other hand, its quality is poorer.

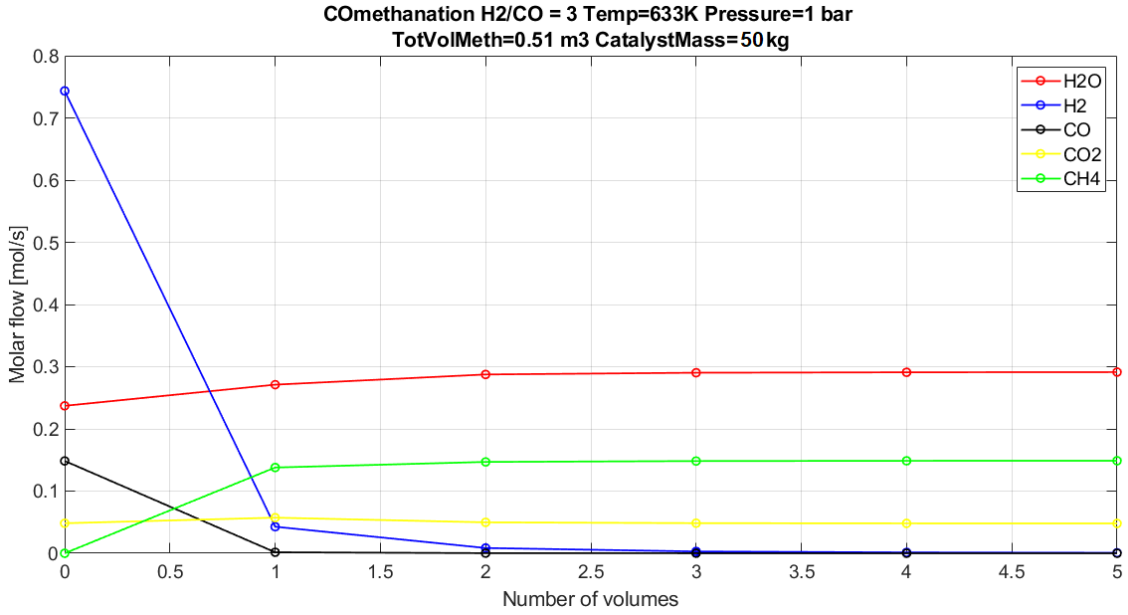

FIG: 3.26. Trends inside methanator $H_2/CO = 3$

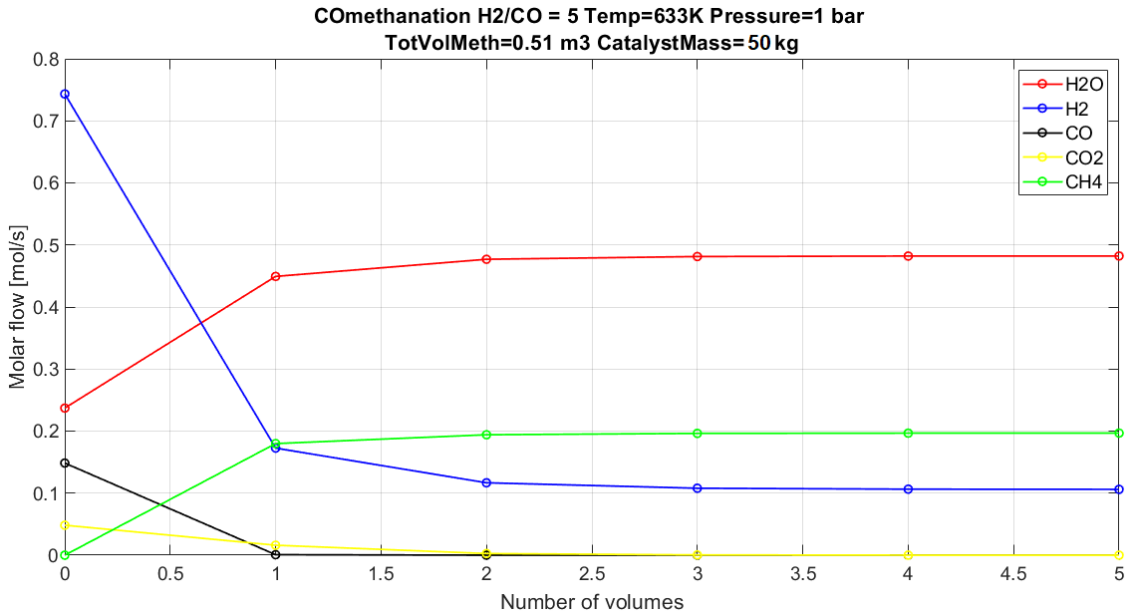

FIG: 3.27. Trends inside methanator $H_2/CO = 5$

3.3.3 Temperature influence

As previously explained in the model description, the simulated methanator can operate in the temperature range 473-673 K; in fig.3.28, the outputs compared with the working isothermal temperature are plotted: increasing the temperature, the methane and water productions raise. On the opposite, hydrogen and carbon monoxide, whose conversion is low below 550 K due to the catalyst chosen [44], are always better converted. These trends are valid until the operating temperature of 633 K: afterwards no variations are appreciable. The results are also in good agreement with a similar study conducted in the paper [44] used as reference; furthermore, in the range 563-573 K, CO_2 and H_2 increase even if CO is completely converted: this is due to the WGSR's influence. In the paper, while, in this work, they are different (H_2O/CH_4 almost 2). It has been supposed that one reason could be the different methodology used to compute the pressure drop (Ergun momentum balance equation [44]); another one could be the different simulator used (Aspen Plus in [44]). Anyway, no further investigation has been carried out. During the choice of the operating temperature of this device, when it is coupled with the CO-electrolyser, this graph has played an important role. It has been decided, indeed, to work at 633 K: operating at higher temperatures it is not convenient because an higher amount of heat would be required and no advantages in CH_4 produced are expected.

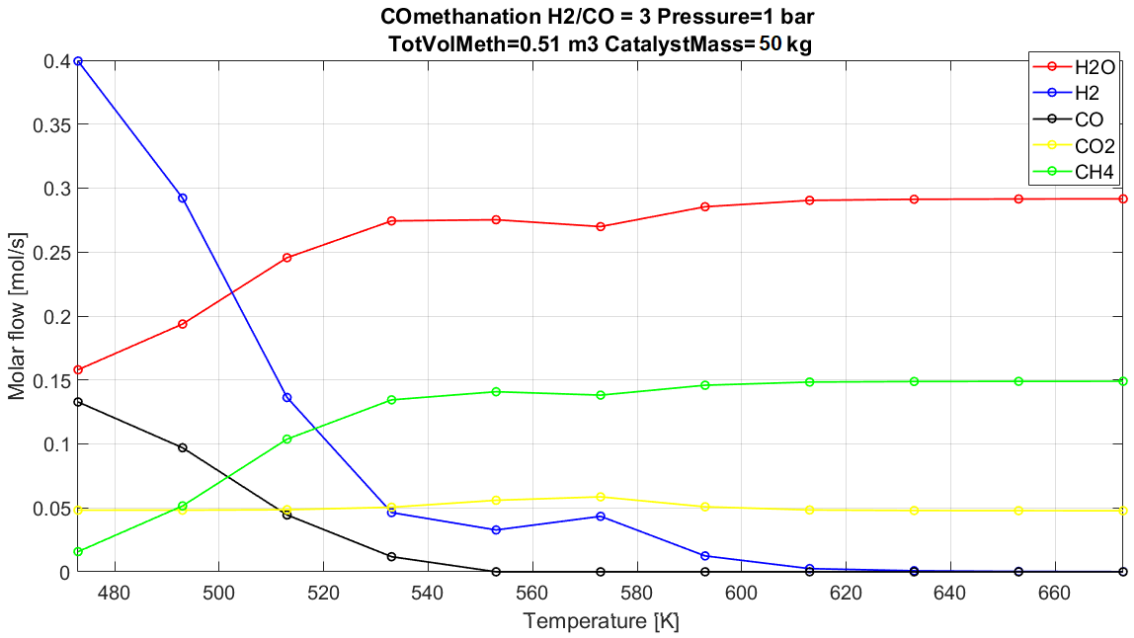

FIG: 3.28. Temperature influence on methanator outputs

3.3.4 Pressure influence

In fig.3.29 and 3.30, the trends of the outputs of the methanator are plotted considering a pressure range between 1 and 10 bar and two different isothermal temperatures. As shown in fig.3.29, the increase of pressure leads to a better steam and methane production; similarly, the other reactants are better consumed. These behaviours are in good agreement with a similar study conducted in [44]; differences in methane and steam produced are ev-

ident and the causes could be searched in the different methodologies adopted with respect to the paper, as already highlighted. Increasing the operating temperature in the model, the pressure effect is reduced and no appreciable differences are evident (fig.3.30); this means that, assuming 633 K as the operating temperature in this study, it is not necessary to increase the pressure and the system can work at the ambient pressure.

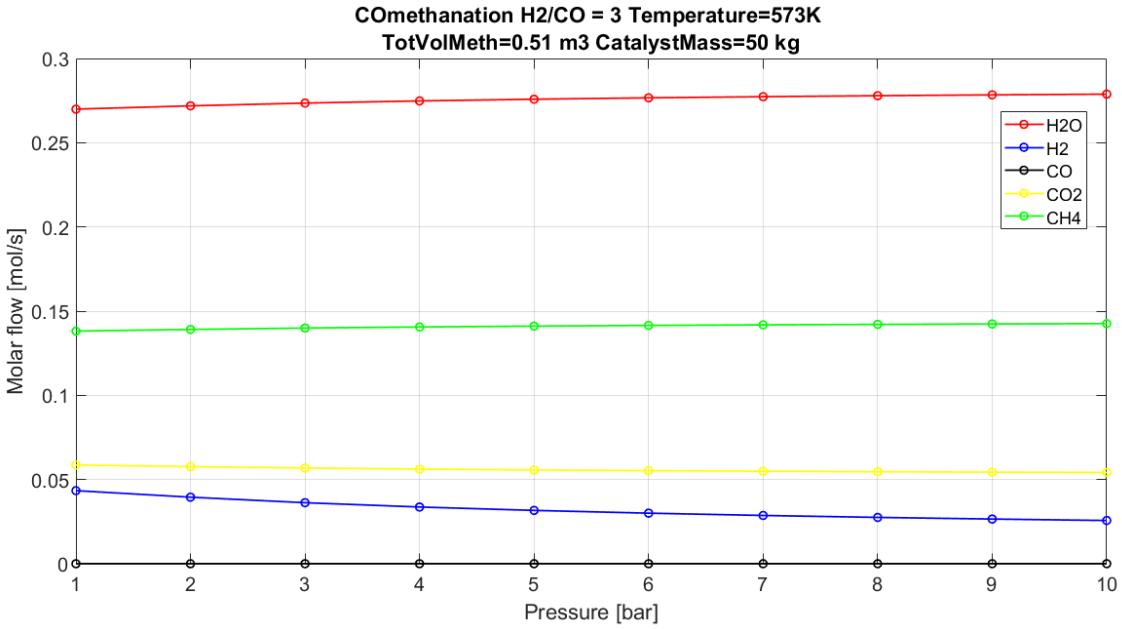

FIG: 3.29. Pressure influence on methanator outputs

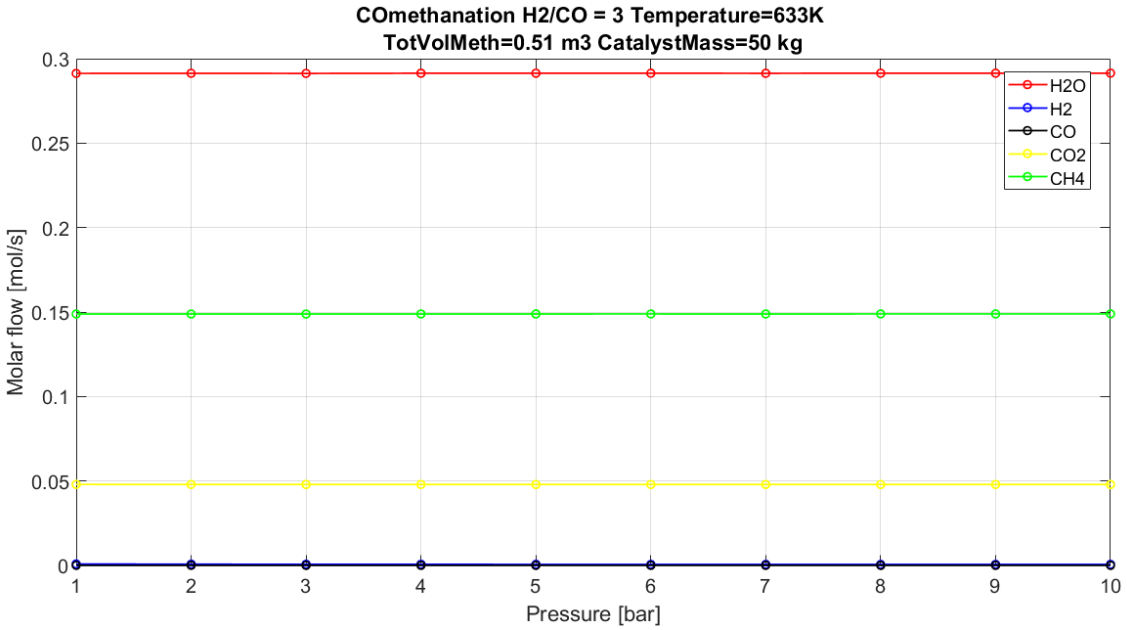

FIG: 3.30. Pressure influence on methanator outputs

3.4 CO_2 Methanator

3.4.1 Model

Similarly to CO-methanator model, a model for the CO_2-methanator has been realized; the two models are almost identical. The main difference is that, in this case, three reactions occur within the volumes of the device. The first two reactions are the ones already implemented in the previous model and they are: CO-methanation and WGSR (3.14) and (3.15); additionally, the CO_2 methanation reaction is taken into account:

$$CO_2(g) + 4H_2(g) \leftrightarrow CH_4(g) + 2H_2O(g) \tag{3.28}$$

The CO_2-methanator presents as input a gas mixture: the main elements are hydrogen, steam (coming from the solid oxide electrolyser) and carbon dioxide (coming from the WWTP); in the model two more inputs are considered: CO and CH_4. However, they are fixed to zero but they are needed to compute the mass balances inside the model. It is important to notice that the inlet ratio H_2/CO_2 is always equal to 4. As already explained for the CO-methanator, the volume of the system has been subdivided in more sections for a better analysis even if its limitations are still valid. The scheme of the model is presented in fig.3.31:

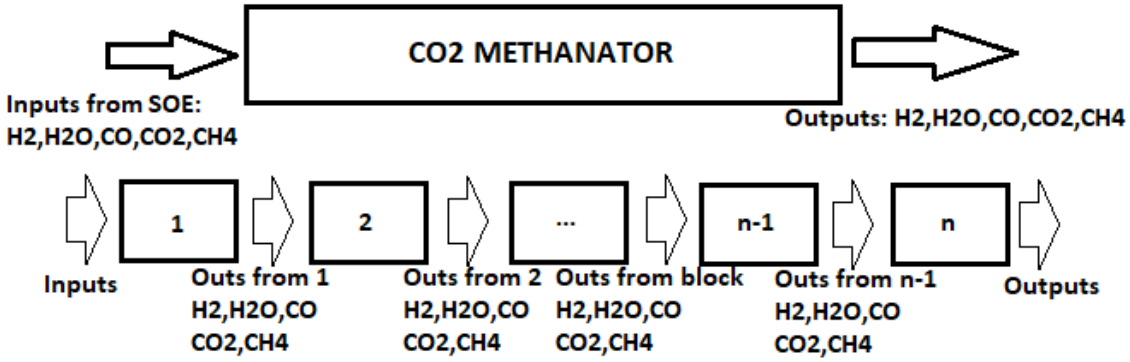

FIG: 3.31. Volumes of the CO2-methanator

Inside each volume, the reaction rates of the three chemical processes are implemented; the intrinsic rate equation for the CO_2-methanation has been taken from [58] and it has been derived using the Langmuir-Hinshelwood-Hougen-Watson (LHHW) approach:

$$R_{CO_2 methanation} = \frac{k_{CO_2} \cdot p_{CH_4} \cdot p_{CO_2}}{(1 + K_{CH_4} \cdot p_{CH_4}) \cdot (1 + K_{CO_2} \cdot p_{CO_2})} \cong \frac{k_{CO_2} \cdot p_{CH_4} \cdot p_{CO_2}}{(1 + K_{CO_2} \cdot p_{CO_2})} [\frac{mol}{kg_{cat} \cdot s}] \tag{3.29}$$

The adsorption coefficient of CO_2 and the rate constant are the following:

$$k_{CO_2} = 0.207 \cdot exp(-\frac{9920}{R \cdot T})[\frac{kmol}{kg_{cat} \cdot bar^2 \cdot s}] \tag{3.30}$$

$$K_{CO_2} = 2.24 \cdot 10^{-3} \cdot exp(\frac{77500}{R \cdot T})[bar^{-1}] \tag{3.31}$$

3.4.2 Methanation process

In this section the operation of the CO_2-methanator model is presented; in this case study, the inputs of the device are the outputs of a solid oxide electrolyser, made up of 1000 cells connected in series, operating at 1073K and ambient pressure; the size of the methanator and its working conditions are reported in the title of the graphs. Particularly, fig.3.32 shows the trends of the gas species: steam, hydrogen, carbon monoxide, carbon dioxide and methane. The inlet ratio H_2/CO_2 is equal to 4. As expected, H_2 and CO_2 are consumed and H_2O and CH_4 are produced; inside the first volume the kinetics of the reactions are predominant and, after the third section, no changes are evident. Hydrogen and carbon dioxide are almost fully consumed and just 0.23% molar fraction of H_2 is present; no traces of carbon monoxide are appreciable. In fig.3.33, it is shown how the different gas species react inside the first section of methanator; as a reminder, three reactions occur simultaneously: CO-methanation, CO_2-methanation and WGSR (or its reverse). It can be noticed that, on one hand, part of CO_2 react with hydrogen and produce directly methane and water through CO_2-methanation; on the other hand, the remaining part of CO_2, processed inside the first volume, reacts again with hydrogen producing water and carbon monoxide through the reverse of the water gas shift reaction. The CO produced reacts then with hydrogen producing again methane and water through the CO-methanation reaction; it has to be noticed that the reaction rates of CO-methanation and WGS are the same in absolute value; this means that all the CO produced is then consumed in the CO-methanation process and consequently no traces are present at the output of the system. Even if just the reaction rates inside one control volume are reported, it has to be noticed that the chemical processes occur in the same way in the other sections.

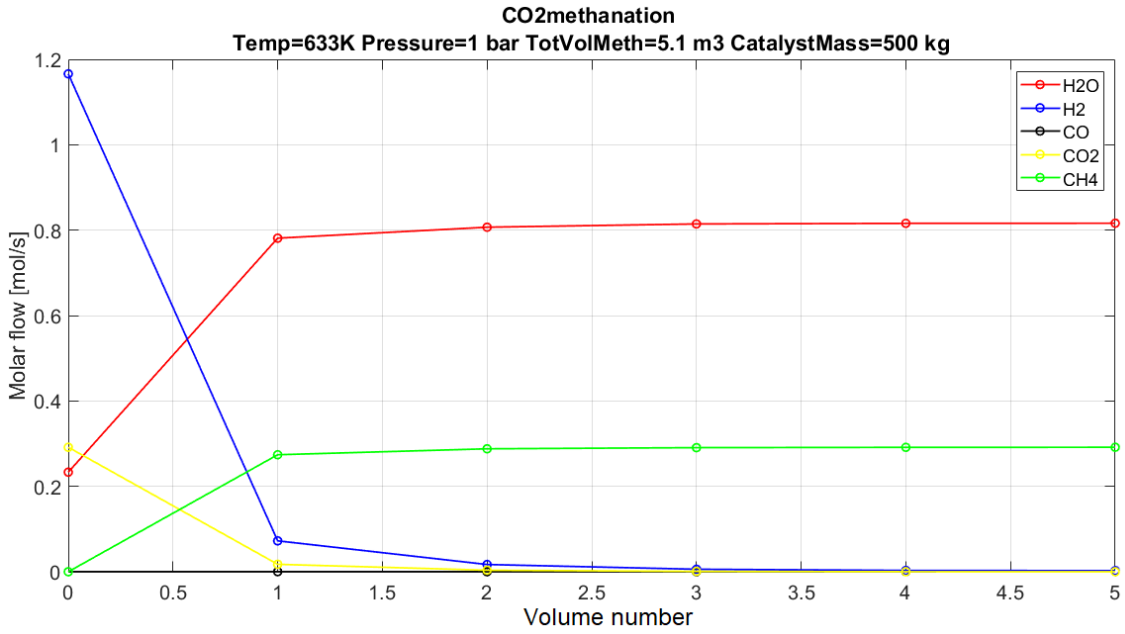

FIG: 3.32. Trends inside the methanator

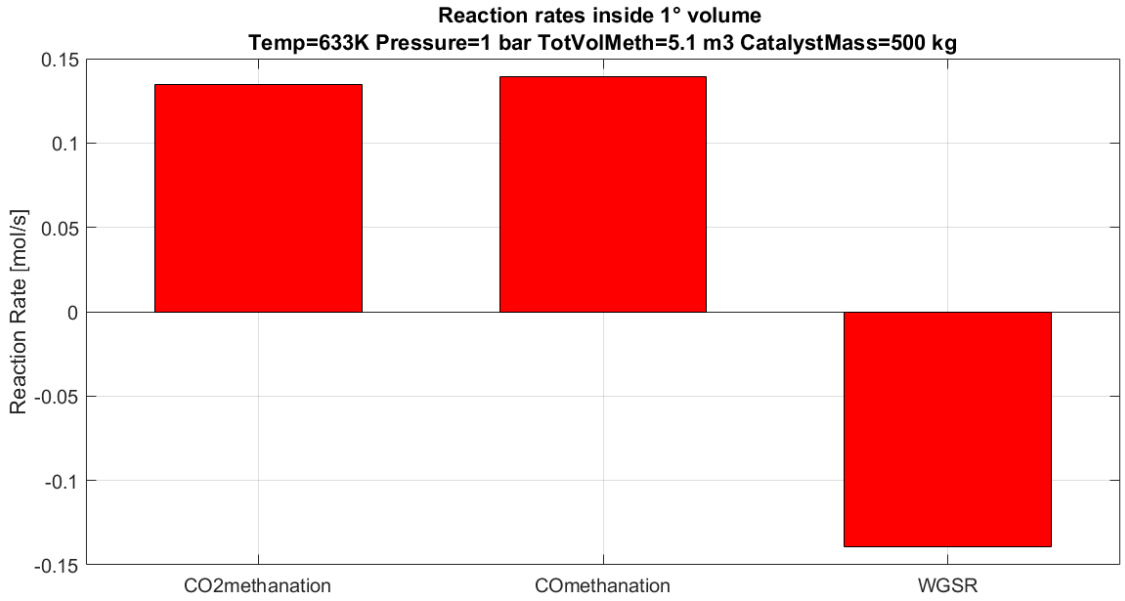

FIG: 3.33. Reaction rates 1° volume

3.4.3 Temperature-pressure influence

Being the CO-methanator and the CO_2-methanator models almost identical, the same reasonings carrying out for the first process concerning temperature and pressure influence are still valid for the CO_2-methanator. The pressure influence study is not reported here. In fig.3.34, the temperature influence can be seen and the temperature range where the model is valid [44] is analysed; with this methanator size, under 520 K the three reactions are almost not activated and no H_2-CO_2 conversion takes place. Increasing the temperature, instead, leads to better conversion and thus methane production; the trend is valid until 633 K; afterwards, a temperature increase does not change the methanator outputs. These trends are again in good agreement with the paper [44] used as reference to build the models but do not match exactly what is explained in the literature where lower temperatures lead to better CH_4 production; possible explanations may be searched in the simplifications and assumptions adopted for this models; however, no further investigations have been conducted and the working conditions chosen are isothermal temperature at 633 K and 1 bar.

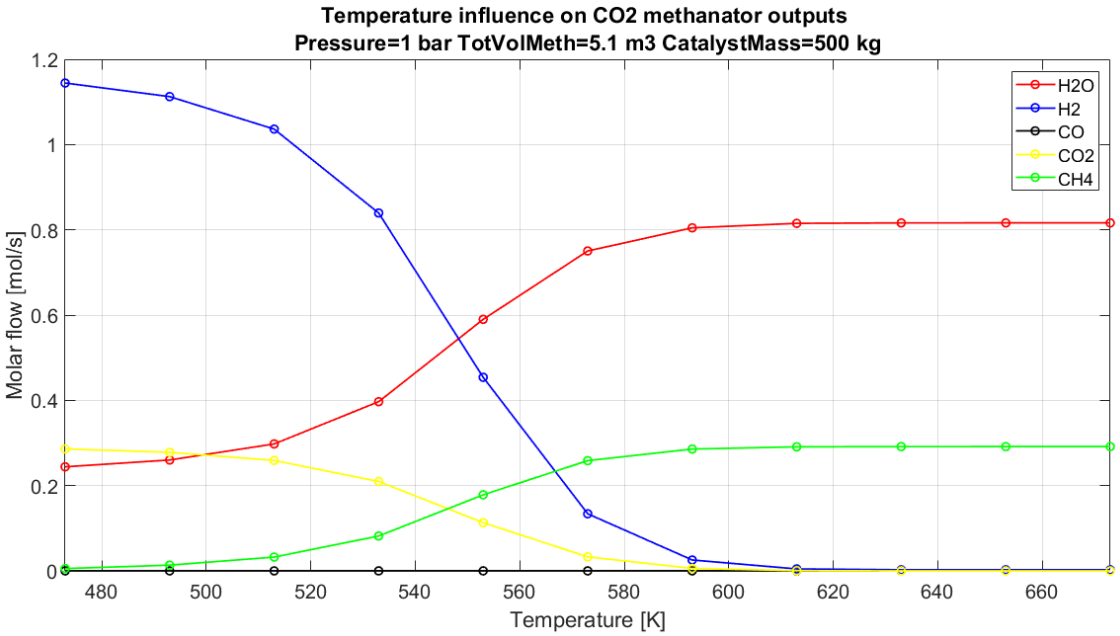

FIG: 3.34. Temperature influence on methanator outputs

Chapter 4

Description of the two Power to Gas systems

4.1 General overview on the two compared system configurations

As already explained in section 'Objectives', the main goal of this work is to capture the CO_2, coming from a Waste Water Treatment Plant, and its conversion into methane that feeds the natural gas grid. Particularly, the CO_2 comes from the upgrading process, where the biogas is converted into a mixture of bio-methane and carbon dioxide; the CH_4 can feed the natural gas grid and CO_2 is normally released to the atmosphere. Thus, the aim of the work is to collect this gas and to produce methane. Moreover, the data processed derives from *EDAR Riu Sec* WWTP; this plant, that works 24/24 h 365 days per year, is situated in Sabadell (Barcelona). In particular, inside the upgrading process of this plant, the amount of biogas processed is practically constant all over the year (an average of 45 m^3/h) and the output CO_2/CH_4 ratio is 35/65; consequently, the CO_2 source is always assumed constant and in every hour the CO_2 production is given by the following relationship:

$$CO_2 = 45\frac{m^3}{h} \cdot 0.35 = 15.75\frac{m^3}{h} = 708.59\frac{mol}{h} \tag{4.1}$$

Moreover, in the simulations performed, a value of mol/s of CO_2 is considered:

$$CO_2 = \frac{708.59\frac{mol}{h}}{3600\frac{s}{h}} = 0.1968\frac{mol}{s} \tag{4.2}$$

It is out of the scope of this work the process of collecting and transport the carbon dioxide from the upgrading process to the Power to Gas plant. Therefore, no costs associated to the collecting/pumping and relative losses are taken into account. However, this CO_2 is processed inside a Power to Gas plant; in this work, two different systems are analysed and compared to evaluate the most efficient one: i.e. the system configuration that requires the least amount of photovoltaic nominal power to fulfil the 100% CO_2 capture is installed.

In fig.4.1 and 4.2, the two system configurations are presented; fig.4.1 shows the "SOE + CO_2-Methanator" and fig.4.2 the "COSOE + CO-Methanator". Both work with a photovoltaic plant as electric power source, a DC/DC power converter to transfer the electrical

power from the PV plant to the electrolysers and CO_2 storage. Moreover, they only operate when power is available. The main difference between the two schemes is how the carbon dioxide is processed; in the "SOE + CO_2-Methanator", the CO_2 feeds the methanator directly where it reacts with the H_2 produced in the solid oxide electrolyser. In the "COSOE + CO-Methanator", the CO_2 is one of the two inputs of the solid oxide co-electrolyser where a mixture containing H_2 and CO is produced. The small amount of hydrogen needed to feed both SOE and COSOE has not been drawn in these schemes. All information concerning the working conditions and physical setup of the two system configurations are explained more detailed in the following sections.

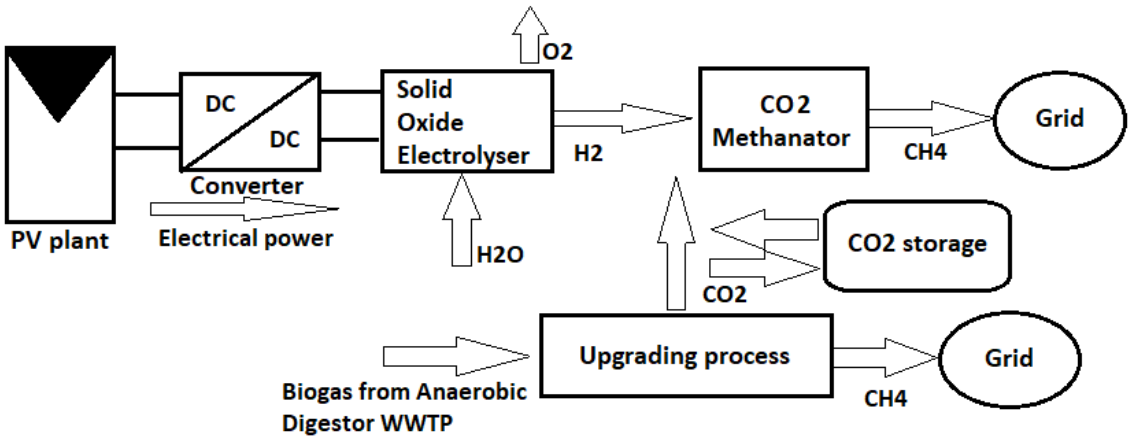

FIG: 4.1. SOE + CO_2-Methanator Scheme

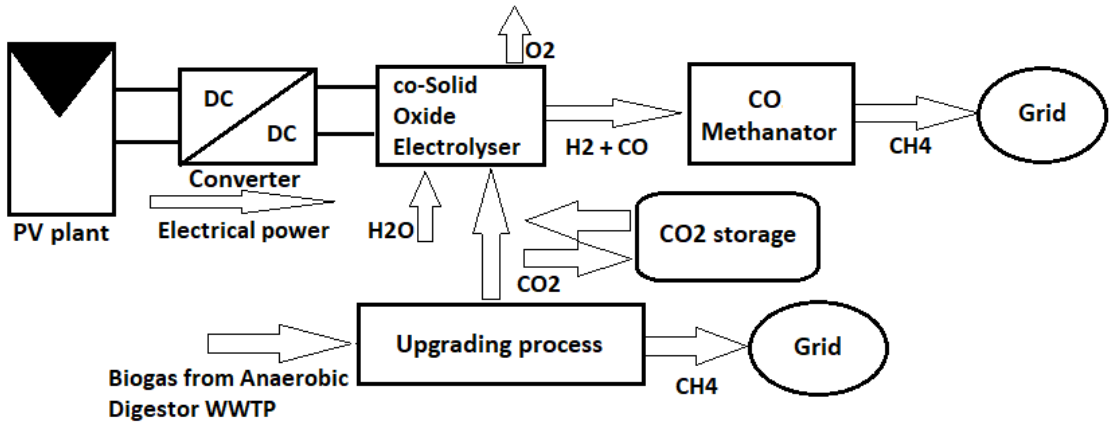

FIG: 4.2. COSOE + CO-Methanator Scheme

4.2 Power profile

At this point, it is important to understand the procedure carried out to evaluate the power profile of the PV plant and how it is converted into a current density value. As already explained in SOE and COSOE modelling, it represents one input of these systems; the current density takes the information of the power coming from the PV plant into account.

First of all, it is now explained how the power profile is obtained and this is done using a programme, named *PV*SOL* (*Valentine Energy Software*) [59]. This programme allows in a professional way to design and size photovoltaic plants in a certain location with meteorological data averaged over the last fifteen years; different libraries are available to choose PV panels, inverters and other components existing on the market.
Moreover, *PV*SOL* can provide the energy production every hour all over the year starting from the midnight of the 1^{st} January until 11 p.m. of the 31^{st} of December of a PV plant placed in a certain location. An energy profile of a PV plant, with a certain rated power, situated in Barcelona has been obtained. To perform these simulations, the PV panel indicated in [61] has been chosen: in particular, the model with the rated power equal to 300 W. Knowing the energy produced in one hour, the power produced in that hour can easily be obtained:

$$actualpower = \frac{E}{\Delta T} = \frac{E[Wh]}{1[h]}[W] \tag{4.3}$$

Furthermore, it has been observed that, knowing the nominal power, the PV production can be extrapolated in percentage per hour in this way:

$$\frac{\text{actual power}}{P_{rated}} \tag{4.4}$$

This power profile expressed in percentage contains values between 0 and 1; thus, on one hand, when the percentage is zero it means no power produced; on the other hand, when it is 1 the plant is producing the rated power. All the other values in this range define different powers produced by the plant. Furthermore, comparing different simulations, it has been noted that these profiles are so similar; thus, it has been assumed that one is valid per any rated power. As a consequence, one profile that expresses the actual power produced in percentage all over one year has been saved. Then, multiplying this profile with the rated power simulated, it is possible to determine the real power profile all over one year. Fig.5.1 compares two PV profiles in July and December.

4.3 From power to current density

Once the power profile has been obtained, this information has to be transferred to the electrolysers that operate as loads and use the electrical power to make the electrochemical reactions; between the PV plant and the electrolysers a DC/DC power converter has been added; it is able to convert one direct current source from one voltage to another one; the output voltage represents the one that can feed the load. Two different types exist: step-up or step-down [77].
However, having just the power profile information of the PV plant (no current and voltage), no more detailed studies have been carried out on this device. The operation of a DC/DC converter is, indeed, out of the scope of this thesis and thus just the power losses associated to this device are taken into account in the efficiency term ($\eta_{DC/DCconverter}$ = 0.95). Furthermore, no other power losses are taken into account in this study. It is clear that this is a simplification but, it is important to remember, that the main efforts in this work have been focused on the modelling and designing of the electrolysers and the two different methanators.

At this point, it is needed to convert the power information into current density that is the input of the electrolysers; the followed procedure is synthetized in fig.4.3. The main element is the second block drawn, that in Simulink represents a '1-D Lookup Table'. This table puts the power absorbed by the electrolyser (y-axis) and the current density (x-axis) in relationship. The power curve is obtained multiplying the power density curve of the electrolyser with the number of cells connected in series and their area. In next section 'SO-COSOE design', it is explained more detailed the size of the electrolyser and how this power curve is obtained precisely. However, for the moment, it is important to notice that this table receives as input the power value with a time discretization of 1 second. This power matches the relative current density that is the output. The current density expressed in A/cm^2 is converted in A/m^2 and then it is passed inside a filter to smooth the profile; the following block, a 'Switch' in Simulink, is needed to set the input current density equal to zero when it is very low (approximately zero). At this point, the current density value feeds the relative electrolyser and the amounts of the inlet reactants are also computed with the procedure explained in SOE/COSOE modelling sections.

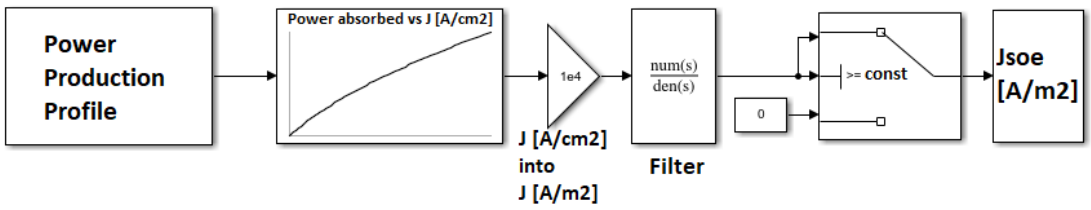

FIG: 4.3. Strategy to find out the current density from the power value

4.4 Solid Oxide Electrolyser and Co-Electrolyser design

In this section, the adopted procedure to size the solid oxide electrolyser and the solid oxide co-electrolyser is explained; the sizing is carried out according to the amounts of power that have to be processed inside these devices. It is useful to explain that the procedure is identical for the two systems. To size these systems, the cells can be connected in series and/or parallel to increase, respectively, the voltage and/or current; in this way, different amounts of power can be exploited. The electrical power is, indeed, defined in this way:

$$P = V \cdot I[W] \tag{4.5}$$

Where:

- $V[V]$ is the voltage;
- $I[A]$ is the current.

Therefore, during the sizing process, one of these two parameters can be varied to absorb different powers; however, fixing the surface of the cell (225 cm^2), the current flowing in the cell is defined. In this work, it has been decided that just a series connection of cells is performed (no parallel circuits); as a consequence, the only parameter, that can be varied to process different power profiles, is the voltage. Clearly, every time, the

rated power of the PV plant requires a different number of cells connected in series. The number of cells is evaluated through the following procedure: first of all, it is important to define the maximum working condition of the system. To do that, it has been chosen the maximum current density that the system can receive as input; through the polarization curve, the relative maximum voltage of the single cell is defined. The nominal current of the device is then easily evaluated. The nominal current-voltage values represent the operating conditions of one cell when the electrolyser is absorbing the rated power of the PV plant. Whenever the power is not the rated one, the electrolyser works with lower current and voltage defined by the polarization curve. Knowing at this point the nominal values of current and voltage, the number of cells to be connected in series is defined as follows:

$$N = \frac{P_{PV\,rated} \cdot \eta_{DC/DC converter}}{I_{cell-nominal} \cdot V_{cell-nominal}} \tag{4.6}$$

The $\eta_{DC/DC converter}$ is assumed to be 0.95.
Now it is easy to compute the power curve of the electrolyser; this curve represents, indeed, all the power values that the system can process with a certain rated power of the PV system. The power curve is obtained multiplying all the current densities (from zero to the nominal one) with the relative voltages taking also into account the area of the cells and its number. The equation synthetizes this calculation:

$$PowerCurveElectrolyser[W] = J[\frac{A}{m^2}] \cdot V[V] \cdot A[m^2] \cdot N \tag{4.7}$$

4.5 Assumptions

It has to be clarified that, due to the complexity of the whole project, a series of assumptions and simplifications have been taken into account during the modelling of these two system configurations. They are:

- The solid oxide electrolyser and the solid oxide co-electrolyser operate under isothermal conditions, precisely at 1073 K and at ambient pressure; thus, any consideration concerning the different heat fluxes (exothermic-endothermic operation or heat losses), involved in these devices, have been carried out;
- It has been assumed to have free and unlimited amounts of water and hydrogen feeding the electrolysers; this means that, whenever these flows are required, they are always available;
- It has to be noted that this project is based on a realistic WWTP placed in Sabadell (Barcelona); however, the space occupation of the PV panels has been neglected; this means that, whichever rated power can be installed and in the WWTP's site there is always enough space to host all the panels needed;
- During the designing process of the SOE and COSOE, no parallel circuits but simply a series connection of cells has been taken into account; moreover, the area of the cells has been considered constant; in this way, it has been fixed, consequently, the maximum amount of current flowing in the device; to sum up, just the operating voltage of the device has been varied every time to process the power available;

- During the simulations, apart the realistic efficiency of the DC/DC converter, no other power losses have been considered; all the PV power available is transferred to the electrolysers;
- In these plant configurations just a CO_2 storage has been implemented; no other storages, for instance batteries to store electrical power or H_2 storages, have been included; their presence may improve a lot the performances of the system allowing a better CO_2 exploitation and, probably, requiring a less amount of rated power of the PV plant;
- In the "SOE + CO_2-Methanator" system, the CO_2 storage has been designed and sized following the hydrogen production of the electrolyser; moreover, no constraints, in terms of space occupation, have been imposed: therefore, the dimensions do not represent a problem for the overall system. Another simplification adopted is that the storage is working at ambient pressure; realistically, storages of gases operate under pressure but, in this project, no costs associated to the compression have been considered;
- The CO_2 storage for the "COSOE + CO-Methanator" is sized comparing every second the CO_2 available with the CO_2 that the COSOE could process according to the power produced in that moment; similar to the other system configuration, space occupation is not taken into account and ambient pressure is the operating one;
- No costs, in terms of energy, associated to the extraction or transport of the different gas species have been considered; moreover, all the gas species are ideally processed at ambient pressure;
- The CO_2-methanator and the CO-methanator work under isothermal conditions, precisely at 633 K and at ambient pressure; as already explained for the electrolysers, no consideration on the heat that has to be removed, due to the exothermicity of the reactions, from these devices has been carried out;
- It has been assumed that the outlet mixture of the methanators can feed directly the natural gas grid, whenever it is necessary, without any restrictions on the gas composition or economical/legal constraints. Clearly, this is an important simplification because the natural gas grid has strict rules to be respected in terms of gas mixture composition. Usually, in the PtG plants, the mixture is then again processed to get an higher methane content;
- No energetic consideration, concerning the cooling down of the output mixture of the electrolysers from 1073 K to 633 K, has been performed; all the other analysis needed in a similar plant about the heat or cold required by the various fluxes to feed the different devices have been neglected;
- No economic analysis, useful to understand the investment cost of the two different system designs, has been performed.

4.6 Physical setup and working conditions of the SOE+CO_2-methanator system

In this section, the system drawn in fig.4.1 is explained more detailed showing the overall setup and the working conditions of the whole system. The same explanation is carried out for the other system configuration in following section. As already clarified, the main devices of this configuration are the solid oxide electrolyser and the CO_2-methanator. Now, step by step, the working conditions are explained:

1. The power, coming from the PV plant, feeds the solid oxide electrolyser; the reactants of this device are steam and a small amount of hydrogen. The outputs are hydrogen, oxigen and remaining steam not converted. The system works under isothermal conditions (1073K) and at ambient pressure;

2. Hydrogen and steam are then mixed with carbon dioxide, coming from the upgrading process, and they feed the CO_2-methanator;

3. The CO_2-methanator works under isothermal conditions (633K) and at ambient pressure; inside this system, through the chemical reaction presented above, H_2 and CO_2 are consumed and CH_4/H_2O are produced; the outlet is then a mixture of methane and other gases.

4.6.1 Carbon dioxide exploitation

The solid oxide electrolyser is fed with a certain power profile considering a certain time period; in the model, the time discretization used is one second and each power value is constant for one hour, thus 3600 seconds. During the simulations of the SOE model the amounts of hydrogen and steam at the outlet section are computed every second. On one hand, the carbon dioxide source is always constant; moreover, it is known that the inlet ratio H_2/CO_2 of the methanator has to be 4; thus, knowing, the mol/s of CO_2, the relative mol/s of the hydrogen needed to react are computed. Clearly, this quantity is fixed and it is evaluated through the following relationship:

$$H_2needed = CO_2source \cdot 4 = 0.1968 \cdot 4 = 0.7873[\frac{mol}{s}] \tag{4.8}$$

On the other hand, the hydrogen that is produced in the SOE is not constant all over the time but it changes according to the electrical power provided by the PV plant. Moreover, when the hydrogen production is zero or too low, a CO_2 storage has been considered to store the CO_2 in excess. On the contrary, when the H_2 production is greater than the necessary, a part of the CO_2 stored can be extracted from the storage and feeds the methanator. Now, more detailed, the four situations, that can occur during the period analysed, are illustrated.

1) No hydrogen produced

The first case is when, for instance during the night, there is no power and, consequently, no mol/s of hydrogen are produced. Fig.4.4 schematizes this case. When this situation

occurs, all the CO_2 captured during that time is stored in the CO_2 storage (green arrow); thus, the amount of CO_2 stored raises. The CO_2-methanator is not working due to the fact that no H_2 and CO_2 are feeding the device; therefore, no methane is produced.

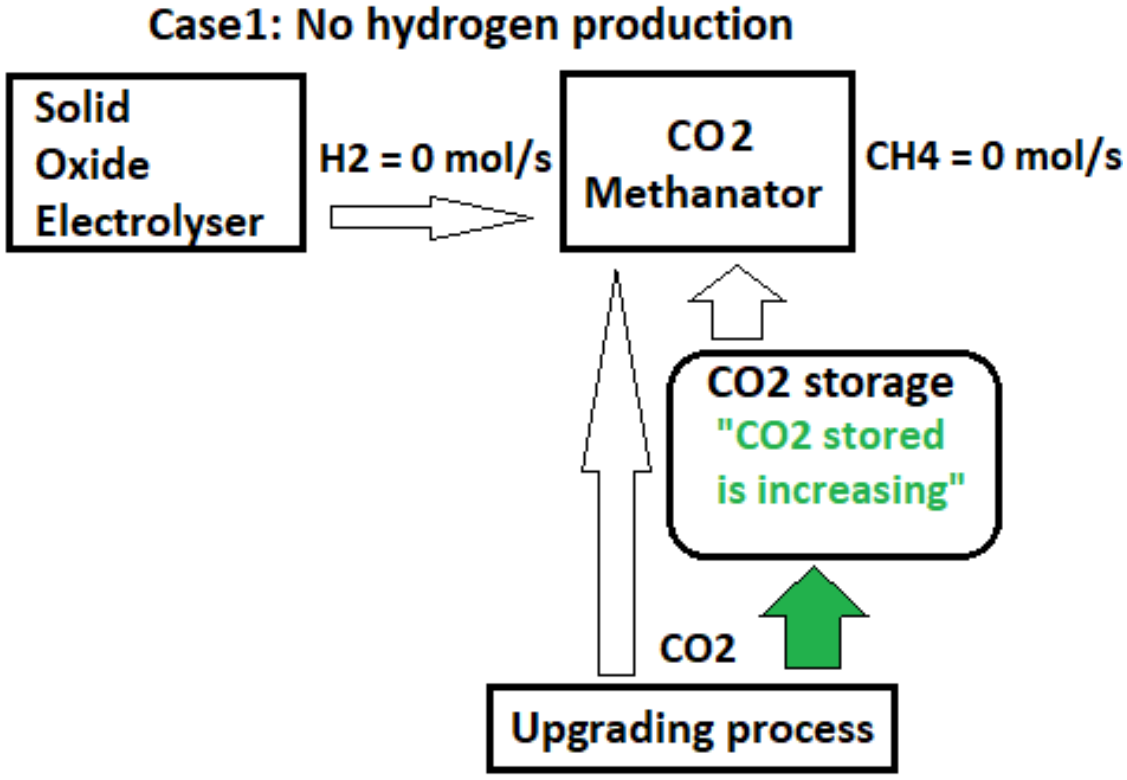

FIG: 4.4. Case1 SOE+CO_2-methanator

2) Hydrogen produced greater than hydrogen needed; CO_2 storage full enough to exploit all the H_2 produced

The second case is when the hydrogen produced is greater than the hydrogen needed to react with the mol/s of CO_2 produced. When this situation occurs, a certain amount of carbon dioxide can be extracted from the storage in order to exploit all the hydrogen available. The surplus of carbon dioxide, respect to the standard production, is evaluated through the following relationship:

$$CO_2surplus = \frac{H_2soeprod - H_2need}{4}[\frac{mol}{s}] \tag{4.9}$$

The surplus of CO_2 is, thus, taken from the storage; however, in this moment, two different situations can occur:

1. The storage contains a quantity of CO_2 greater than the surplus;
2. The storage contains a quantity of CO_2 smaller than the surplus

The first situation is analysed in this section; the second one is explained in the case 3. Thus, if the storage is full enough, all the CO_2 surplus can be extracted from the storage: the amount of CO_2 inside the storage goes down and afterwards the device is not empty. The green arrows of fig.4.5 show that the CO_2 methanator is then fed with hydrogen and carbon dioxide (normal production + surplus). To sum up, in this situation, methane is produced and all the hydrogen available is exploited.

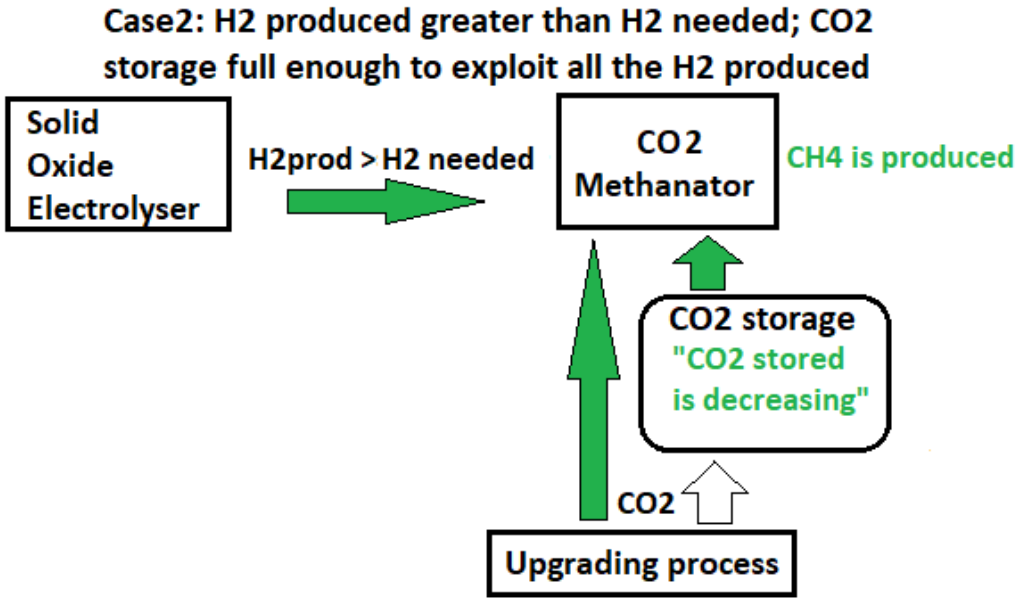

FIG: 4.5. Case2 SOE+CO_2-methanator

3) Hydrogen produced greater than hydrogen needed; CO_2 storage empty and H_2 surplus

The third case, shown in fig.4.6, is similar to the previous one; the main difference is that the amount of CO_2 stored, in that moment, is lower than the surplus required. Therefore, when this situation occurs, not all the hydrogen available is reacted, due to the lack of CO_2, and the storage is emptied. The green arrows show that the H_2 not used is considered as a surplus; in this work, no hydrogen storages are studied or other uses are considered. As a consequence, this surplus of H_2 is lost: it is assumed that it is easily released to the atmosphere without any further consideration. To conclude, methane is again produced but its amount will be smaller than case 2 due to the lack of carbon dioxide available.

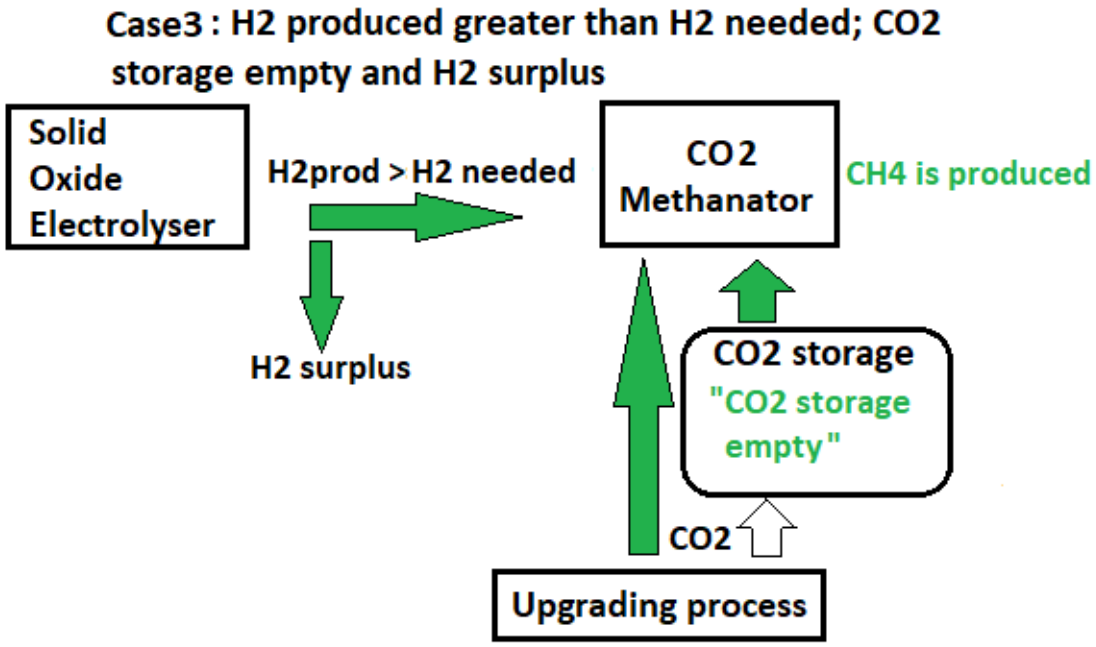

FIG: 4.6. Case3 SOE+CO_2-methanator

4) Hydrogen produced smaller than hydrogen needed

The fourth case analysed is shown in fig.4.7. This situation occurs when the hydrogen produced in the SOE is smaller than the hydrogen needed to exploit the CO_2 extracted from the upgrading process. Thus, the CO_2 is split in two flows: one stream is going to the methanator to react with the hydrogen and the remaining part is stored. The two flows are computed following these relationships:

$$CO_2 methanator = \frac{H_2 soeprod}{4}[\frac{mol}{s}] \tag{4.10}$$

$$CO_2 stored = \frac{H_2 needed - H_2 soeprod}{4}[\frac{mol}{s}] \tag{4.11}$$

Therefore, when this situation takes place, the amount of CO_2 stored increases and methane is produced too. Clearly, the CH_4 obtained is quite small: the hydrogen available is not enough to exploit, at least, the carbon dioxide captured. The green arrows in fig.4.7 help to understand the different flows. The presence of an H_2 storage may improve the methane production; in fact, if available, a certain quantity of hydrogen could be taken from the storage and reacts with the CO_2 available.

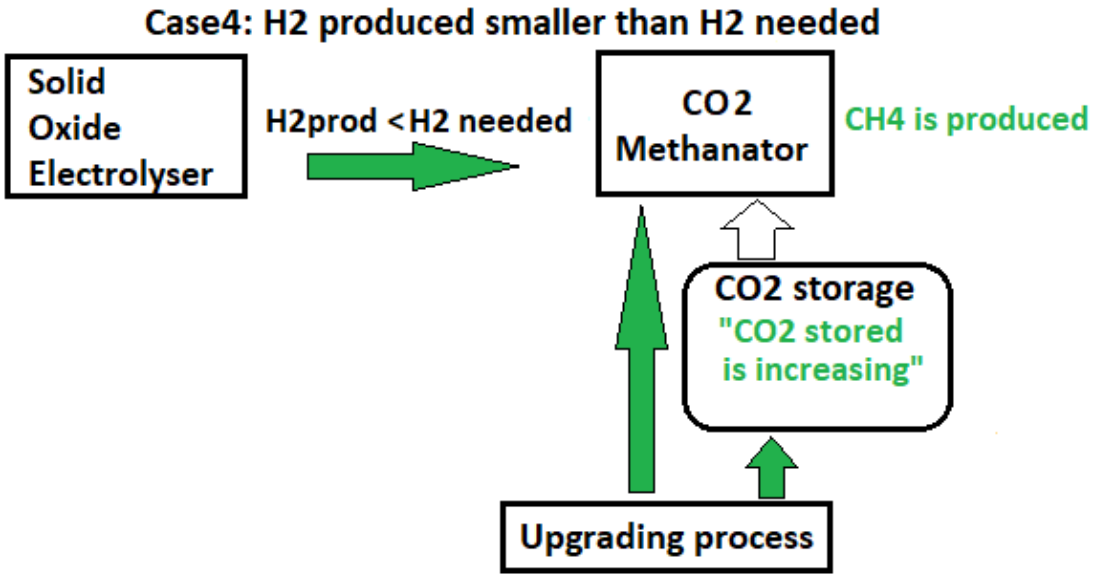

FIG: 4.7. Case4 SOE+CO_2-methanator

4.7 Physical setup and working conditions of the COSOE+CO-methanator system

In this section, the system, represented in fig.4.2, is explained more detailed showing the overall setup and the working conditions of the whole system. As already clarified, the main devices of this configuration are the solid oxide co-electrolyser and the CO-methanator. Now, step by step, the working conditions are explained:

1. The power, coming from the PV plant, feeds the solid oxide co-electrolyser; the reactants of this device are steam, carbon dioxide and a small amount of hydrogen. The outputs are mainly H_2, CO but also H_2O and CO_2 are still present; in this project two operating conditions of co-electrolyser are studied. The main difference is the desired outlet ratio H_2/CO: one model works with ratio of 3, the other with ratio of 5. The component works under isothermal conditions (1073K) and at ambient pressure;

2. The mixture feeds then the CO-methanator; this component works under isothermal conditions (633K) and at ambient pressure; through the chemical reactions presented above, mainly H_2 and CO are consumed and CH_4/H_2O are produced; therefore, the outlet is a mixture of methane, steam and other gases.

4.7.1 Carbon dioxide exploitation

The solid oxide co-electrolyser is fed with a certain power profile considering a certain time period; the time discretization used is one second and each power value is constant for one hour, i.e. 3600 seconds. This device converts, through the electrochemical reactions and WGSR, H_2O and CO_2 into H_2 and CO; at the outlet section also traces of

steam and carbon dioxide are still present. As a matter of fact, no 100% conversion of H_2O and CO_2 is realized; however, as expected, the production is expressed in mol/s and it changes according to the electrical power provided by the PV plant. As already known, the carbon dioxide production is always constant all over the time period analysed. It is important to remember that, in the "COSOE + CO-Methanator", two electrolysers with different outlet ratios (i.e. 3 and 5) are used and compared. However, the strategy adopted to exploit the CO_2 available does not depend on the ratio used and it is now explained.
First of all, the power information is converted in current density, through the procedure explained in section "From power to current density". Therefore, a profile of the current density over the time is realized; secondly, by means of the Faraday's law and the relative molar fractions, the amounts of H_2, CO_2 and H_2O needed to feed the co-electrolyser are computed. Clearly, fixed the power profile, the amounts of reactants are different in every moment. Thus, given a certain rated power and consequently the relative power profile over a certain time period, the carbon dioxide required, with time discretization equal to one second, is evaluated. At this point, the CO_2 required can be compared with the CO_2 available and four situations can occur.

1) No PV power available

The first case is when, for instance during the night, there is no power and consequently no mol/s of H_2, H_2O and CO_2 are required to feed the co-electrolyser. Fig.4.8 schematizes this case. When this situation occurs, all the CO_2 captured, from the upgrading process, is stored in the CO_2 storage (green arrow); thus, the amount of CO_2 stored raises. The CO-methanator is not working due to the lack of reactants; as a consequence, no methane is produced.

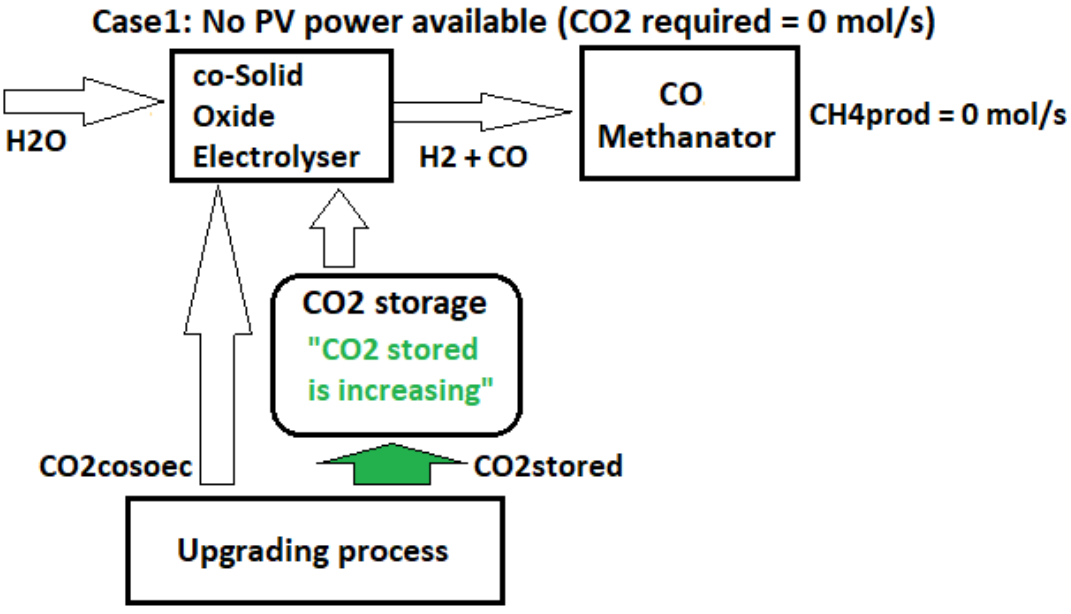

FIG: 4.8. Case1 COSOE+CO-methanator

2) Carbon dioxide produced in the upgrading process greater than carbon dioxide required by the co-electrolyser

The second case, shown in fig.4.9, takes place when the CO_2 produced is greater than the CO_2 required to feed the co-electrolyser. When this situation occurs, the CO_2 flow is separated in two stream: one goes, together with steam, to the COSOE ($CO_2cosoec$ = $CO_2required$); the remaining part is stored inside the CO_2 storage. Therefore, when this situation happens, the amount of CO_2 stored increases and methane is produced too. Clearly, the CH_4 obtained is small: the electrical power available is not enough to exploit, at least, the CO_2 coming from the upgrading process in that moment. The green arrows in fig.4.9 help to better understand the different streams.

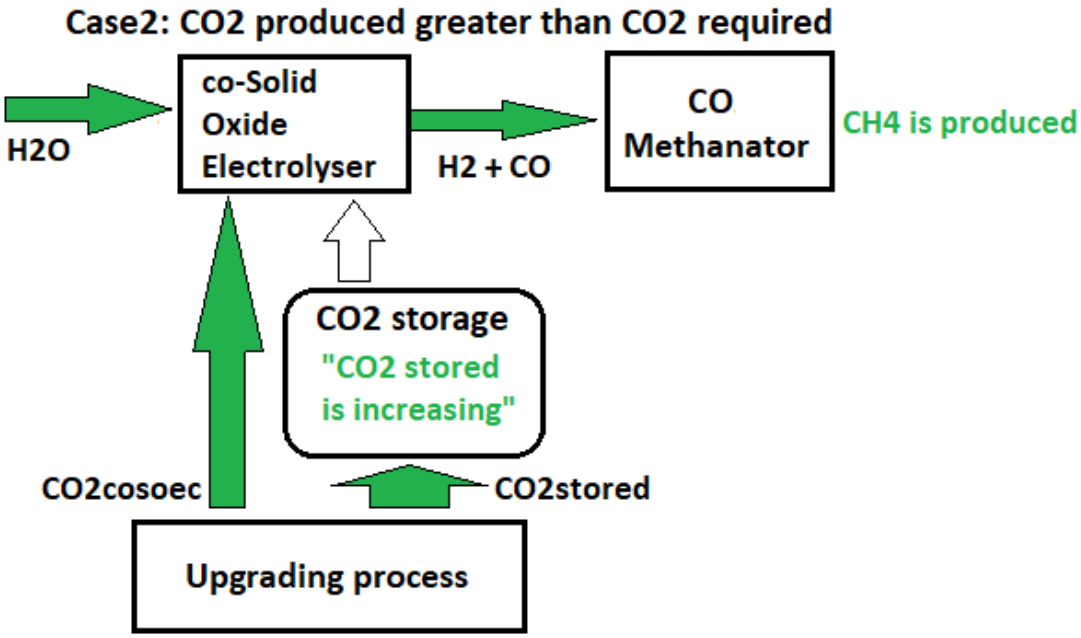

FIG: 4.9. Case2 COSOE+CO-methanator

3) Carbon dioxide required greater than carbon dioxide produced; CO_2 storage full enough to cover the CO_2 demand

The third case, shown in fig.4.10, takes place when the carbon dioxide required is greater than the carbon dioxide produced in the upgrading process. When this situation occurs, a certain amount of carbon dioxide can be extracted from the storage in order to satisfy the CO_2 demand. The surplus of carbon dioxide, respect to the standard production, is evaluated through the following relationship:

$$CO_2surplus = CO_2required - CO_2upgrading[\frac{mol}{s}] \tag{4.12}$$

The surplus of CO_2 is, thus, taken from the storage; however, in this moment, two situations can occur:

1. The storage contains a quantity of CO_2 greater than the surplus;

2. The storage contains a quantity of CO_2 smaller than the surplus.

The first situation is analysed in this section; the second one is explained in next case. Thus, if the storage is full enough, all the CO_2 surplus can be extracted from the storage: the amount of CO_2 inside the storage goes down but, afterwards, the device is not empty. The green arrows of fig.4.10 show that the co-electrolyser uses all the PV power available; moreover, all the CO_2 required is satisfied thanks to the presence of the CO_2 storage. Downstream of the COSOE, the mixture of H_2/CO and remaining traces of H_2O and CO_2 is then transferred to the CO-methanator, where methane is produced.

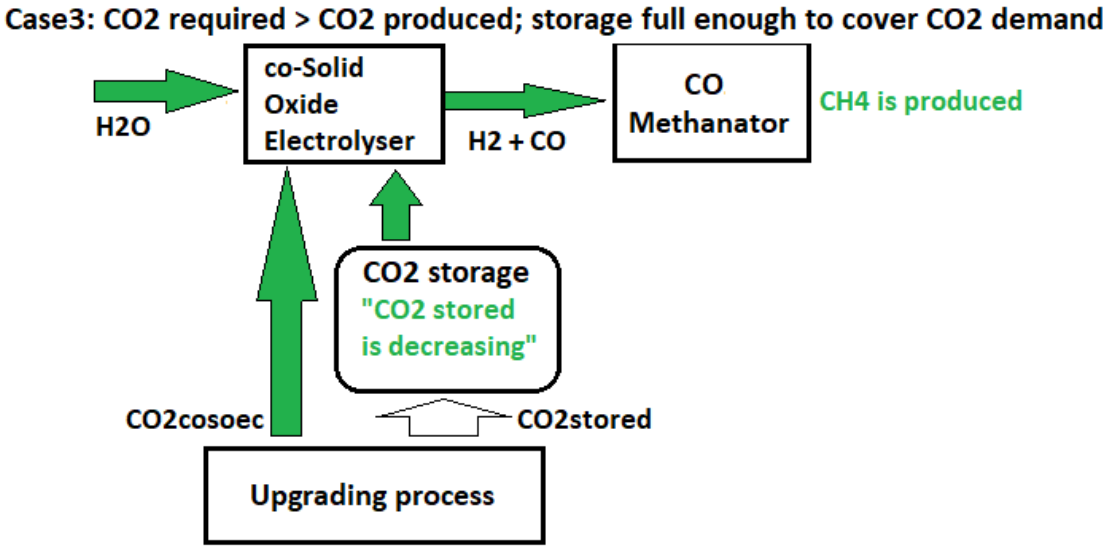

FIG: 4.10. Case3 COSOE+CO-methanator

4) Carbon dioxide required greater than carbon dioxide produced; CO2 storage empty and surplus of PV power

The last case, shown in fig.4.11, is similar to the previous case; the main difference is that the amount of CO_2 stored, in that moment, is lower than the surplus required. Thus, when this situation occurs, the CO_2 demand is not 100% satisfied and the storage, after this moment, remains empty. Furthermore, the new amounts of steam/hydrogen needed are again evaluated based on the CO_2 available. As a consequence, not all the PV power available is utilised and part of it is lost. As a matter of fact, in this work, no possible batteries or other uses of this power are considered. The green arrows show the various flows and the PV surplus. To conclude, methane is again produced but its amount will be smaller than case 3 due to the lack of carbon dioxide available.

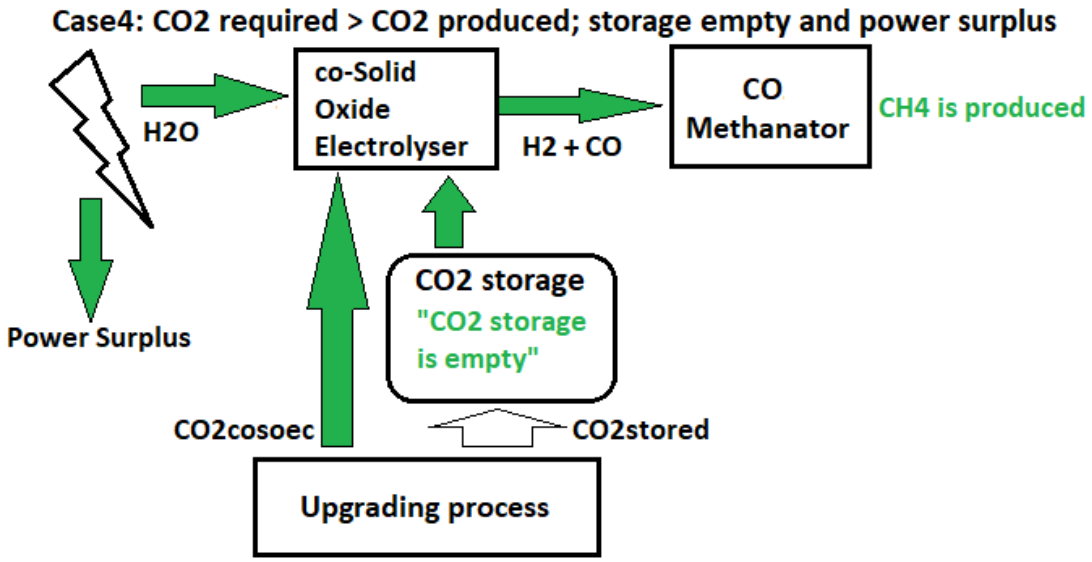

FIG: 4.11. Case4 COSOE+CO-methanator

Chapter 5

Simulations and results

5.1 Simulations 'SOE + CO_2-methanator' system

Now, in the following sections the simulations carried out in this work are presented; first of all, it has to be reminded that the power production of the PV plant of one entire year is known. Secondly, this year has been divided in two different periods: summer and winter. The first period is from 1^{st} November to 28^{th} February; the second one from 1^{st} May to 31^{st} August. Analysis and comparison between these two seasons are carried out.

5.1.1 Winter case - 100% CO_2 exploitation

The main aim of this work is to evaluate the rated power of the PV plant that allows the 100% capture of the CO_2 in the two different system configurations; in this section just the system 'SOE + CO_2-methanator' is taken into account and analysed. Moreover, as already explained above, the power production has been divided into two periods. It is clear that during the colder months the power production will be lower and, in the overall analysis, this represents the 'worst' scenario; this means that the necessary rated power during winter will be larger and also the CO_2 storage is supposed to be greater than summer case, where PV power production is higher. In fig.5.1, the PV power productions in two opposite months (July and December) are shown; as expected, during July, the power profile is almost always higher with respect to December; just few days show a larger power values during the winterly month. It has to be reminded that these profiles are averaged over some years and they do not represent the exact production every day in one year. Furthermore, it can be seen that the areas under the curve, that represents July, are greater: this means that during summer a larger number of Sun hours are available.

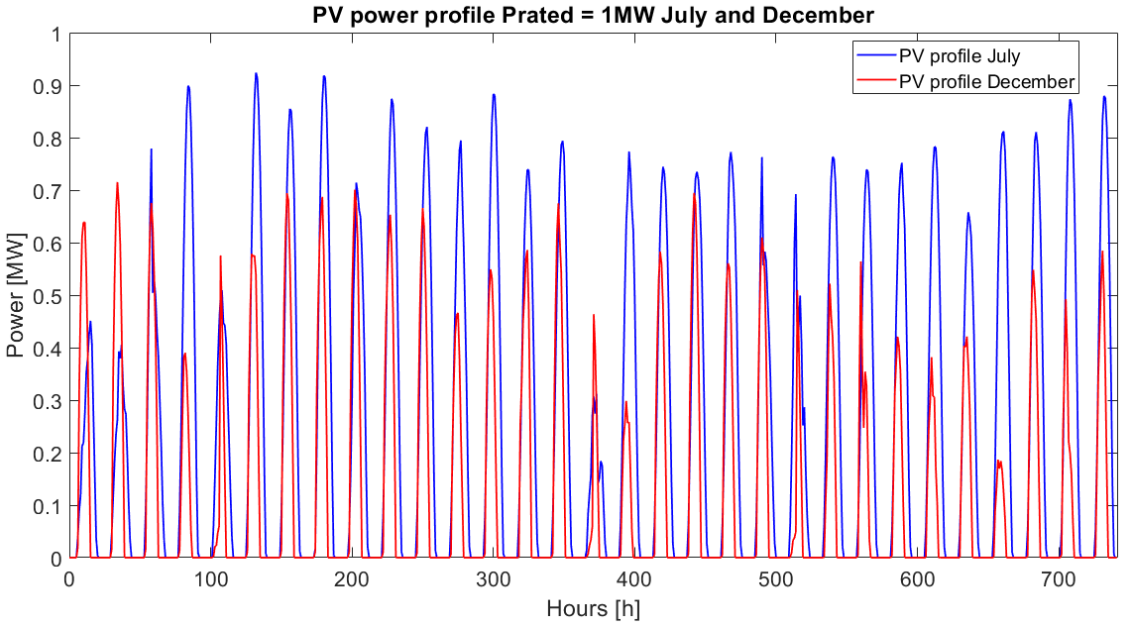

FIG: 5.1. Comparison PV profile July and December

In this section, the four months of winter period are considered and the scope is to evaluate the PV rated power and the CO_2 storage size in order to process all the CO_2 available coming from the upgrading process. To achieve this goal, several rated powers have been tested; it has to be noticed that, given the power profile, it is impossible to feed the methanator with exactly 100% of carbon dioxide; the last hours of the profile are, indeed, night hours and, consequently, without power production. In fig.5.2, considering PV powers between 1 and 2.4 MW the numbers of cells (considered constant area), to be connected in series in the SOE, are presented; as expected, increasing the power a larger number of cells is required.

PV plant size [MW]	Area cell [cm2]	Number of cells in series
1	225	2613
1.2	225	3135
1.4	225	3657
1.6	225	4180
1.8	225	4702
2	225	5225
2.2	225	5747
2.4	225	6269

FIG: 5.2. Number of cells in series

In fig.5.3, the results, according to several powers, in terms of hydrogen produced, carbon dioxide sent to methanator and storage size are presented; it can be observed that, increasing the rated power of the PV plant, there is a larger H_2 production but, on the opposite, the percentage of H_2 used decreases; as a matter of fact, having a larger PV plant, the H_2 produced grows but, consequently, the number of hours where there is a

surplus increases. In these hours there is more hydrogen than CO_2 available and it is assumed that this surplus is lost. Moreover, as expected, increasing the PV plant, the storage size goes down and the CO_2 processed grows; this trend is valid until 2 MW; after that, even if the PV plant becomes larger, the amount of CO_2 processed does not change; the only advantage, that can be achieved, is a further reduction in terms of storage size. It is clear that an economic analysis should be carried out in order to evaluate if it is more convenient having a larger PV plant and a smaller storage size or the opposite situation. However, in this work, this analysis is not present; thus, it is suggested to install a PV plant with a rated power of 2 MW and a storage with a capacity of 909 m^3 to cover the CO_2 produced during the winterly period. In fig.5.4, the total amounts of CO_2 and H_2 produced and then processed in the methanator with a PV plant rated power of 2 MW are presented. It is useful to highlight that the total amount of carbon dioxide available during winter is:

$$CO_2available = 2.04 \cdot 10^6[mol] \tag{5.1}$$

PV size [MW]	H2 prod [mol]	CO2 meth[mol]	H2 used [%]	CO2 used [%]	CO2 storage size [m3]
1.0	5.61·10^6	1.40·10^6	99.7	68.5	14276
1.2	6.74·10^6	1.68·10^6	99.5	82.1	8216
1.4	7.86·10^6	1.95·10^6	99.4	95.7	3871
1.6	8.98·10^6	2.03·10^6	90.5	99.6	1937
1.8	1.01·10^7	2.03·10^6	80.5	99.7	1127
2.0	1.12·10^7	2.04·10^6	72.5	99.8	909
2.2	1.23·10^7	2.04·10^6	66.0	99.8	822
2.4	1.40·10^7	2.04·10^6	58.0	99.8	692

FIG: 5.3. Results comparing different rated powers during winter

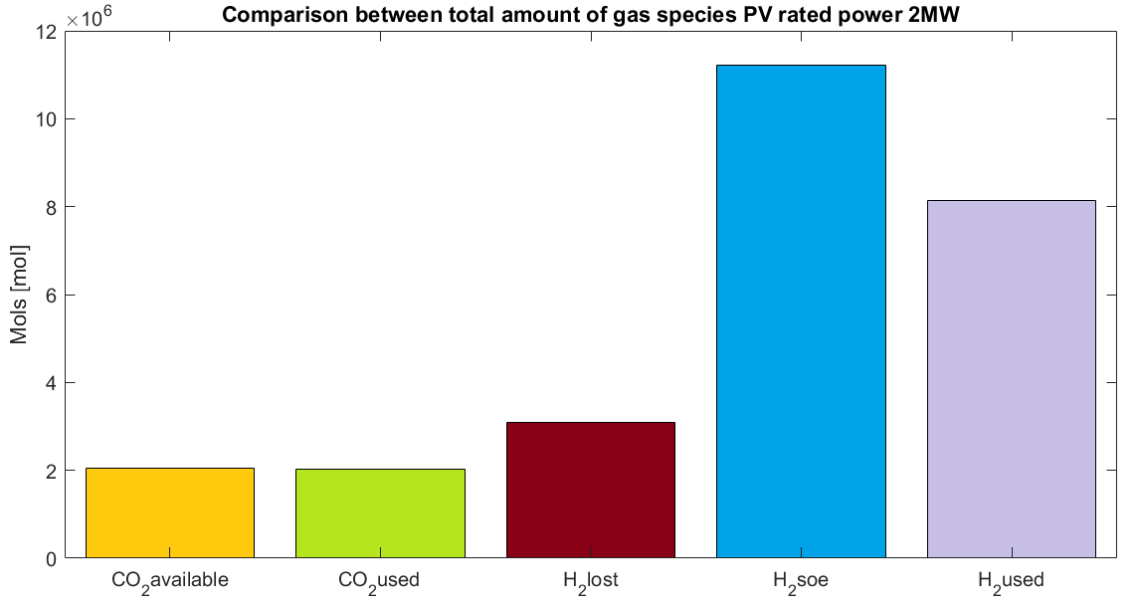

FIG: 5.4. Comparison between CO_2 and H_2 produced and used

In fig.5.5 and 5.6, the comparison between the PV power profile and the amount of

CO_2 stored during the winter is presented; it can be observed that the trend is the following: during the nights, without PV power, the CO_2 stored increases and then it goes to zero during the daylight hours. In some days this trend is not respected because the power produced is too small and part of the carbon dioxide available has to be stored.

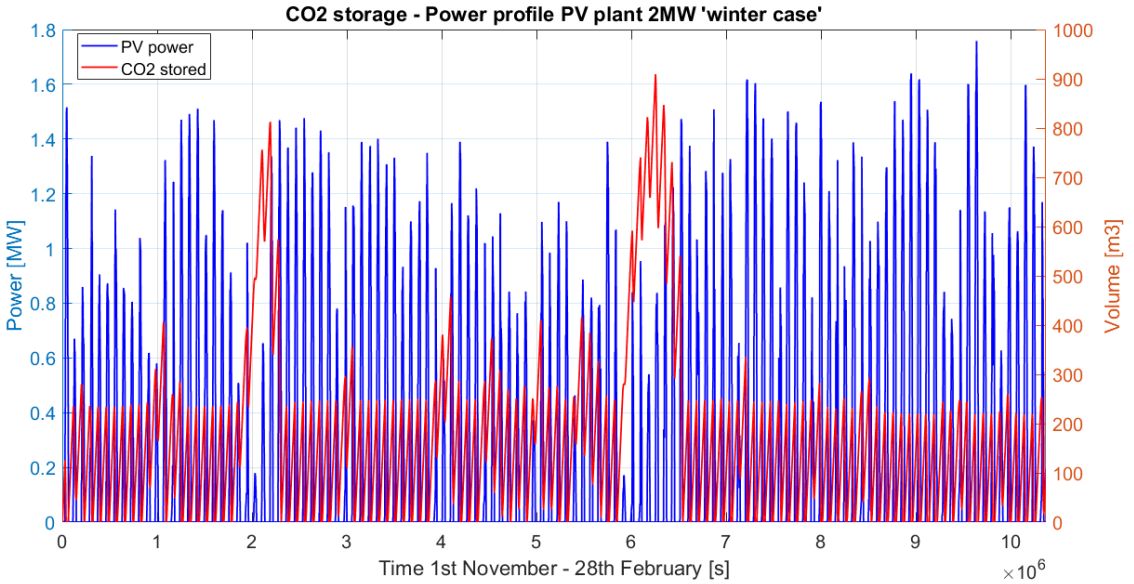

FIG: 5.5. CO_2 stored and PV power profile during winter

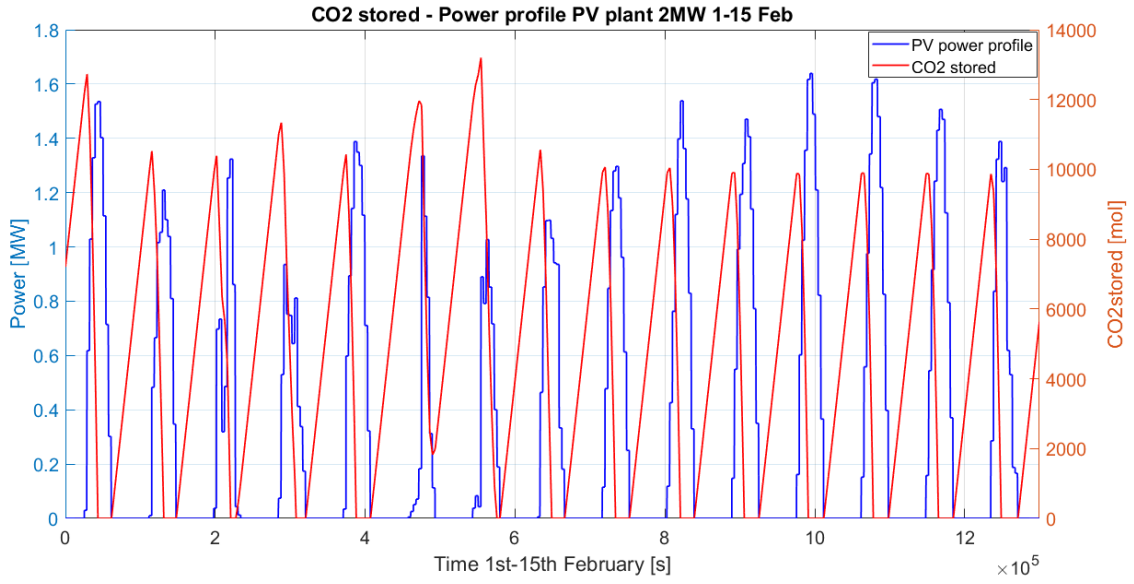

FIG: 5.6. CO_2 stored and PV power profile during first two weeks in February

In fig. 5.7 and 5.8, the H_2 and CO_2 molar flows are presented considering two weeks in December and January: particularly, the green curve represents the outlet H_2 of the solid oxide electrolyser and the blue one the amount of CO_2 that should react to consume all the hydrogen produced in that moment. When there is no H_2 surplus , this curve

matches exactly the black one that indicates the H_2 that feeds the CO_2-methanator. However, in some hours, the CO_2 available is not enough to react with the H_2 produced and a mismatch between black and green curves is evident; when this situation occurs, the CO_2 available and, thus feeding the methanator, is represented by the red curve, that has a flat shape. This behaviour is more frequent in January when the PV production is larger.

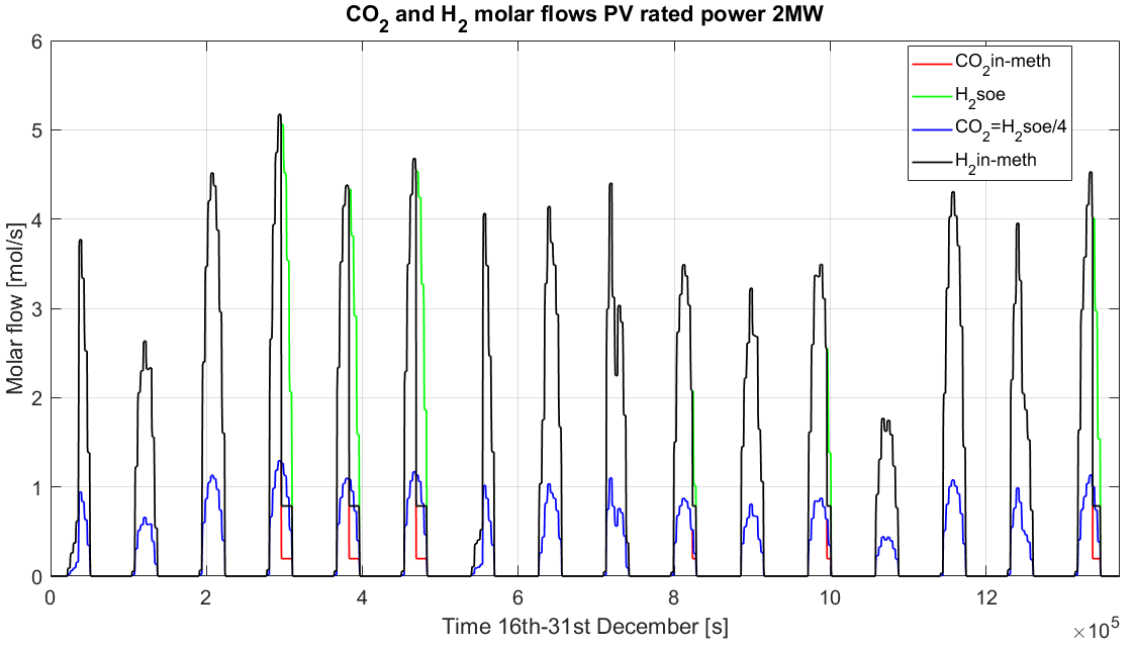

FIG: 5.7. Comparison between H_2 and CO_2 molar flows

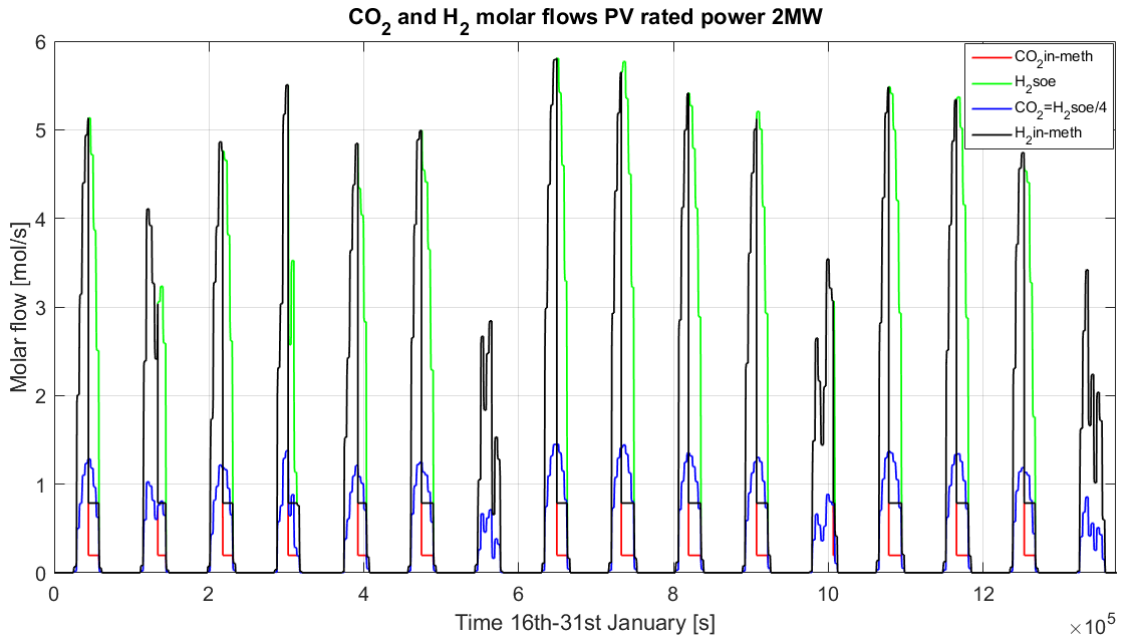

FIG: 5.8. Comparison between H_2 and CO_2 molar flows

At this point it is important to figure out the dimensions and the operating conditions

of the CO_2 methanator used in these simulations. In fig.5.9, the main characteristics of this device are summarized; it has been observed that, during all simulations performed in this work, the reactions are completely developed; in particular, the worst case (highest amount of inlet mixture) has been tested. The system is, then, able to provide the correct amounts of outlet mixture produced. For smaller inlet mixtures, the component could be oversized. However, no economic analysis is carried out and no further considerations have been done. The same dimensions and operating conditions have been chosen for the CO-methanator too.

Reactor dimensions and operating conditions CO2-methanator	
Length [m]	10.57
Inner diameter [m]	2.44
Outside diameter [m]	2.64
Number of tubes	336
Tube diameter [m]	ID = 0.092, OD = 0.102
Tube length [m]	6.86
Catalyst mass [kg]	1500
Temperature [K]	633
Pressure [bar]	1

FIG: 5.9. Methanator dimensions and operating conditions from open literature (Davis, 1981)

It has been considered that the catalytic reactions occur inside the tubes where the catalyst is present. The whole active volume has been computed with this formula:

$$ActiveVolume = \frac{\pi \cdot ID^2}{4} \cdot Tubelength \cdot NumberTubes \tag{5.2}$$

$$ActiveVolume = \frac{\pi \cdot 0.092^2}{4} \cdot 6.86 \cdot 336 = 15.32[m^3] \tag{5.3}$$

In fig. 5.10, the inlet molar flows that feed the methanator in the first two weeks of November are plotted; as already explained in the modelling of CO_2-methanator, there are three inputs: steam water, hydrogen and carbon dioxide. It has to be noticed that when there is lack of CO_2 and, consequently, H_2 surplus there is an amount of steam water in excess as well. It has been decided that, similarly to H_2, a part of steam water is lost keeping always fixed the output molar ratio H_2/H_2O equal to 5.

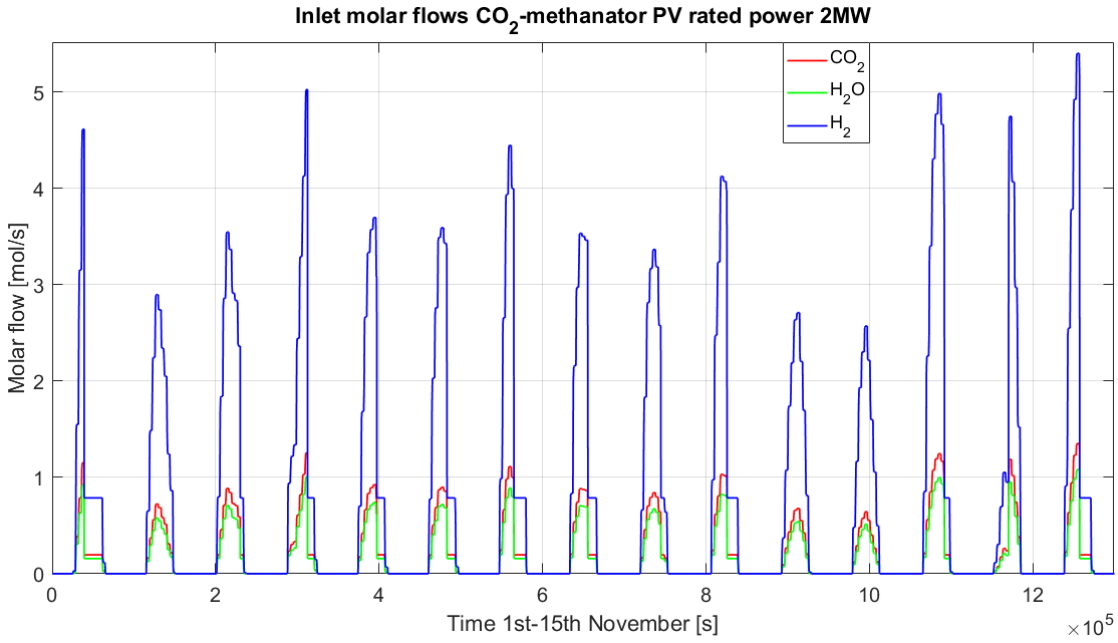

FIG: 5.10. Inlet molar flows CO_2-methanator

In fig.5.11, the total amounts of outputs of the methanator during the whole winterly period are presented; as expected, CH_4 and H_2O are produced and, on the contrary, CO_2 and H_2 are totally consumed. No traces of CO have been found. Morever it can be commented that the relative molar fractions among the outputs are: $73.5\%H_2O$, $26.25\%CH_4$ and $0.25\%H_2$. Almost all the CO_2 at the inlet has been converted into methane; thus, the methanator works with a quasi-ideal efficiency of 100%. Furthermore, in fig.5.12, the outlet molar flows of the methanator are shown during two weeks in December; the exiting hydrogen is negligible and the predominant flows are methane and steam water. As already highlighted in the modelling section, the methane is produced mainly through the CO_2 methanation reaction and the remaining through the CO methanation process; in fact, the reverse of WGSR takes place and CO is produced inside the device. The steam water derives mainly from the CO_2 methanation reaction; two lower equal contributions are due to the other two reactions involved that are in equilibrium. In fig. 5.13 and 5.14, other comparison between inlet and outlet flows are shown.

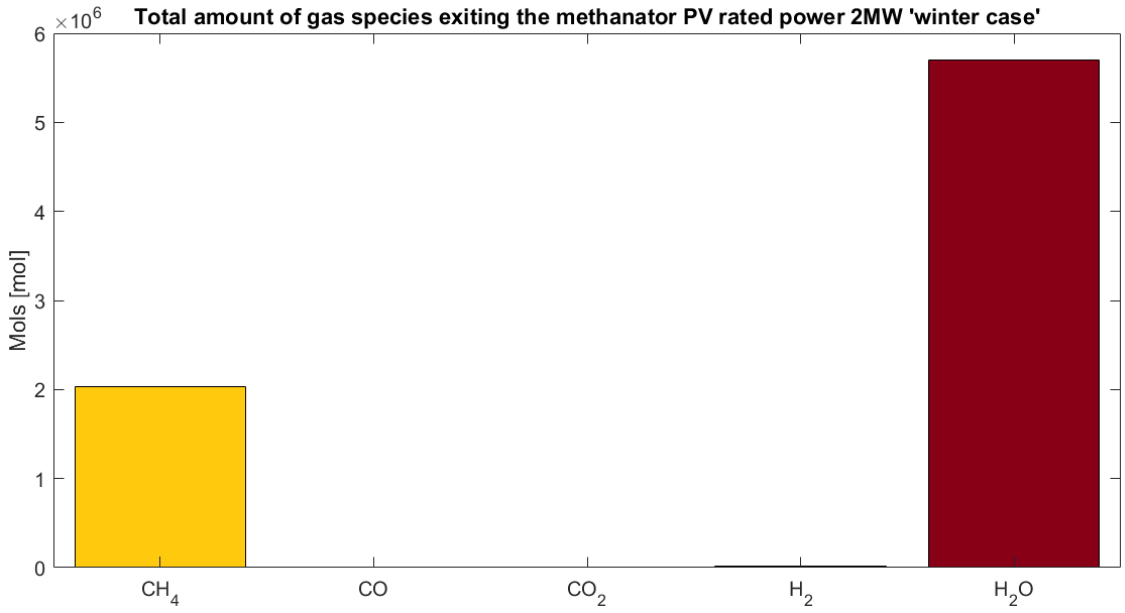

FIG: 5.11. Total amounts of outputs CO_2-methanator during winter

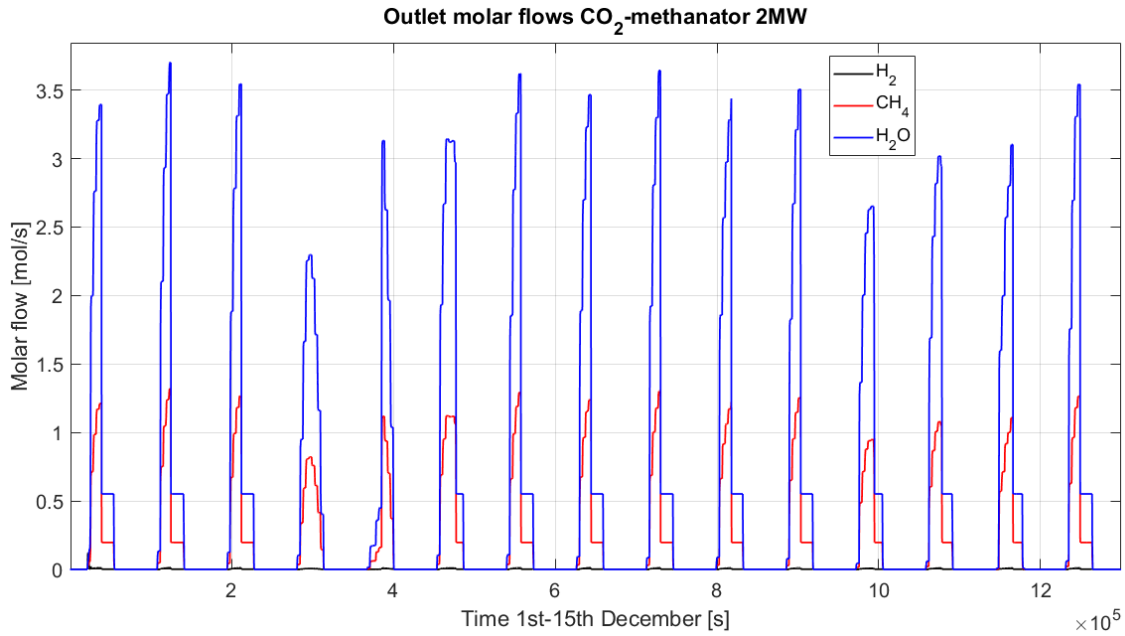

FIG: 5.12. Outlet molar flows CO_2-methanator

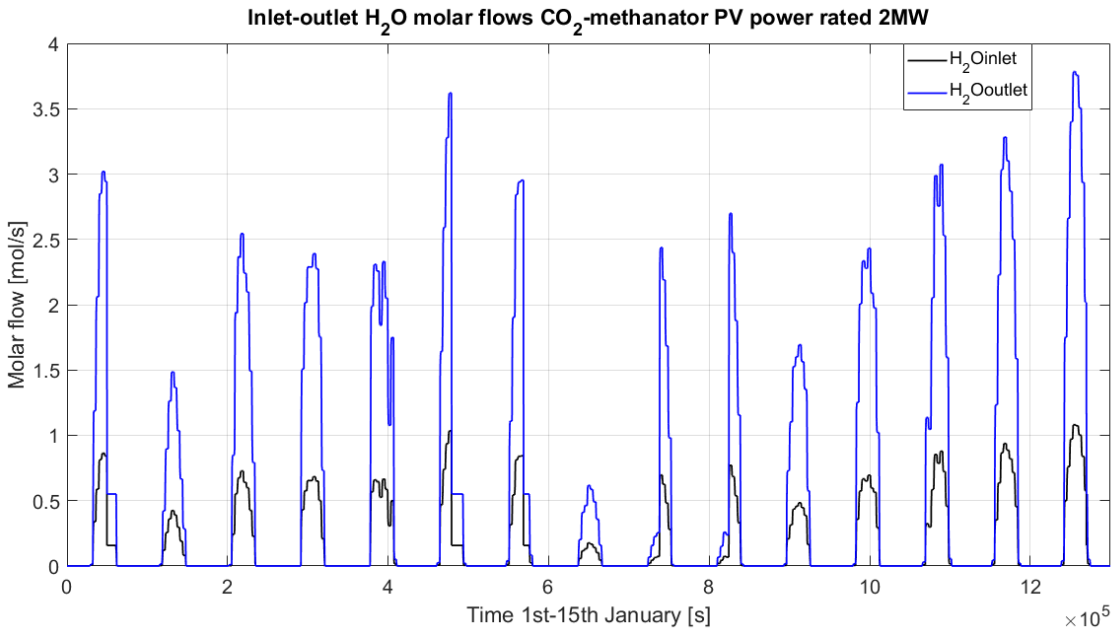

FIG: 5.13. Inlet-outlet steam water CO_2-methanator PV power rated 2MW

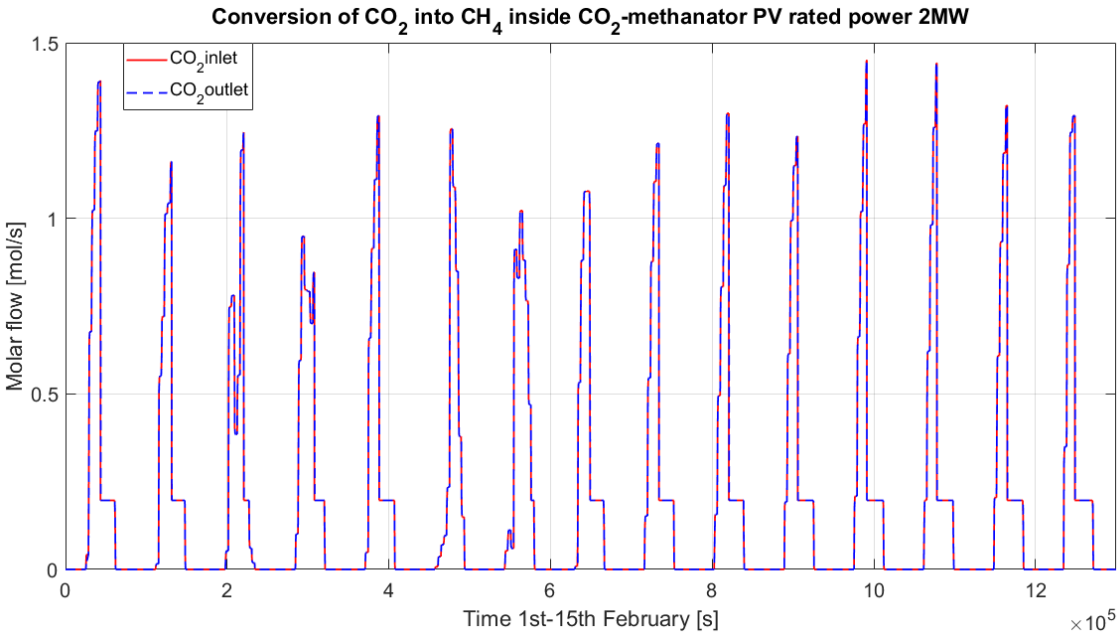

FIG: 5.14. Inlet CO_2 converted into CH_4 inside the methanator

5.1.2 Summer case - 100% CO_2 exploitation

In the first part of this section, the idea is to present the results in terms of hydrogen used, carbon dioxide processed and storage size for the summer period when the PV plant rated power is the one that allows 100% CO_2 conversion during winter, thus 2MW. In fig. 5.15, all data are summarized; it can be seen that this PV plant for the summer case is widely oversized; in fact, more than 50% of H_2 produced is a surplus. Moreover, the storage size

is almost half of the capacity required for the winter case. However, looking at fig. 5.16, the capacity of this device may also be chosen around 200 m^3 because a larger storage is required just to host the CO_2 for few days; it is clear that part of the CO_2 would be lost but great savings in economic terms would be reached. In fig. 5.17, the different amounts of hydrogen and carbon dioxide produced and processed are presented.

PV size [MW]	H2 prod [mol]	CO2 meth[mol]	H2 used [%]	CO2 used [%]	CO2 storage size [m3]
2.0	1.97·10^7	2.09·10^6	47.1	99.7	456

FIG: 5.15. Results during summer case with a PV rated power 2MW

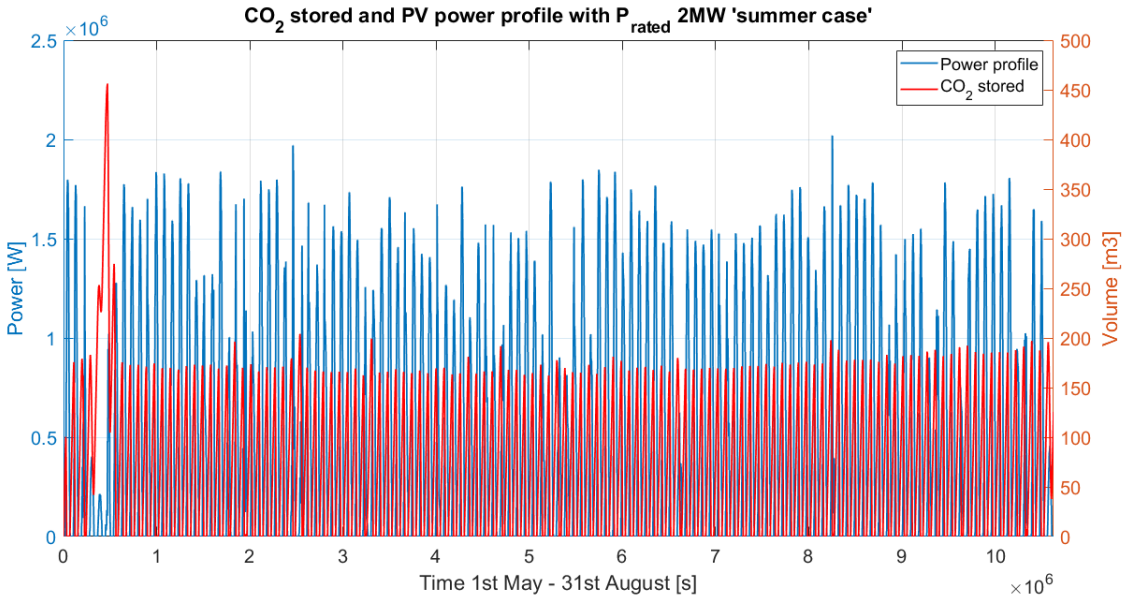

FIG: 5.16. CO_2 stored and PV power profile during summer

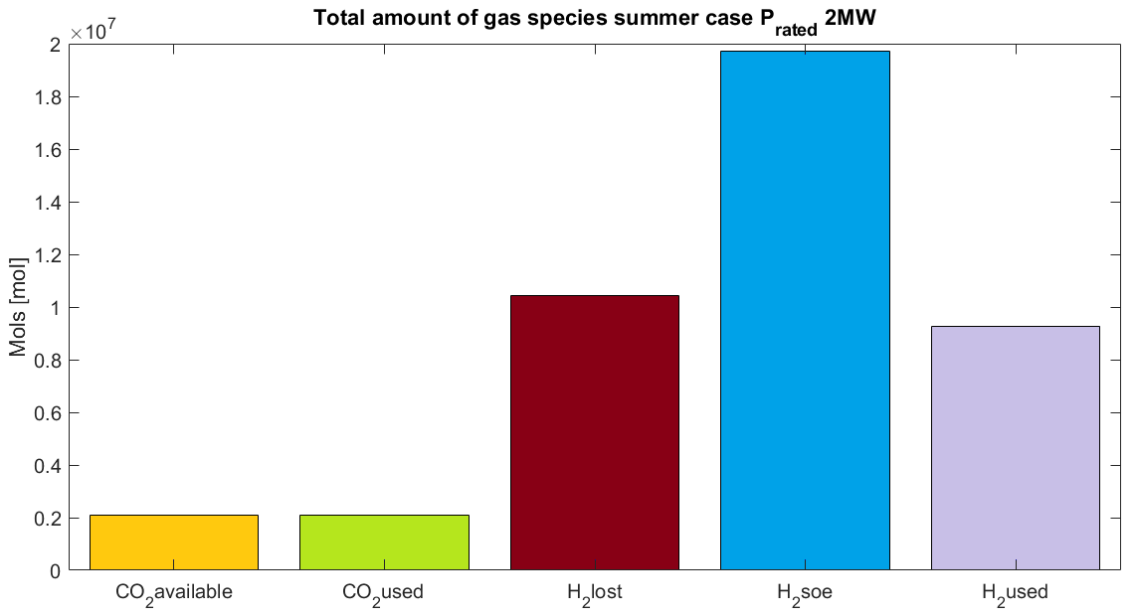

FIG: 5.17. Comaparing between CO_2 and H_2 produced during summer

Now, the PV rated power to exploit as much CO_2 as possible, assuming the system working just during summer, is searched. The total amount of carbon dioxide available during summer is:

$$CO_2available = 2.092 \cdot 10^6[mol] \tag{5.4}$$

As already done for the winter case, different powers have been considered. Looking at fig.5.18, the simulations carried out and the results are presented. It has been chosen 1.2MW as the power to be installed in the PV plant. It is true that this is not the maximum percentage of CO_2 processed but, on the other side, it allows to limit the H_2 surplus equal to around 28%. In fig.5.19 and 5.20, the different amounts of gases before and after the methanation process are highlighted. The molar fractions after the methanator are: 71.4% H_2O, 25.3% CH_4 and 3.3% H_2; the conversion of carbon dioxide into methane is 99.8%. The other reasonings carried out for the methanation process in the winter case are still valid and, for brevity, are not again reported here.

PV size [MW]	H2 prod [mol]	CO2 meth[mol]	H2 used [%]	CO2 used [%]	CO2 storage size [m3]
0.8	7.89·10^6	1.96·10^6	99.6	93.9	2845
1.0	9.86·10^6	2.08·10^6	85.2	99.3	870
1.2	1.18·10^7	2.08·10^6	72.5	99.4	700
1.5	1.48·10^7	2.08·10^6	59.8	99.5	595
1.8	1.77·10^7	2.08·10^6	51.3	99.7	511
2.0	1.97·10^7	2.09·10^6	47.1	99.7	456

FIG: 5.18. Comparison between H_2 and CO_2 produced and processed

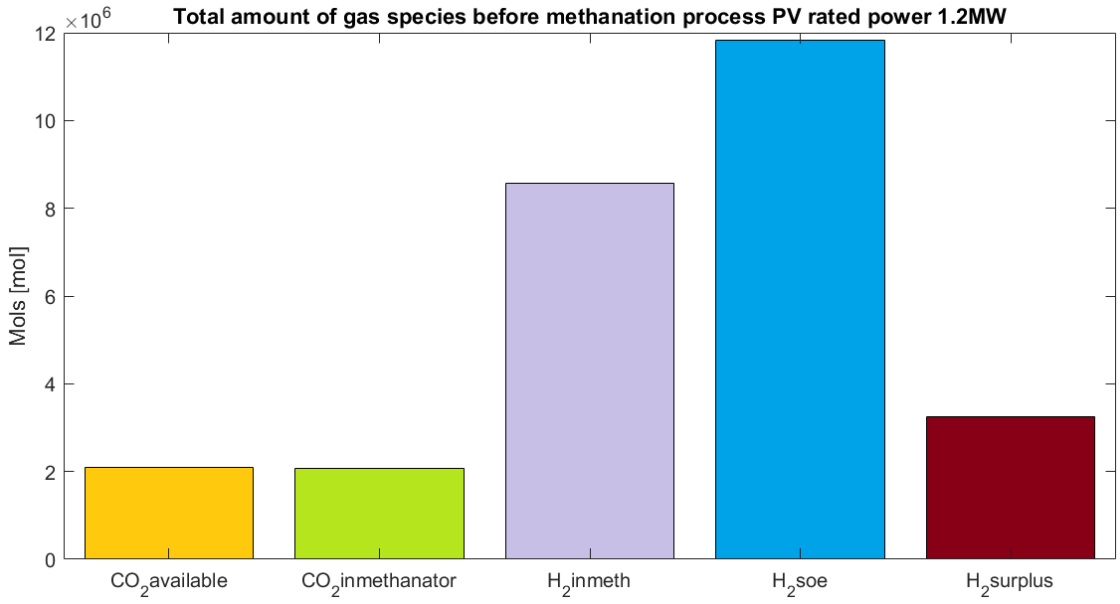

FIG: 5.19. Comparison between H_2 and CO_2 produced and processed

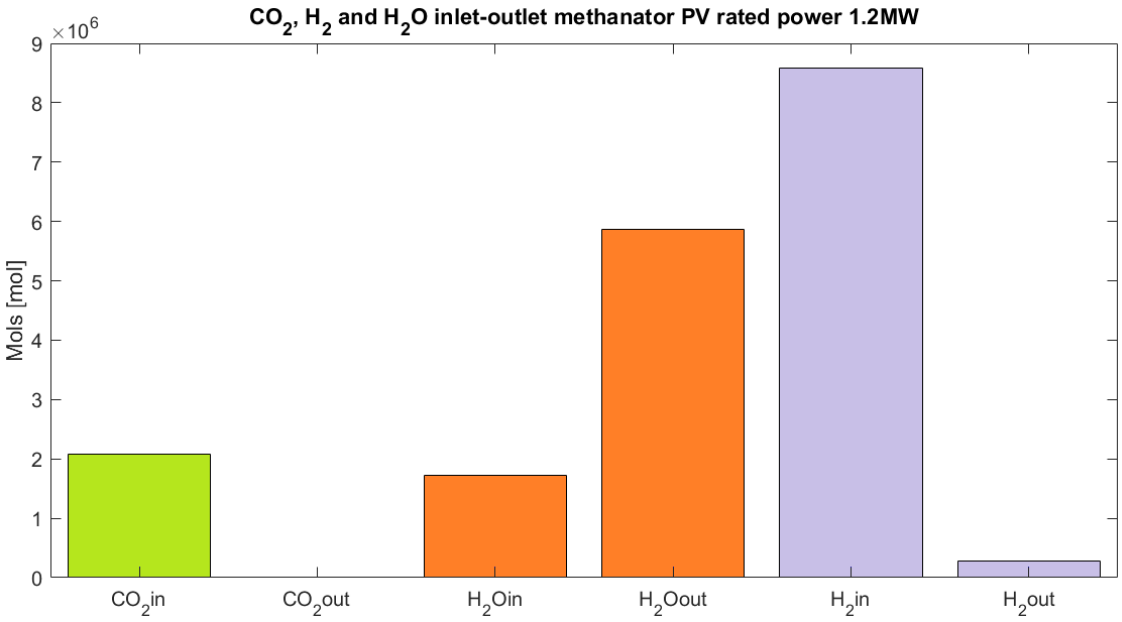

FIG: 5.20. Comparison between inlet and outlet methanator summer case

5.2 Simulations 'COSOE + CO-methanator' system

5.2.1 Comparison different outlet H_2/CO-ratio co-electrolyser

In this section, the system 'COSOE + CO-methanator' is analysed. Firstly, a comparison between the system, where the co-electrolyser works with different output ratio (i.e. 3 or 5) is carried out. The main scope is to determine which one produces the greatest amount of methane. This comparison is carried out considering two weeks and the same rated power of the PV plant. Furthermore, there are no constraints in terms of steam water, carbon dioxide and hydrogen required to feed the co-electrolyser; in other words, in this particular study, the real amounts of CO_2 available in that time period do not influence the operation of the system. The PV rated power chosen is 1MW and the period is the two first weeks in December. In fig. 5.21, the different amounts of CO_2 and H_2O feeding the co-soe in the two different situations are shown. As already explained in modelling section, to reach the proper output H_2/CO different molar fractions are needed at the input. Particularly, in the case of ratio 5, a lower amount of CO_2 and a greater amount of H_2O are needed with respect to output ratio equal to 3.

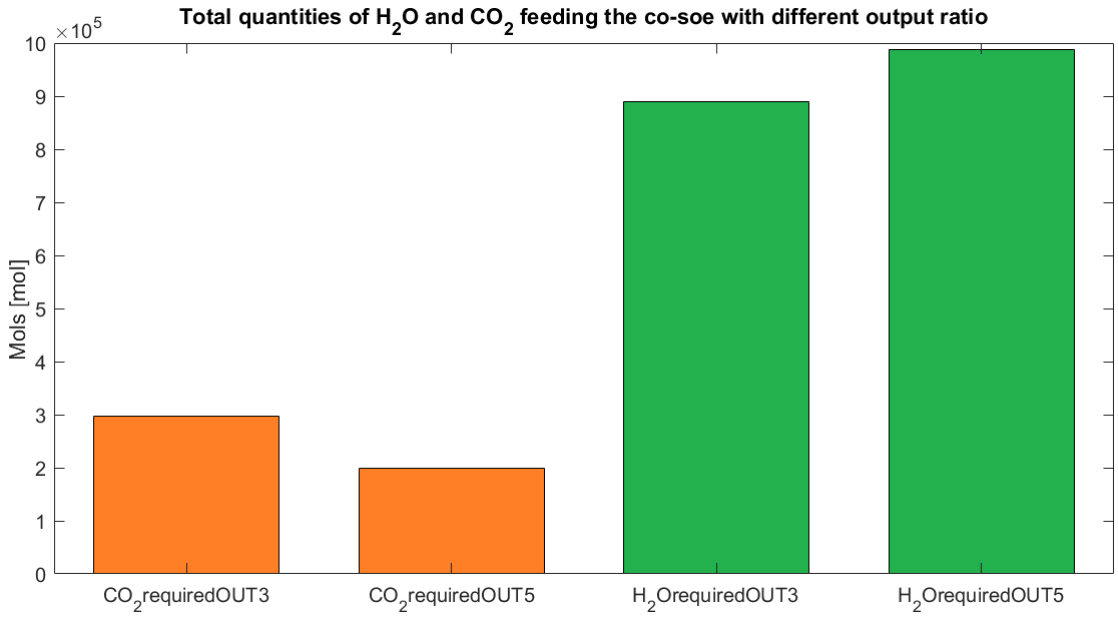

FIG: 5.21. Comparison between H_2O and CO_2 needed for co-soe

In fig.5.22, the H_2 and CO COSOE outflows are presented. Furthermore, looking also at fig.5.23, the total quantities produced by the COSOE are visible. Firstly, it can be noticed that the H_2 is the predominant quantity in both cases. Secondly, considerable amounts of H_2O and CO_2 are still present. Then, just considering carbon oxides, it is clear that their total quantity is greater in the case with ratio of 3.

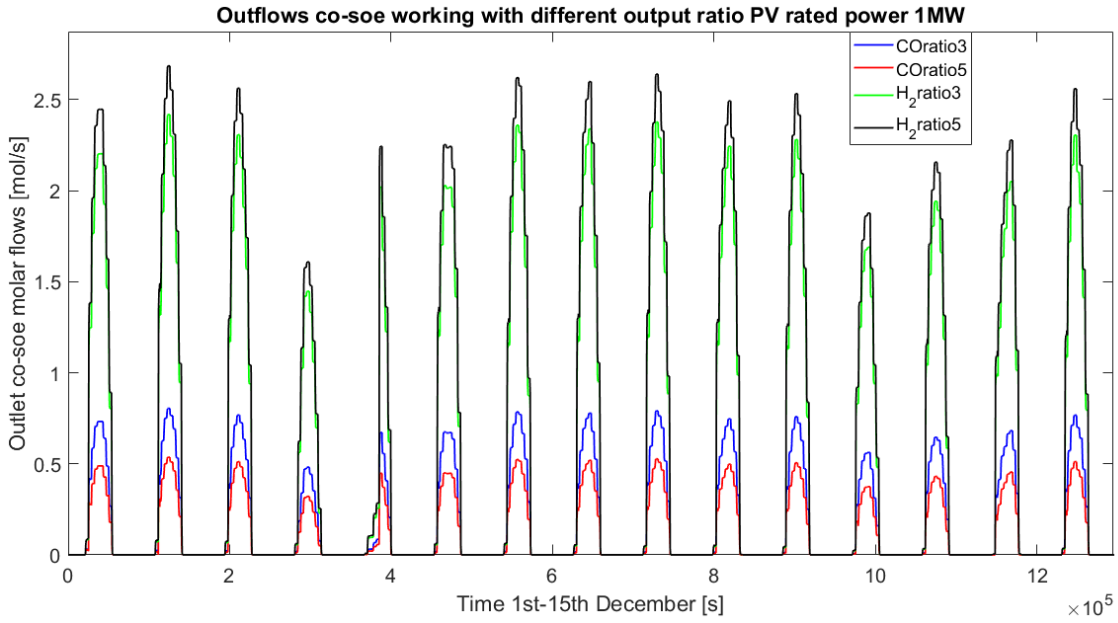

FIG: 5.22. Comparison between outflows co-soe different H_2/CO

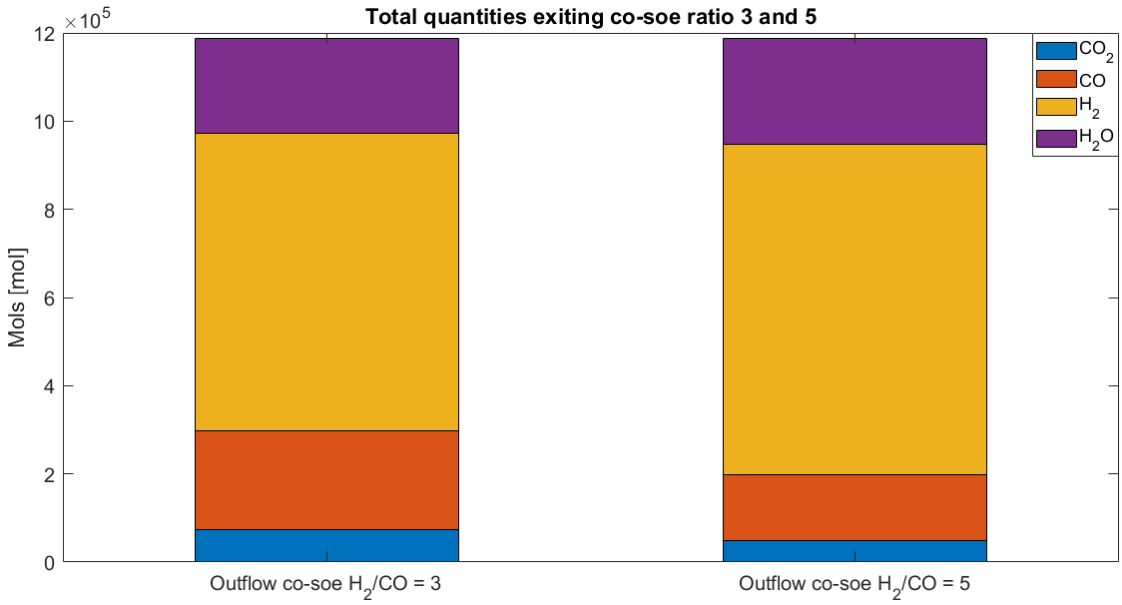

FIG: 5.23. Comparison between total outputs co-soe different H_2/CO

The total amounts exiting the CO-methanator are highlighted in fig.5.24. The CO-methanator dimensions and operating conditions are reported in 5.9. It is evident that, in this work, with the coupling of a COSOE and a CO-methanator, the best operating ratio is 3. A larger amount of methane is, indeed, produced. However, it has to be commented that with ratio of 3 the inlet-outlet CO_2 is almost the same; with this configuration, inside the methanator, the predominat reaction is the CO methanation and the effect of WGSR is quasi-negligible. In the other situation, the reverse of the WGSR plays an important role; the CO_2 is totally converted in new CO that produces other methane through CO-

methanation. At the output, there is a surplus of H_2 that has not reacted. To conclude in both cases all the CO is consumed.

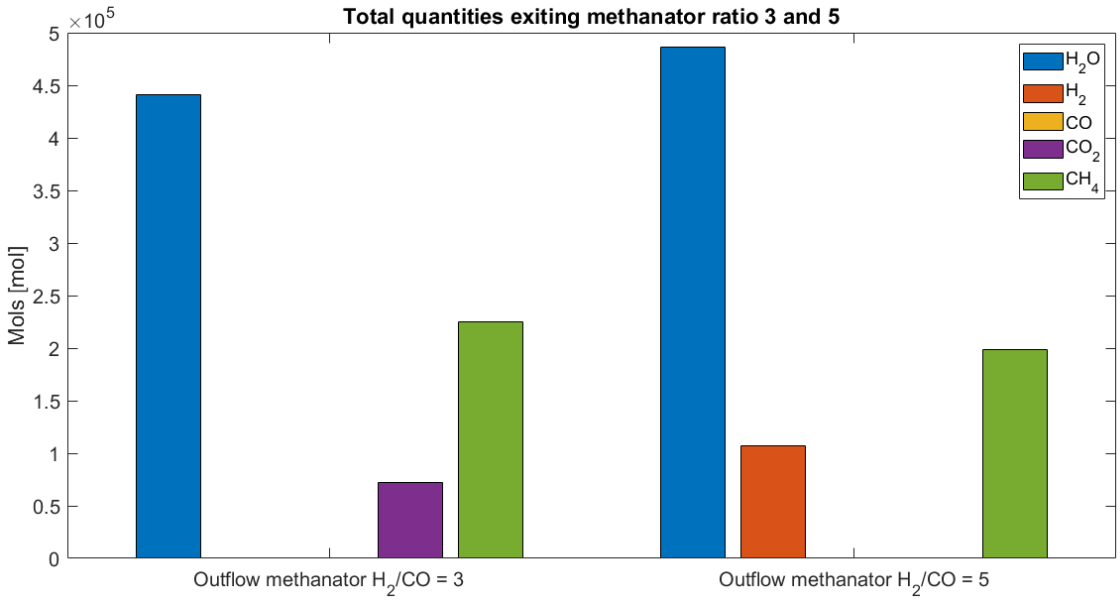

FIG: 5.24. Comparison between total outputs methanator different H_2/CO

5.2.2 Winter case - 100% CO_2 exploitation ratio 3

In this section, the goal is to evaluate the PV rated power that allows 100% CO_2 during winter considering the system "COSOE + CO-methanator"; firstly, the output COSOE ratio between H_2 and CO equal to 3 is analysed. In fig.5.25, different PV rated powers are studied and some results are presented. Looking at this table, the reasonable PV rated power to be installed is 1.2 MW. It is true that, with 1.4 MW, a better exploitation of CO_2 is reached but the increment is very very small. Furthermore, with 1.2 MW, it can be noticed that there is a CO_2 lack equal to almost 29%; this means that there is a surplus of power due to the fact that there is no enough CO_2 available.

PV size [MW]	Cells co-soe	CO2 co-soe[mol]	H2O co-soe[mol]2	CO2 used [%]	CO2 lack [%]	Storage size [m3]
0.8	2587	1.74·10^6	5.20·10^6	85.4	0.45	7055
1.0	2613	2.03·10^6	6.07·10^6	99.6	7.70	2258
1.2	3135	2.03·10^6	6.07·10^6	99.7	29.05	995
1.4	3657	2.04·10^6	6.10·10^6	99.8	50.42	864
1.6	4180	2.04·10^6	6.10·10^6	99.8	71.88	733
1.8	4702	2.04·10^6	6.10·10^6	99.8	93.33	625

FIG: 5.25. Comparison between different PV rated powers winter case ratio 3

In the following figures the results of the whole system can be appreciated. Particularly, in fig. 5.26, the power profile and the CO_2 stored during the winterly period are shown. Secondly, in fig.5.27, the comparison between the CO_2 available and used is highlighted; the red curve represents the CO_2 needed according to the power available. On the other side, the blue one shows the CO_2 available and, thus, processed in the COSOE. When the two curves are not overlapped, it means that there is a surplus in the electric

power produced. Then, in fig.5.28, the total amounts of gases feeding and leaving the COSOE are plotted. It can be seen that H_2O and CO_2 react and H_2 and CO are obtained with a relative ratio of 3. According to the utilization factor used, considerable amounts of CO_2 and H_2O are still present.

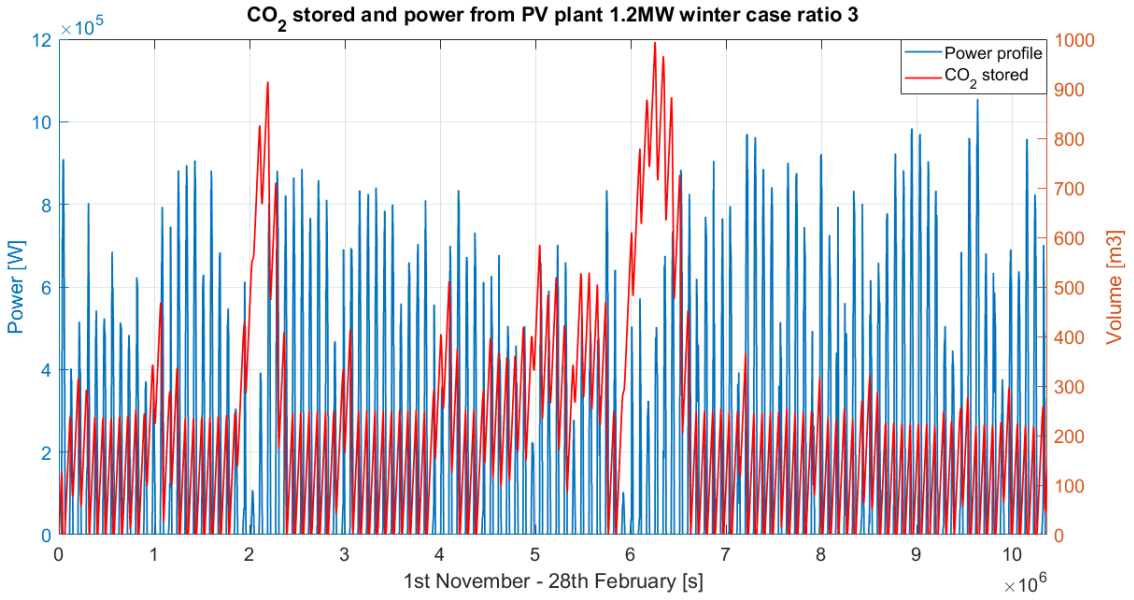

FIG: 5.26. Comparison between CO_2 stored and PV power profile

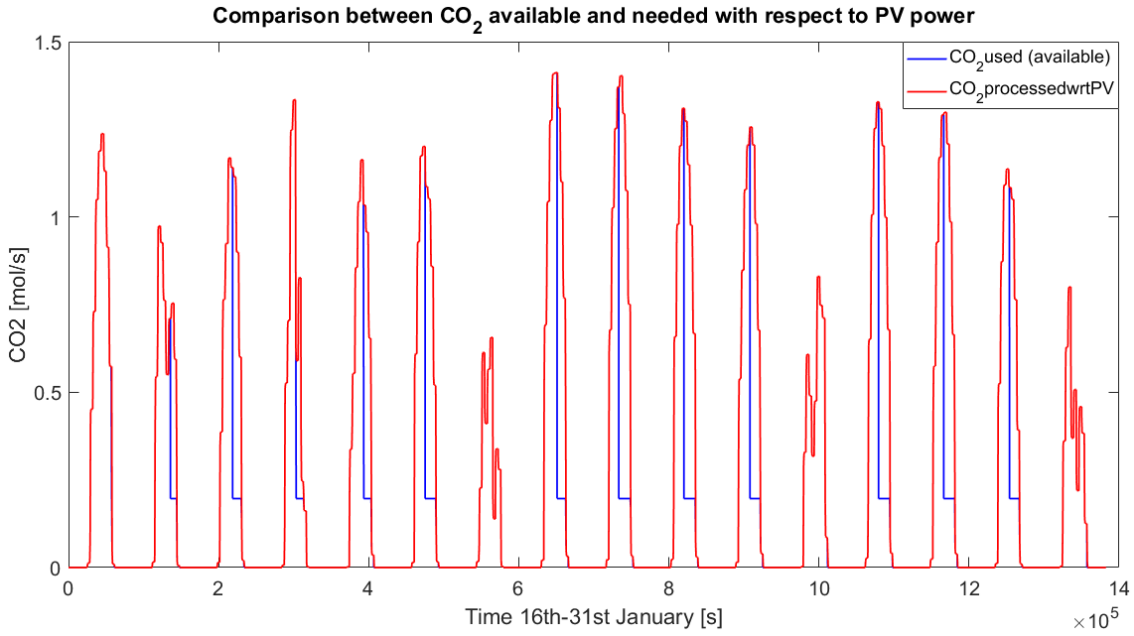

FIG: 5.27. Comparison between CO_2 available and used winter case ratio 3

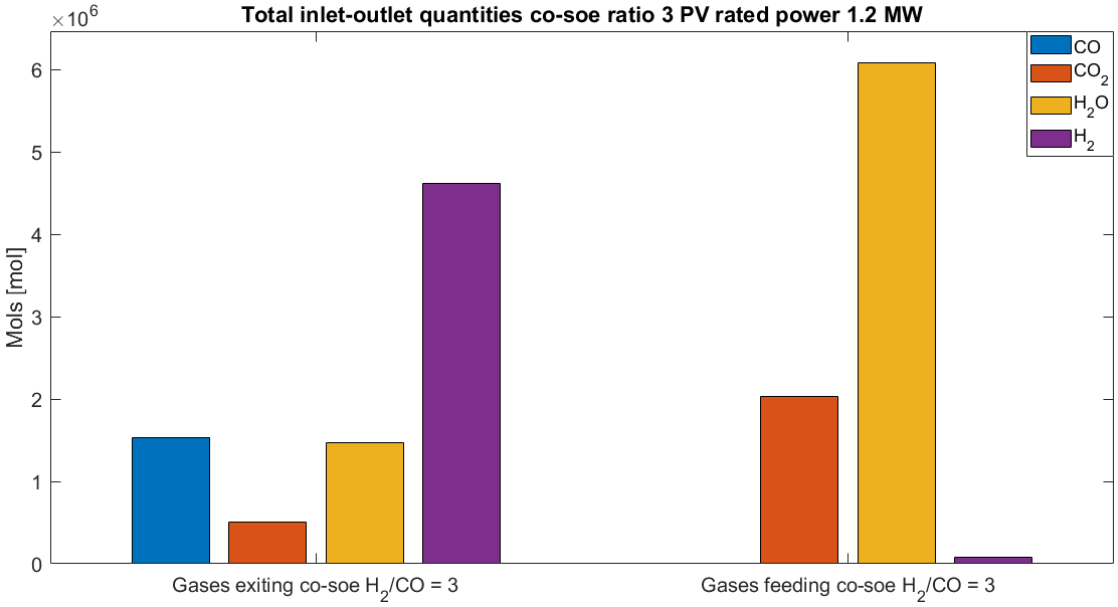

FIG: 5.28. Comparison between inlet-outlet quantities co-soe winter case ratio 3

The CO methanator dimensions and operating conditions are reported into 5.9. In fig.5.30, H_2-CO inlet molar flows and CH_4-H_2O outlet molar flows of the CO-methanator in two weeks of November are plotted. It can be seen that all the CO is converted into CH_4 and, at the same time, H_2O is produced. In fig.5.29, the comparison between the total amounts feeding and leaving the CO-methanator are shown; as expected, the inlet/outlet CO_2 is the same because inside the device the CO-methanation reaction is the predominant one. The H_2 and CO are, indeed, totally converted and CH_4 and H_2O are produced. The outlet molar fractions are: 30.5% CH_4, 59.8% H_2O and 9.7% CO_2.

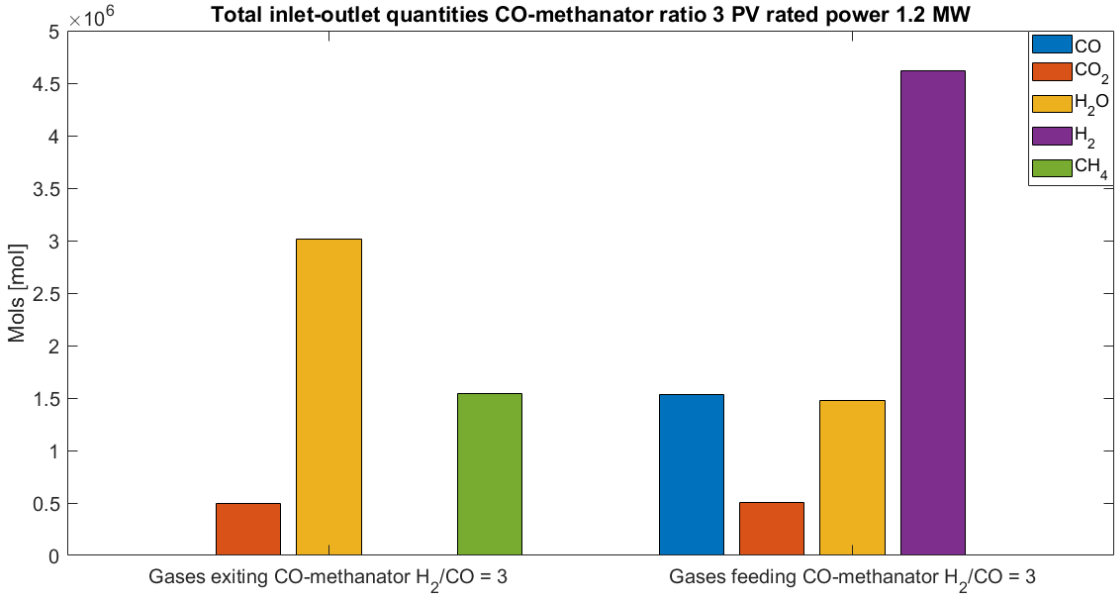

FIG: 5.29. Comparison between inlet-outlet quantities methanator winter case ratio 3

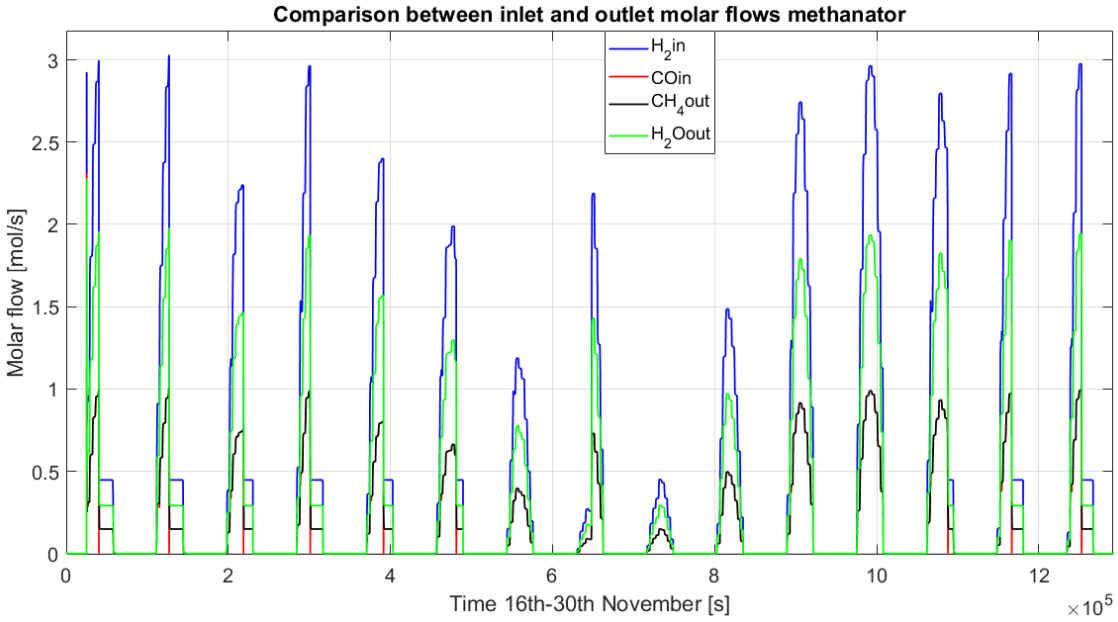

FIG: 5.30. Inlet-Outlet molar flows methanator ratio 3

5.2.3 Winter case - 100% CO_2 exploitation ratio 5

In this section, the same system and the same period of the year is considered but in this case the output COSOE ratio H_2/CO is equal to 5. The results, according to the PV rated power, are shown in fig. 5.31. Looking at the table, it can be seen that the amounts of CO_2 and H_2O are, respectively, lower and larger with respect to ratio 3. The nominal power to be installed in the PV plant should be around 1.8 MW. With this power, practically 100% of CO_2 exploitation is reached and the lack od carbon dioxide is limited. Increasing the nominal power, the storage size decreases and the power surplus becomes always more larger; the gain in terms of CO_2 usage is negligible.

PV size [MW]	Cells co-soe	CO2 co-soe[mol]	H2O co-soe[mol]2	CO2 used [%]	CO2 lack [%]	Storage size [m3]
1.0	2613	1.46·10^6	7,27·10^6	71.3	0.28	13010
1.2	3135	1.74·10^6	8.67·10^6	85.5	0.45	7027
1.4	3657	2.02·10^6	1.01·10^7	99.2	0.70	3006
1.6	4180	2.03·10^6	1.01·10^7	99.6	14.94	1775
1.8	4702	2.03·10^6	1.01·10^7	99.7	29.17	995
2.0	5225	2.04·10^6	1.02·10^7	99.8	43.41	907
2.2	5747	2.04·10^6	1.02·10^7	99.8	57.72	820
2.4	6269	2.04·10^6	1.02·10^7	99.8	72.04	733

FIG: 5.31. Comparison between different PV rated powers winter case ratio 5

In fig.5.32, the inlet-outlet total quantities of the co-soe working with ratio 5 are presented. In fig.5.33, the amounts relative to methanator are highlighted; with this inlet ratio between H_2 and CO, all the CO and CO_2 feeding the system are consumed. In fact, even if the CO methanation reaction is the predominant, the reverse of WGS plays an important role, converting CO_2 in CO; this is, then, converted in new methane. The output mixture is made up of: CH_4, H_2O and not reacted H_2 with these molar fractions respectively: 25.1%, 61.4% and 13.5%.

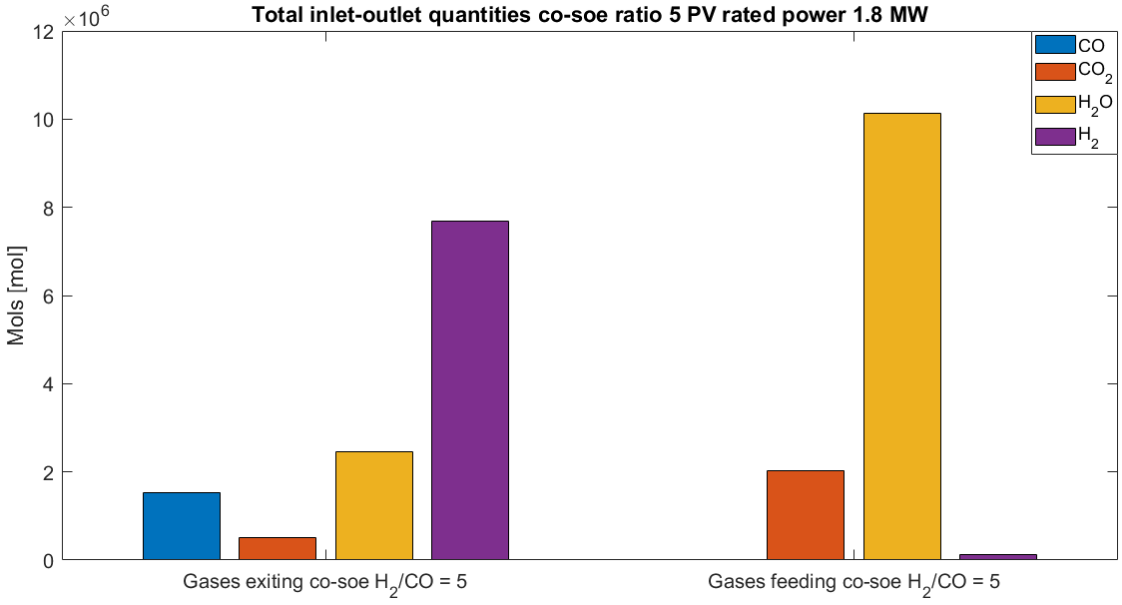

FIG: 5.32. Comparison between inlet-outlet quantities co-soe winter case ratio 5

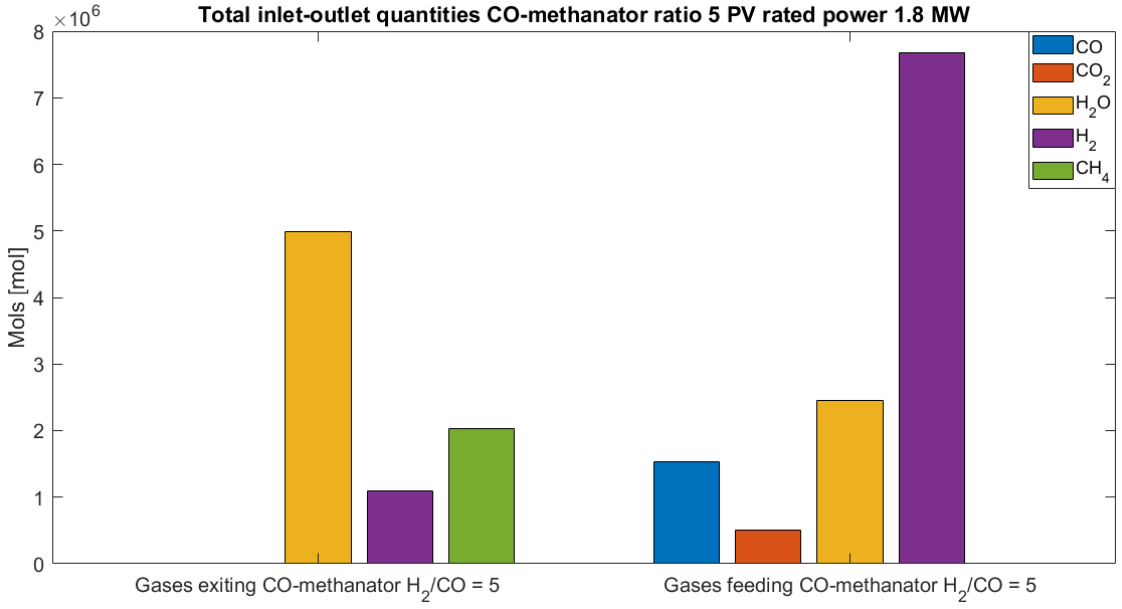

FIG: 5.33. Comparison between inlet-outlet quantities methanator winter case ratio 5

5.2.4 Summer case - 100% CO_2 exploitation ratio 3

As already done for the other system configuration, a similar study for the summer season is portrayed. Concerning the coupling of co-electrolyser and CO methanator, just the case with ratio 3 is considered due to the better results in terms of nominal PV power needed. The results are presented in fig.5.34. Similarly, the nominal power 1.2 MW, evaluated for the winter case, is tested; if this plant was installed for summer operation, it would require a storage almost the half; on the other side, there would be a super amount

of power surplus that is not used. Practically, more than the double quantity of CO_2 available would be needed. Concerning the sole operation in summer season, the rated power of the PV plant to be installed would be 0.8 MW. In fig.5.35, the CO_2 stored and the power profile with 0.8 MW as rated power are shown. It can be seen that, as previously commented, the size of the storage is due to few days in May where the power production is low; if these days were not considered the capacity required would be around 300 m^3.

PV size [MW]	Cells co-soe	CO2 co-soe[mol]	H2O co-soe[mol]2	CO2 used [%]	CO2 lack [%]	Storage size [m3]
0.6	1940	2.07·10^6	6,19·10^6	99.1	12.47	949
0.8	2587	2.08·10^6	6.22·10^6	99.4	49.33	698
1.0	2613	2.08·10^6	6.22·10^6	99.5	86.41	609
1.2	3135	2.08·10^6	6.22·10^6	99.6	123.48	529
1.4	3657	2.09·10^6	6.25·10^6	99.8	160.57	450

FIG: 5.34. Comparison between different rated powers summer case ratio 3

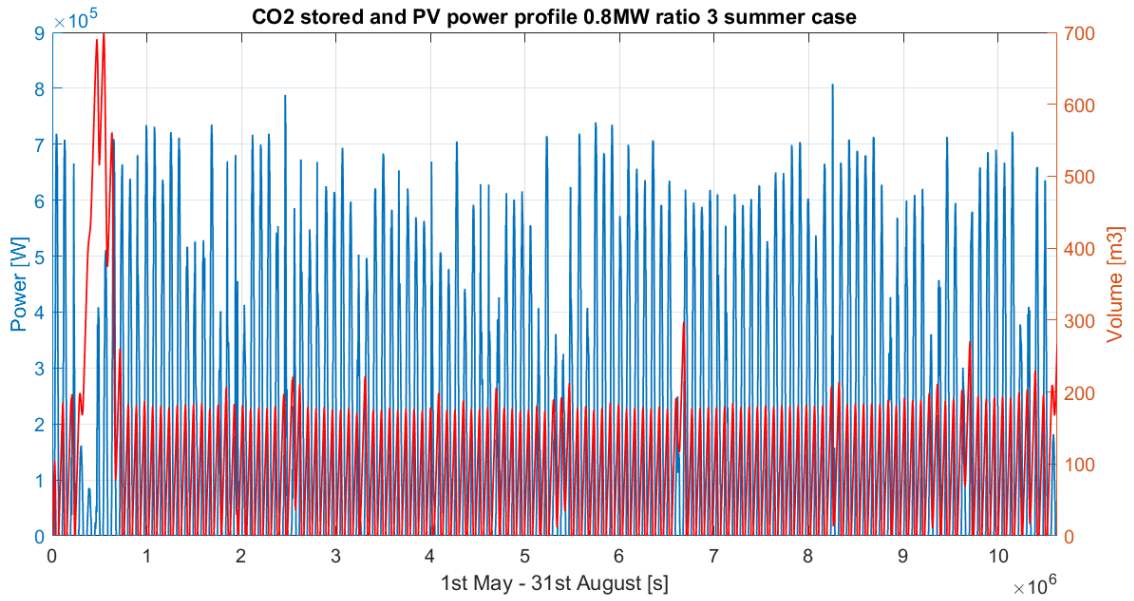

FIG: 5.35. CO_2 stored and PV power profile summer case

5.3 Comparison between the two Power to Gas systems

In this section, the results of the two systems are shown and compared. In fig.5.36, the power plants to be installed, the design of the SOE or COSOE, the storage size and the CO_2 exploited during winter case are presented. The most efficient system is the 'COSOE + CO-methanator' with outlet COSOE H_2/CO-ratio equal to 3. The nominal power is, indeed, 1.2 MW and the storage size is just a bit greater than the one required for the 'SOE + CO_2-methanator'. The percentages of CO_2 expolited are almost identical. In fig.5.37, the summer case is presented; as expected, also in this situation, the system 'COSOE + CO-methanator' is the most efficient one.

System	PV size [MW]	Cells	Storage size [m3]	CO2 used [%]
SOE + CO2 meth	2.0	5225	909	99.8
COSOE + CO meth ratio 3	1.2	3135	995	99.7
COSOE + CO meth ratio 5	1.8	4702	995	99.7

FIG: 5.36. Comparison between the three system configurations winter case

System	PV size [MW]	Cells	Storage size [m3]	CO2 used [%]
SOE + CO2 meth	1.2	3135	700	99.4
COSOE + CO meth ratio 3	0.8	2587	698	99.4

FIG: 5.37. Comparison between the three system configurations summer case

In fig.5.38 and 5.39, the outputs and the molar fractions of the methanators are presented. Looking at these two graphs, it can be seen that in 'COSOE + CO-methanator', operating with H_2/CO-ratio of 5, and 'SOE + CO_2-methanator' the amount of methane produced is maximised: all the carbon atoms available are indeed consumed to get CH_4. Furthermore, it is evident that the outlet gas mixture is different in the three cases; thus, different molar fractions are obtained. In the case of 'SOE + CO_2-methanator', the mixture is made up of methane and steam. In the other PtG configuration, in case of outlet COSOE H_2/CO-ratio of 3 CO_2 is still present; in case of outlet COSOE H_2/CO-ratio of 5, unreacted H_2 is observed.
In the 'COSOE + CO-methanator', operating with an outlet COSOE H_2/CO-ratio of 3, the highest methane molar fraction is obtained. However, as explained above, unreacted and unwanted carbon dioxide is still present; this gas should be then separated, before feeding the natural gas grid, but this is out of the scope of this work.
To sum up, according to the main scope of this work, the system that allows to exploit, in the most efficient way, all the CO_2 available is the 'COSOE + CO-methanator', working with an outlet COSOE H_2/CO-ratio equal to 3.

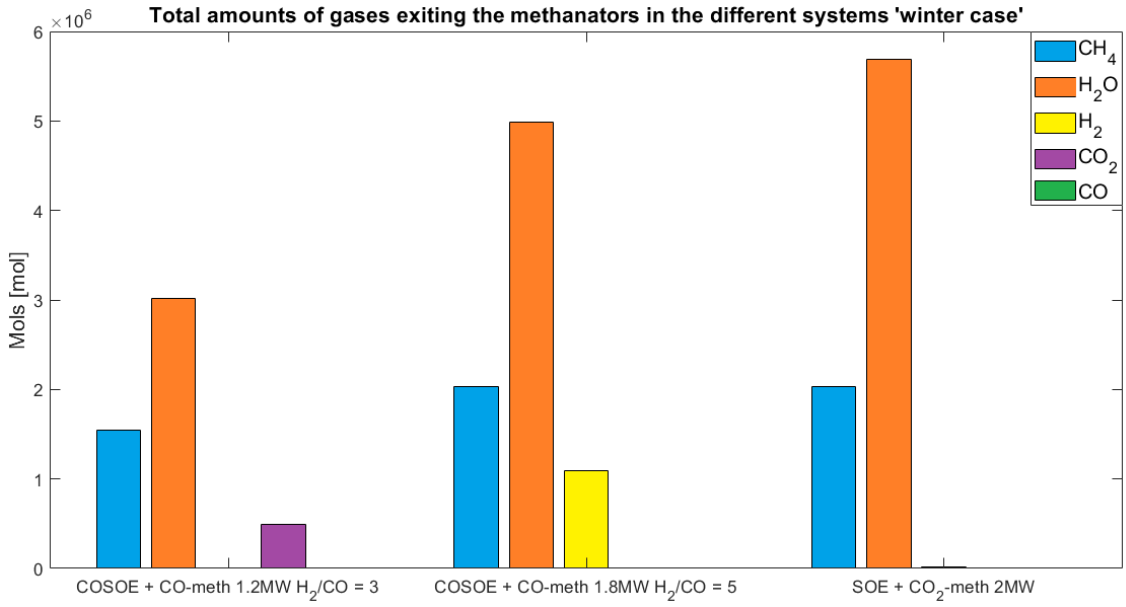

FIG: 5.38. Comparison between the three system configurations

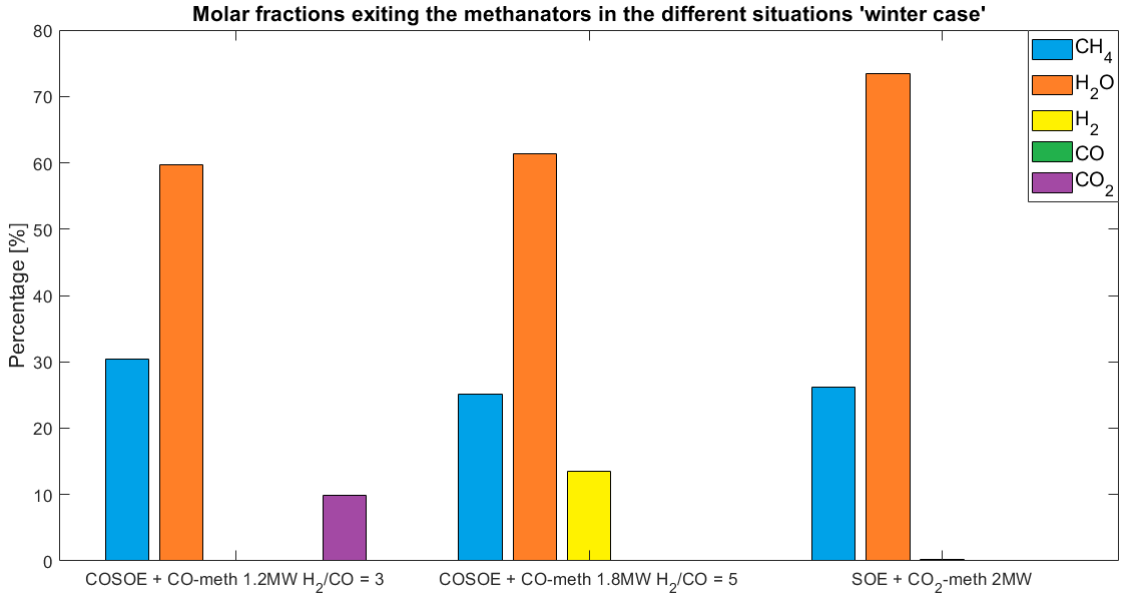

FIG: 5.39. Comparison between the three system configurations

Chapter 6

Budget and enviromental impact

6.1 Budget

In this section all the costs supposed to develop this Master Thesis project are presented. The whole budget is made up of:

- 750 working hours junior engineer with the following subdivision:
  - 30 hours: Case Study and Master Thesis Objectives definition;
  - 150 hours: Literature Review;
  - 20 hours: Self-Learning of MATLAB - Simulink and PV*SOL programmes;
  - 50 hours: Self-Learning of Solid Oxide Electrolyser Model provided by supervisors;
  - 120 hours: Modelling and Simulations of Solid Oxide CO-Electrolyser, CO and CO_2 methanators;
  - 80 hours: Modelling and Simulations of operations inside the two different Power to Gas plants including the strategies to exploit the carbon dioxide produced;
  - 150 hours: Simulations to identify the most efficient technology in two different periods accordingly to MT objectives;
  - 150 hours: Editing of the Master Thesis document.
- Computer;
- MATLAB-Simulink licence;
- PV*SOL licence;
- Microsoft Office 365;
- Office Expenses.

In table 6.1 and 6.2 all the costs associated are presented:

Junior Engineer salary	20 €/hour
Computer	800 €
Annual MATLAB-Simulink licence	1200 € (*)
PV*SOL licence	895 € (**)
Microsoft Office 365 (personal licence)	7 €/month (***)
Electricity, lighting and heating-cooling systems	20 €/month

FIG: 6.1. Different costs associated with the MT project

(*) This is the cost of the annual MATLAB-Simulink licence for a standard end user; thanks to the UPC's licences the author of the work used this programme for free.
(**) This is the cost associated to a standard end user; in this work a 1-month free version is used.
(***) This is the monthly cost for a personal use; thanks to the POLITO's agreements the author of the work used this programme for free.

Budget	Units (u)	Unit price (€/u)	Total price (€)
Engineering	750	20	15000
Hardware	1	800	800
Software	1	2095	2095
Software	7	7	49
Office expenses	7	20	140
Total without I.V.A			18084
I.V.A (21%)			3797,64
TOTAL			**21881,64**

FIG: 6.2. Total cost to develop the project

6.2 Enviromental impact

The topic treated in this Master Thesis is related with the reduction of the environmental impact due to the carbon dioxide emissions of the upgrading process installed inside the Waste Water Treatment Plant "EDAR Riu Sec" based in Sabadell (Barcelona). The main goal is, indeed, the carbon dioxide capture and its subsequent conversion into methane using, during the process, renewable power. At the same time, producing methane in this way, the environmental impact linked with the production of fossil-based natural gas is reduced. Different schemes for the CO_2 conversion into methane have been assessed and compared. During the development of the project, the author tried to limit as much as possible the usage of sheets of papers and when it was needed recycled ones have been used. Moreover, the author is committed to use the lighting and heating-cooling systems in the office just when it was strictly necessary. While travelling, bicycle and public transport have been used.

Chapter 7

Conclusions and future work

7.1 Conclusions

In this Master Thesis work, the analysis of 'Power to Gas' systems, where carbon dioxide is processed to produce methane, has been developed. It has been considered to install the studied technology inside *EDAR Riu Sec*, a Waste Water Treatment Plant, situated in Sabadell (Barcelona). The upgrading process of this plant, where biogas is converted into methane, produces a constant amount of CO_2 all over the year, usually released to the atmosphere. The main goal was to compare two different P2G systems, converting CO_2 into CH_4, in order to evaluate the most efficient one.
Using Matlab-Simulink, simplified dynamic models of the different devices involved have been developed. On the one hand, the Solid Oxide Electrolyser and Co-Electrolyser models have been helpful to evaluate the involved electrochemical reactions to convert steam and/or carbon dioxide into hydrogen and carbon oxide. Furthermore, inlet and outlet molar flows and their relationship have been investigated. The operating conditions, in terms of isothermal temperature and pressure, have been analysed to achieve the more suitable conversion using, at the same time, the least amount of power possible. The computation of the cell voltage, depending on the inlet current density, has been carried out to estimate the polarization curve.
On the other hand, the CO_2 and CO-methanator models have been useful to estimate the methane production and the final outlet gas composition. Similar to electrolysers models, studies on the relationship between inlet and outlet flows have been developed; the more suitable operating conditions have been investigated too.
The developed models have been used to compare the two different P2G plants: 'SOE + CO_2-methanator' and 'COSOE + CO-methanator'. Furthermore, it has been necessary to develop careful strategies to process the carbon dioxide according to the power available. It has been demonstrated that the most efficient P2G plant, among the considered systems, in terms of power needed, is the 'COSOE + CO-methanator' with an outlet co-electrolyser H_2/CO-ratio of 3. This PtG system requires the least amount of PV rated power to be installed to process all CO_2 available during the four winterly months. The PV size is 1.2 MW, compared to 1.8 MW for the same P2G system but with outlet co-electrolyser H_2/CO-ratio of 5; installing a 'SOE + CO_2-methanator', the rated power would be 2 MW. Regarding CO_2 storage, the capacity needed is around 995 m^3 for 'COSOE + CO-methanator' (ratio 3 and 5); for the other PtG configuration, the size

results a bit smaller, around 909 m^3.
During winterly months, the solar energy available is the lowest; it represents the worst case in terms of power installed and CO_2 storage capacity. Therefore, sizing the system in this period, allows to evaluate the rated power and the storage capacity needed to convert CO_2 into methane all over the year.
Repeating the analysis for the summer months, from May to August, the results are similar: the best P2G system is the 'COSOE + CO-methanator' (ratio 3). However, due to the greater amounts of sunlight hours available the capacity of the PV power plant and CO_2 storage are smaller. The 'COSOE + CO-methanator' (ratio 3) needs a PV plant of 0.8 MW and a storage of 698 m^3; the other PtG system 1.2 MW and 700 m^3, respectively.
Concerning the 'COSOE + CO-methanator' system, another comparison had to be established. This comparison analyzed the most profitable co-electrolyser outlet H_2/CO-ratio in terms of produced methane. In this analysis, the same rated power of the PV plant and the design of the components have been considered. In this work, it has been found that the outlet co-electrolyser H_2/CO-ratio of 3 is the optimal solution. An higher methane content is observed with respect to ratio of 5. However, the outlet gas mixture is made up of steam, methane and carbon dioxide; this latter gas can not be injected to natural gas grid and it should be separated afterwards with, consequently, higher costs. Analysing a H_2/CO-ratio of 5, the methanator oulet mixture contains less methane, steam and a significative quantity of unreacted H_2. On the other side, all the carbon oxides are consumed.
It has to be noted that, in this P2G system, the inlet mixture of the CO-methanator comes from the COSOE; this device fixes the amounts of hydrogen, carbon monoxide, steam and carbon dioxide. If it was possible to change the composition, for instance adding CO_2, it can be supposed that the ratio of 5 or an intermediate between 3 and 5 would be the more suitable solution, as highlighted in the literature. However, these investigations have not been carried out.

7.2 Future work

To conclude, during the development of a similar work, a lot of aspects have to be considered and carefully studied. Due to the complexity of the systems, some assumptions and simplifications have been made and it has not been possible going further in the analysis. This work helps to evaluate the most efficient PtG system to exploit the CO_2 produced in *EDAR Riu Sec* WWTP. However, further investigations could bring to find more precise results in terms of gas flows converted and produced. Firstly, additional reactions, that could occur inside the devices should be considered. Secondly, heat flows inside the devices should be accounted. Then, pressurized systems could be studied.
Focusing more on the plant configuration, some improvements could be apported too; for instance, a set of batteries or a H_2 storage could be included to reduce the PV power plant installation and CO_2 storage. Energetic costs in pumping and managing the different gases should be considered to evaluate the total energy required, not just electricity, for the operation of the whole PtG system. Between the electrolysers and methanators, a steam water separator could be included to reduce the amount of steam feeding the methanator improving therefore the methane content in the outlet mixture. A similar device could be installed, after the methanation process, to match the exact gas composition

feeding the natural gas grid.
An economical analysis would be needed to evaluate the investment cost of the whole Power to Gas plant.

Bibliography

[1] Salomone, F., Giglio, E., Ferrero, D., Santarelli, M., Pirone, R. and Bensaid, S. (2018). Techno-economic modelling of a Power-to-Gas system based on SOEC electrolysis and CO2 methanation in a RES-based electric grid. Chemical Engineering Journal.

[2] Götz, Manuel & Lefebvre, Jonathan & Mörs, Friedemann & Koch, Amy & Graf, Frank & Bajohr, Siegfried & Reimert, Rainer & Kolb, Thomas. (2016). Renewable Power-to-Gas: A technological and economic review. Renewable Energy. 85. 1371–1390. 10.1016/j.renene.2015.07.066.

[3] Bachmann, N. (2015). Sustainable biogas production in municipal wastewater treatment plants. [ebook] IEA BIOENERGY.

[4] Ni, M., Leung, M. K. H.,Leung, D. Y. C. (2008). Technological development of hydrogen production by solid oxide electrolyzer cell (SOEC). International Journal of Hydrogen Energy, 33, 2337–2354. doi:10.1016/j.ijhydene.2008.02.048

[5] Laguna-Bercero, M. (2012). Recent advances in high temperature electrolysis using solid oxide fuel cells: A review. Journal of Power Sources, 203, pp.4-16.

[6] Sapountzi, F., Gracia, J., Weststrate, C., Fredriksson, H. and Niemantsverdriet, J. (2017). Electrocatalysts for the generation of hydrogen, oxygen and synthesis gas. Progress in Energy and Combustion Science, 58, pp.1-35.

[7] Rendine, A. (2018). ANALISI NUMERICA DI UN INNOVATIVO SISTEMA "POWER-TO-GAS" PER L'ACCUMULO ENERGETICO. Tesi di Laurea Magistrale. UNIVERSITÀ DI BOLOGNA.

[8] Dragsbæk Duhn, J. (2017). Development of highly efficient solid oxide electrolyzer cell systems. PhD Thesis Doctor of Philosophy. DTU Chemical Engineering.

[9] Giglio, Emanuele & Lanzini, Andrea & Santarelli, Massimo & Leone, Pierluigi. (2015). Synthetic natural gas via integrated high-temperature electrolysis and methanation: Part II—Economic analysis. Journal of Energy Storage. 2. 74-69. 10.1016/j.est.2015.06.004.

[10] Gondolini, A. (2013). Celle ad ossidi solidi per elettrolisi ad alta temperatura. Dottorato di ricerca in chimica industriale. Università di Bologna.

[11] Luiso, S. (2013). Elettrolisi dell'acqua con energia fotovoltaica: analisi di un impianto per la produzione di idrogeno da fonti rinnovabili. Laurea Magistrale. Università di Bologna.

[12] Harrison, K., Remick, R., Martin, G. and Hoskin, A. (2010). Hydrogen Production: Fundamentals and Cas Study Summaries.

[13] Ni, Meng & Leung, Michael K.H. & Leung, Dennis. (2006). An Electrochemical Model of a Solid Oxide Steam Electrolyzer for Hydrogen Production. Chemical Engineering & Technology. 29. 636 - 642. 10.1002/ceat.200500378.

[14] Stempien, Jan & Sun, Qiang & Chan, S.H.. (2013). Solid Oxide Electrolyzer Cell Modeling: A Review. Journal of Power Technologies. 93. 216.

[15] Ni, Meng. "An electrochemical model for syngas production by co-electrolysis of H2O and CO2." (2012).

[16] J. R. Ferguson, J. M. Fiard, R. Herbin, J. Power Sources 1996, 58 (2), 109. DOI: 10.1016/0378–7753 (95) 02269–4

[17] Wang, Yao & Liu, Tong & Lei, Libin & Chen, Fanglin. (2016). High temperature solid oxide H2O/CO2 co-electrolysis for syngas production. Fuel Processing Technology. 161. 10.1016/j.fuproc.2016.08.009.

[18] R. Suwanwarangkul, E. Croiset, M.W. Fowler, P.L. Douglas, E. Entchev, M.A. Douglas, J. Power Sources 122 (2003) 9–18.

[19] Redissi, Y. and Bouallou, C. (2013). Valorization of Carbon Dioxide by Co-Electrolysis of CO2/H2O at High Temperature for Syngas Production. Energy Procedia, 37, pp.6667-6678.

[20] Rivera-Tinoco R, Mansilla C, Bouallou C. Competitiveness of hydrogen production by high temperature electrolysis: impact of the heat source and identification of key parameters to achieve low production costs. Energy Conversion and Management 2010;51;2623-2634.

[21] Jensen OJ, Jensen SH, Tophoj N, Bandur V, Ebbesen S, et al. Pre-investigation of water electrolysis. Risø DTU National Laboratory for Sustainable Energy; 2008. Available on ¡http://130.226.56.153/rispubl/NEI/NEI DK-5057.pdf.¿.

[22] D. Ferrero, A. Lanzini, M. Santarelli, P. Leone, A comparative assessment on hydrogen production from low-and high-temperature electrolysis, Int. J. Hydrog. Energy 38 (2013) 3523–3536.

[23] M. Ni, An electrochemical model for syngas production by co-electrolysis of H2O andCO2, J. Power Sources 202 (2012) 209–216.

[24] X. Sun, M. Chen, S.H. Jensen, S.D. Ebbesen, C. Graves, M. Mogensen, Thermodynamic analysis of synthetic hydrocarbon fuel production in pressurized solid oxide electrolysis cells, Int. J. Hydrog. Energy 37 (2012) 17101–17110.

[25] S.D. Ebbesen, S.H. Jensen, A. Hauch,M.B.Mogensen, High temperature electrolysis in alkaline cells, solid proton conducting cells, and solid oxide cells, Chem. Rev. 114 (2014) 10697–10734.

[26] S.H. Chan, Z.T. Xia, J. Appl. Electrochem. 32 (2002) 339–347.

[27] M. Ni, M.K.H. Leung, D.Y.C. Leung, Energy Convers. Manage. 48 (2007) 1525–1535.

[28] H.F. Rase, Handbook of Commercial Catalysts: Heterogenous Catalysts, CRC Press, Boca Raton, 2000.

[29] M.V. Twigg, London, Catalyst Handbook, 2nd ed., Manson Publishing Ltd., 1996.

[30] Appl M (1999) Ammonia: principles and industrial practice. Wiley-VCH,Weinheim, Chichester. ISBN 3527295933

[31] Xu G, Chen X, Zhang ZG (2006) Temperature-staged methanation: an alternative method to purify hydrogen-rich fuel gas for PEFC. Chem Eng J 121:97–107

[32] Miguel, C., Mendes, A. and Madeira, L. (2018). Intrinsic kinetics of CO2 methanation over an industrial nickel-based catalyst. Journal of CO2 Utilization, 25, pp.128-136.

[33] Frontera, P.; Macario, A.; Ferraro, M.; Antonucci, P. Supported Catalysts for CO2 Methanation: A Review. Catalysts 2017, 7, 59.

[34] Su, X.; Xu, J.; Liang, B.; Duan, H.; Hou, B.; Huang, Y. Catalytic carbon dioxide hydrogenation to methane: A review of recent studies. J. Energy Chem. 2016, 25, 553–565.

[35] Ronsch, S.; Schneider, J.; Matthischke, S.; Schluter, M.; Gotz, M.; Lefebre, J.; Prabhakaran, P.; Bajohr, S. Review on methanation—From fundamentals to current projects. Fuel 2016, 166, 276–296.

[36] Schaaf, T., Grünig, J., Schuster, M., Rothenfluh, T. and Orth, A. (2014). Methanation of CO2 - storage of renewable energy in a gas distribution system. Energy, Sustainability and Society, 4(1).

[37] E.Z. Golosman, V.N. Efremov, Industrial catalysts for the hydrogenation of carbon oxides, Catal. Ind. 4 (2012) 267–283.

[38] G.H. Watson, Methanation Catalysts, International Energy Agency Coal Research, London, 1980.

[39] Pedersen K, Skov A, Rostrup Nielsen JR (1980) Symposium on catalytic reactions involving synthesis gas, Houston. pp 89–100

[40] Kopyscinski J, Schildhauer TJ, Biollaz SMA (2009) Employing catalyst fluidization to enable carbon management in the SNG-production from biomass. Chem Eng Technol 32(3):343–347

[41] Kunii D, Levenspiel O (1991) Fluidization engineering. Butterworth-Heinemann, Boston

[42] Hedden K (1986) Fachinformationszentrum Energie. Physik, Mathematik, Karlsruhe

[43] Kopyscinski J, Schildhauer TJ, Biollaz SMA (2010) Production of synthetic natural gas (SNG) from coal and dry biomass - a technology review from 1950 to 2009. Fuel 89(8):1763–1783

[44] Er-rbib, H. and Bouallou, C. (2019). Methanation catalytic reactor.

[45] Kopyscinski, J., Schildhauer, T. and Biollaz, S. (2011). Methanation in a fluidized bed reactor with high initial CO partial pressure: Part I—Experimental investigation of hydrodynamics, mass transfer effects, and carbon deposition. Chemical Engineering Science, 66(5), pp.924-934.

[46] Jiajian, Gao & Wang, Yingli & Ping, Yuan & Hu, Dacheng & Xu, Guangwen & Gu, Fangna & Su, Fabing. (2012). A thermodynamic analysis of methanation reactions of carbon oxides for the production of synthetic natural gas. RSC Adv.. 2. 2358-2368. 10.1039/C2RA00632D.

[47] G.H. Watson, Methanation catalysts,, Technical report of International Energy Agency Coal Research, London, England, 1980.

[48] C. Yang, A. Coffin, F. Chen, High temperature solid oxide electrolysis cell employing porous structured (La0.75Sr0.25)0.95MnO3 with enhanced oxygen electrode performance, Int. J. Hydrog. Energy 35 (2010) 3221–3226.

[49] M. Laguna-Bercero, Recent advances in high temperature electrolysis using solid oxide fuel cells: a review, J. Power Sources 203 (2012) 4–16.

[50] C. Yang, J. Li, J. Newkirk, V. Baish, R. Hu, Y. Chen, F. Chen, Co electrolysis of H2O and CO2 in a solid oxide electrolysis cellwith hierarchically structured porous electrodes, J. Mater. Chem. A 3 (2015) 15913–15919.

[51] C.M. Stoots, J.E. O'Brien, J.S. Herring, J.J. Hartvigsen, J. Fuel Cell Sci. Technol. 6 (2009) 011014.

[52] S.D. Ebbesen, C. Graves, M. Mogensen, Int. J. Green Energy 6 (2009) 646–660.

[53] Aicart, J., Laurencin, J., Petitjean, M. and Dessemond, L. (2014). Experimental Validation of Two-Dimensional H2O and CO2Co-Electrolysis Modeling. Fuel Cells, 14(3), pp.430-447.

[54] Aicart, J., Petitjean, M., Laurencin, J., Tallobre, L. and Dessemond, L. (2015). Accurate predictions of H2O and CO2 co-electrolysis outlet compositions in operation. International Journal of Hydrogen Energy, 40(8), pp.3134-3148.

[55] Effects of Pressure on High Temperature Steam and Carbon Dioxide Co-electrolysis L. Bernadeta, J. Laurencina,*, G. Rouxa, D. Montinarob, F. Mauvyc, M. Reytiera

[56] J. Kopyscinski, Production of synthetic natural gas in a fluidized bed reactor: Understanding the hydrodynamic, mass transfer, and kinetic effects, Thesis for the degree of Doctor of Sciences, Paul Scherrer Institute, Villigen, Switzerland, 2010.

[57] K. Khorsan, M.A. Marvast, N. Pooladian, M. Kakavan, Petroleum Coal 49 (2007) 46.

[58] Iliuta, I., Tahoces, R., Patience, G., Rifflart, S. and Luck, F. (2010). Chemical-looping combustion process: Kinetics and mathematical modeling. AIChE Journal, p.NA-NA.

Sitography

[59] PV*SOL Valentine Software. (2019). [online] Available at: $http$: $//www.valentin-software.com/it/prodotti/pvsol[Accessed19Sep.2019]$.

[60] Iea.org. (2019). Statistics: Key electricity trends 2016. [online] Available at: $https$: $//www.iea.org/newsroom/news/2017/april/statistics-key-electricity-trends-2016.html[Accessed18Sep.2019]$.

[61] Oksolar.it. (2019). [online] Available at: $https$: $//www.oksolar.it/datasheet/SF-PM096B00_dsit.pdf[Accessed18Sep.2019]$.

[62] Climate Change: Vital Signs of the Planet. (2019). Climate Change: Vital Signs of the Planet. [online] Available at: $https$: $//climate.nasa.gov/[Accessed18Sep.2019]$.

[63] En.wikipedia.org. (2019). Wastewater treatment. [online] Available at: $https$: $//en.wikipedia.org/wiki/Wastewater_treatment[Accessed18Sep.2019]$.

[64] ClearCove. (2019). Primary vs. Secondary Sludge - ClearCove. [online] Available at: $http$: $//www.clearcovesystems.com/primary-vs-secondary-sludge/[Accessed18Sep.2019]$.

[65] Foodandbeverage.pentair.com. (2019). Pentair - Biogas Upgrading for Biogas Plants - Haffmans — Pentair Food and Beverage Process Solutions. [online] Available at: $https$: $//foodandbeverage.pentair.com/en/products/haffmans-biogas-upgrading-technology[Accessed18Sep.2019]$.

[66] US EPA. (2019). Overview of Greenhouse Gases — US EPA. [online] Available at: $https$: $//www.epa.gov/ghgemissions/overview-greenhouse-gases[Accessed18Sep.2019]$.

[67] Ec.europa.eu. (2019). [online] Available at: $https$: $//ec.europa.eu/eurostat/documents/2995521/9779945/8-08052019-AP-EN.pdf/9594d125-9163-446c-b650-b2b00c531d2b[Accessed18Sep.2019]$.

[68] Unfccc.int. (2019). The Paris Agreement — UNFCCC. [online] Available at: $https$: $//unfccc.int/process-and-meetings/the-paris-agreement/the-paris-agreement[Accessed18Sep.2019]$.

[69] Europarl.europa.eu. (2019). Reducing carbon emissions: EU targets and measures — News — European Parliament.

[70] Wikipedia. (2019). Main Page. [online] Available at: $https$: $//en.wikipedia.org/wikiSolid_oxide_electrolyser_cell[Accessed18Sep.2019]$.

[71] Press Room - Naturgy. (2019). CoSin Project. [online] Available at: $https$: $//prensa.naturgy.com/en/gas-natural-fenosa-launches-pilot-project-to-produce-renewable-gas-in-catalonia/[Accessed18Sep.2019]$.

[72] Wikipedia. (2019). Main Page. [online] Available at: $https$: $//en.wikipedia.org/wikiHeterogeneous_catalytic_reactor[Accessed18Sep.2019]$.

[73] Sciencedirect.com. (2019). Fixed Bed Reactor - an overview — ScienceDirect Topics. Available at: $https$: $//www.sciencedirect.com/topics/engineering/fixed-bed-reactor[Accessed18Sep.2019]$.

[74] Sciencedirect.com. (2019). Fluidized Bed Reactor - an overview — ScienceDirect Topics. [online] Available at: $https$: $//www.sciencedirect.com/topics/engineering/fluidized-bed-reactor[Accessed18Sep.2019]$.

[75] En.wikipedia.org. (2019). Ideal gas law. [online] Available at: $https$: $//en.wikipedia.org/wiki/Ideal_gas_law[Accessed18Sep.2019]$.

[76] En.wikipedia.org. (2019). Molar mass. [online] Available at: $https$: $//en.wikipedia.org/wiki/Molar_mass[Accessed18Sep.2019]$.

[77] It.wikipedia.org. (2019). Convertitore DC-DC. [online] Available at: $https$: $//it.wikipedia.org/wiki/Convertitore_DC-DC[Accessed18Sep.2019]$.